Universitat de Girona

NOMINAL STRENGTH AND SIZE EFFECT OF QUASI-BRITTLE STRUCTURES WITH HOLES

Abdallah Mahmoud Bayoumi KABEEL

Dipòsit legal: Gi. 866-2015
http://hdl.handle.net/10803/289985

Universitat de Girona

PhD Thesis

Nominal Strength and Size Effect of Quasi-brittle Structures with Holes

Abdallah Mahmoud Bayoumi Kabeel

2014

Universitat de Girona

PhD Thesis

Nominal Strength and Size Effect of Quasi-brittle Structures with Holes

Abdallah Mahmoud Bayoumi Kabeel

2014

Technology Doctorate Programme

Advisor

Dr. Pere Maimí Vert

Universitat de Girona, Spain

A thesis submitted for the degree of Doctor of Philosophy by the Universitat de Girona

To whom it might concern,

Dr. Pere Maimí Vert, Associate Professor at the *Universitat de Girona* of the Department of *Enginyeria Mecànica i de la Construcció Industrial*

CERTIFY that the study entitled *Nominal Strength and Size Effect of Quasi-brittle Structures with Holes* has been carried out under his supervision by Abdallah Mahmoud Bayoumi Kabeel to apply for the doctoral degree. I also certify that Abdallah Mahmoud Bayoumi Kabeel was a full time graduate student at Universitat de Girona, Girona, Spain, from April 2012 to present.

Dr. Pere Maimí Vert
Universitat de Girona, Spain

IN THE NAME OF ALLAH

Acknowledgements

I would like to express my gratitude to my advisor, Dr. Pere Maimí, for the indefatigable help and for the key contributions that have allowed the development of the present thesis. Also, his experienced advice, patience and guiding me through this work are much appreciated.

I also would like to thank the help received from Dr. Narcís Gascons. He spent a lot of time making the work easy and clarified many things. Also, I would like to thank Dr. Emilio González for his support and encouragement during my work.

Many thanks should also be pointed towards all members of AMADE research group of the University of Girona, for their cooperation during my stay with them.

Thanks to my friends: Tamer Sebaey, Ibrahim Attia, Mohammed Emran, Ahmed Wageih and Mohammed Emara for nice moments that I have spent with them in Girona.

I'm extremely grateful to my friends: Ayman Sadoun, Mohammed Eltaher, Mahmoud Khater, Mohammed Samir and Tarek Alsayed for heir continuous support and encouragement.

I must acknowledge my parents, my brothers and my sisters for their support during my whole life.

Last but not least, I would like to express my deepest gratitude to my wife, my daughter Mennah and my sons Ahmed and Mohammed for their sacrifices and being alone for long time during my travel abroad. I'm also very thankful to my relatives and to the people whom I didn't mention their names but they were always there.

Funding

The period of this research has been funded by the Comissionat per a Universitats i Recerca del Departament d'Innovació, Universitats i Empresa de la Generalitat de Catalunya, under a research grant FI pre-doctorate grant 2012FI-B00102, started in July of 2012 until present.

Also, the present work has been partially funded the Ministerio de Economía y Competitividad under the projects MAT2012-37552-C03-03 and MAT2013-46749-R.

Publications

The papers published during the development of this thesis are listed below:

1. **A. M. Kabeel**, P. Maimí, N. Gascons, E.V. González. Nominal strength of quasi-brittle open hole specimens under biaxial loading conditions. *Composites Science and Technology*, 87: pp. 42-49, 2013.

2. **A. M. Kabeel**, P. Maimí, N. Gascons, E.V. González. Net-tension strength of double lap joints taking into account the material cohesive law, *Composite Structures*, 112: pp. 207-213, 2014.

3. **A. M. Kabeel**, P. Maimí, E.V. González, N. Gascons. Net-tension strength of double-lap joints under bearing-bypass loading conditions using the cohesive zone model, *Composite Structures*,119: pp. 443-451, 2015.

List of Symbols

Symbol	Description
b	Empirical parameter used in fastener stiffness calculation.
E	Modulus of elasticity (Young's modulus).
E_f	Young's Modulus of the fastener's material.
E_I	Young's Modulus of the inner plate in the double-lap joints.
E_O	Young's Modulus of the outer plates in the double-lap joints.
e	End distance in bolted joints.
G_C	Critical fracture energy.
H	Initial slope of the cohesive law.
K	Total stress intensity factor.
K_b	Stress intensity factor of the contact stress due to the bolt.
$\bar{K}_b$	Normalized form of K_b .
K_C	Critical stress intensity factor.
K_E	Stress intensity factor due to total external applied loads.
$\bar{K}_E$	Normalized form of K_E .
K_{rB}	Stress intensity factor due to remote stress caused by the bypass load.
$\bar{K}_{rB}$	Normalized form of K_{rB} .
K_{rb}	Stress intensity factor due to remote stress caused by the bearing load.
$\bar{K}_{rb}$	Normalized form of K_{rb} .
K_t	Stress concentration factor.

Symbol	Description
K_{σ_c}	Stress intensity factor due to the cohesive stresses.
$\bar{K}_{\sigma_c}$	Normalized form of K_{σ_c} .
$\bar{k}$	Parameter that represents the relative stiffness in bolted joints.
k_f	Fastener stiffness in bolted joints.
k_I	Stiffness of the inner plate in double-lap joints.
$\bar{k}_I$	Relative k_I with respect to k_f, $\bar{k}_I = k_I/k_f$.
k_O	Stiffness of the outer plates in double-lap joints.
$\bar{k}_O$	Relative k_O with respect to k_f, $\bar{k}_O = k_O/k_f$.
L_B	Bypass load in multi-fastener joints.
L_b	Bearing load in bolted joints.
ℓ_{ASM}	Characteristic length according to the average stress method.
$\bar{\ell}_{\text{ASM}}$	Normalized ℓ_{ASM}, $\bar{\ell}_{\text{ASM}} = \ell_{\text{ASM}}/R$.
ℓ_{FFM}	Characteristic length according to the finite fracture mechanics model.
$\bar{\ell}_{\text{FFM}}$	Normalized ℓ_{FFM}, $\bar{\ell}_{\text{FFM}} = \ell_{\text{FFM}}/R$.
ℓ_{FPZ}	Size of the fracture process zone.
$\bar{\ell}_{\text{FPZ}}$	Normalized size of the FPZ, $\bar{\ell}_{\text{FPZ}} = \ell_{\text{FPZ}}/R$.
$\tilde{\ell}_{FPZ}$	Normalized ℓ_{FPZ} with respect to ℓ_M, $\tilde{\ell}_{FPZ} = \ell_{\text{FPZ}}/\ell_M$.
ℓ_{IFM}	Characteristic length according to the inherent flaw model.
$\bar{\ell}_{\text{IFM}}$	Normalized ℓ_{IFM}, $\bar{\ell}_{\text{IFM}} = \ell_{\text{IFM}}/R$.
ℓ_{PSM}	Characteristic length according to the point stress method.
$\bar{\ell}_{\text{PSM}}$	Normalized ℓ_{PSM}, $\bar{\ell}_{\text{PSM}} = \ell_{\text{PSM}}/R$.
ℓ_M	Material characteristic length, $\ell_M = EG_c/\sigma_u^2$.
$\bar{\ell}_M$	Normalized ℓ_M, $\bar{\ell}_M = \ell_M/R$.
ℓ_{SEL} and r	Adjusting parameters in the size effect law.
$\bar{\ell}_{\text{SEL}}$	Normalized ℓ_{SEL}, $\bar{\ell}_{\text{SEL}} = \ell_{\text{SEL}}/R$.
m	Empirical parameter used in fastener stiffness calculation.

Symbol	Description
q	Fastener spacing in bolted joints.
R	Hole radius.
S_b	Bearing strength.
$\bar{S}_b$	Normalized Bearing strength,$\bar{S}_b = S_b/\sigma_u$.
t	Specimen, or joint, thickness .
t_I	Thickness of the inner plate in double-lap joints.
t_O	Thickness of the outer plates in double-lap joints.
$2W$	Specimen, or joint, width.
w	Total crack opening displacement.
$\bar{w}$	Normalized form of the w.
w_b	Crack opening displacement of the contact stress due to the bolt.
$\bar{w}_b$	Normalized form of w_b .
w_c	Critical crack opening displacement.
w_E	Crack opening displacement due to external applied loads.
$\bar{w}_E$	Normalized form of the w_E.
w_{rB}	Crack opening displacement due to remote stress caused by the bypass load.
$\bar{w}_{rB}$	Normalized form of w_{rB} .
w_{rb}	Crack opening displacement due to remote stress caused by the bearing load.
$\bar{w}_{rb}$	Normalized form of w_{rb} .
w_{σ_c}	Crack opening displacement due to the cohesive stresses.
$\bar{w}_{\sigma_c}$	Normalized form of the w_{σ_c}.
σ_b	Bearing stress.
$\bar{\sigma}_b$	Normalized σ_b, $\bar{\sigma}_b = \sigma_b/\sigma_u$.
σ_{bf}	Bearing stress at net-tension failure.
$\bar{\sigma}_{bf}$	Normalized σ_{bf}, $\bar{\sigma}_{bf} = \sigma_{bf}/\sigma_u$.
σ_N	Nominal stress.

Symbol	Description
$\bar{\sigma}_N$	Normalized σ_N, $\bar{\sigma}_N = \sigma_N/\sigma_u$.
σ_{Nf}	Nominal strength in tensile and net-tension failures of open hole and bolted joint problems, respectively.
$\bar{\sigma}_{Nf}$	Normalized σ_{Nf}, $\bar{\sigma}_{Nf} = \sigma_{Nf}/\sigma_u$.
σ_{nB}	Bypass stress with respect to the net area.
$\bar{\sigma}_{nB}$	Normalized σ_{nB}, $\bar{\sigma}_{nB} = \sigma_{nB}/\sigma_u$.
σ_u	Material ultimate tensile strength.
σ_∞	Remote stress in bolted joints.
$\bar{\sigma}_\infty$	Normalized σ_∞, $\bar{\sigma}_\infty = \sigma_\infty/\sigma_u$.
$(\sigma_\infty)_f$	Remote stress at net-tension failure in bolted joints.
$(\bar{\sigma}_\infty)_f$	Normalized $(\sigma_\infty)_f$, $(\bar{\sigma}_\infty)_f = (\sigma_\infty)_f/\sigma_u$.
β and ζ	Measures of the bearing-bypass load ratio in multi-fastener joints, $\zeta = L_B/L_b = (1-\theta_W)/(\beta\theta_W)$.
λ	Biaxiality load ratio in open hole specimens.
θ_e	Geometric parameter, $\theta_e = e/2R$.
θ_W	Geometric parameter, $\theta_W = R/W$.

List of Acronyms

Acronym	Description
ASM	Average Stress Method
CCL	Constant Cohesive Law
CL	Cohesive Law
CDTs	Critical Distance Theories
COD	Crack Opening Displacement
CZM	Cohesive Zone Model
ECL	Exponential Cohesive Law
FEM	Finite Element Method
FFM	Finite Fracture Mechanics
FPZ	Fracture Process Zone
IFM	Inherent Flaw Model
LCL	Linear Cohesive Law
LEFM	Linear Elastic Fracture Mechanics
MASM	Modified Average Stress Method
OH	Open Hole
PSM	Point Stress Method
SEL	Size Effect Law
SIF	Stress Intensity Factor

List of Figures

Contents

Resum

Degut a les seves excel·lents propietats específiques moltes estructures es fabriquen amb materials quasi-fràgils. Aquests materials es caracteritzen per la formació d'una zona de procés de falla relativament gran respecte la mida de l'estructura. L'existència d'aquesta zona provoca que la resistència nominal de l'estructura depengui de la seva mida, efecte conegut com *llei d'escala*. Sovint, és necessari la presència de forats, ja sigui per realitzar finestres, portes o punts d'accés. A més, els forats són necessaris sempre que diferents elements vulguin unir-se mitjançant cargols. Per tant, l'estudi de la resistència nominal i la llei d'escala en estructures quasi-fràgils que continguin forats és un tema de gran importància.

El desenvolupament de models per predir la resistència nominal permet dissenyar aquestes estructures d'una manera econòmica ja que es redueix la necessitat de realitzar costoses campanyes experimentals. Les estructures aeronàutiques i aeroespacials contenten molts forats sota estats multidireccionals de forces que poden provocar l'aparició d'esquerdes que eventualment poden ser causa de la falla de l'estructura. Per tant, la predicció de la resistència nominal d'estructures foradades sota estats biaxials de càrregues és necessari pel disseny de moltes estructures. Les estructures cargolades o reblonades són típiques en moltes aplicacions enginyerils i la seva degradació pot causar el colapse catastròfic de l'estructura. La determinació de la resistència última és essencial per un disseny eficient d'aquestes unions.

A la literatura existeixen models per predir la resistència nominal d'estructures amb forats i cargols per materials quasi-fràgils. No obstant, els models analítics avantatgen als numèrics en la seva velocitat de càlcul permetent agilitzar el proces de disseny.

La principal contribució d'aquest treball és la d'introduïr un model analític capaç de generar diagrames de disseny que permeten obtenir la resistència nomi-

nal d'estructures quasi-fràgils que continguin forats. Els models de zona cohesiva (CZM) permeten predir la resistencia d'estructures amb forats formades de materials quasi-fràgils amb una gran zona de procés de fallada confinada en un pla. Aquests models també són capaços de predir l'efecte de la mida de l'estructura en la resistència nominal. A més els CZM són un dels pocs (o els únics) que consideren d'una manera explítica la llei cohesiva en la seva formulació. Per aquestes raons, la majoria de resultats presentats es basen en els models de zona cohesiva.

L'objectiu global d'aquesta tesis s'obté a partir de la consecució de tres objectius parcials. El primer objectiu del treball es centra en la definició d'un model analític capaç de predir la resistència nominal d'estructures foradades sota estats de càrrega biaxial formades per un material quasi-fràgil i isòtrop. El model considera la llei cohesiva del material i s'estudien diverses formes d'aquesta llei. Els resultats obtinguts es comparen amb altres mètodes de disseny, aquells basats en les teories de les distàncies crítiques.

El segon objectiu de la present tesis és la definició d'un model analític capaç de predir la resistència nominal d'estructures cargolades formades per un sol cargol i de material quasi-fràgil i isòtrop. El model es formula considerant la llei cohesiva del material. El model considera; la forma de la llei cohesiva, la distribució de pressions sota el cargol, la mida del forat i l'amplada de la proveta. Com que la majoria d'unions estan formades per més d'una fila de cargols, el darrer objectiu de la tesis és extendre el model a unions formades per més d'una fila de cargols on sols part de la càrrega externa és transferida per un cargol.

Els resultats obtinguts es comparen amb resultats experimentals obtenint bons ajustos. Alguns dels resultats presentats són novedosos com els diagrames que mostren l'obertura de l'esquerda (COD) en el moment de la fallada. Aquests gràfics són molt útils per entendre certes característiques de la llei cohesiva. Per exemple, mitjançant aquests diagrames es demostra que la primera part de la llei cohesiva és la més important per determinar la resistencia nominal d'estructures amb forats. Finalment, també es demostra que si la llei cohesiva es determina correctament els models presentats permeten substituïr l'ús de complexes models de dany continu implementats en codis d'elements finits. A més, els resultats obtinguts permeten la definició de diagrames de disseny que permeten l'estudi paramètric de la resistència d'estructures foradades sota estats complexes de càrregues.

Resumen

Debido a sus excelentes propiedades específicas muchas estructuras se fabrican con materiales casi-frágiles. Estos materiales se caracteizan por la formación de una zona de proceso de fallo relativamente grande comparada con el tamaño de la estructura. La existencia de esta zona provoca que la resistencia nominal de las estructuras depenga de su tamaño, efecto conocido como *ley de escala*. A menudo, es necesario el diseño de estucturas con agujeros, ya sea para realizar ventanas, puertas o puntos de acceso. Además, los agujeros son necesarios siempre que se quieran unir diferentes partes mediante tornillos o remaches. Por lo tanto, el estudio de la resistencia nominal y la ley de escala en estructuras casi-frágiles con agujeros es un tema de gran importancia práctica.

El dessarrollo de modelos para predecir la resistencia nominal permite diseñar estas estructuras de una manera económica ya que se reducen las costosas campañas experimentales. Las estructuras aeronáuticas y aeroespaciales contienen agujeros bajo estados multiaxiales de fuerzas que provocan la aparición de grietas que eventualmente pueden ocasionar el colapso estructural. Por lo tanto, la predicción de la resistencia nominal de estructuras con agujeros bajo estados biaxiales de carga es un tema necesario para el diseño de muchas estructuras. Las uniones atornilladas o reblonadas son típicas en muchas aplicaciones ingenieriles y su degradación puede resultar en un colapso catastrófico de la estructura. La determinación de su resistencia última es esencial para un diseño eficiente y seguro de estas uniones.

En la literatura existen varios modelos para predecir la resistencia de estructuras agujereadas y atornilladas para materiales casi-frágiles. No obstante, los modelos analíticos aventajan a los numéricos en velocidad de cálculo permitiendo agilizar enormemente el proceso de diseño.

La mayor contribución de este trabajo es la de introducir un modelo analítico

para generar cartas de diseño que permiten obtener la resistencia nominal de estructuras de materiales casi-frágiles que contengan agujeros. Los modelos de zona cohesiva (CZM) son herramientas que permiten predecir la falla a tracción de estructuras con agujeros formados de materiales casi-frágiles con una gran zona de proceso de falla confinada en un plano. Los modelos de zona cohesiva también son capaces de predecir el efecto del tamaño de la estructura en la resistencia nominal. Además, es uno de los pocos modelos (o el único) que permite tener en cuenta la ley cohesiva del material de una manera explícita. Por estas razones, la mayoria de resultados presentados se basan en los modelos de zona cohesiva.

El objetivo global de esta tesis se obtiene a partir de la consecución de tres trabajos. El primero se centra en la definición de un modelo analítico capaz de predecir la resistencia nominal de estructuras agujereadas bajo estados biaxiales de cargas para materiales casi-frágiles e isótropos. El modelo considera la ley cohesiva del material y se estudian diversas funciones entre las tensiones transferidas y la apertura de la grieta. Los resultados obtenidos se comparan con otros métodos de diseño, esos basados en las teorías de las distancias críticas.

El segundo objetivo de la presente tesis es la definición de un modelo analítico capaz de predecir la resistencia nominal de estructuras atornilladas formadas por un sólo tornillo de materiales casi-frágiles e isótropos. El modelo se formula considerando la ley cohesiva del material. El modelo considera; la forma de la ley cohesiva, la distribución de tensiones bajo el tornillo, el diámetro del agujero y el ancho de la probeta. La mayoría de uniones atornilladas constan de más de una hilera de tornillos. El último objetivo de la tesis se centra en extender el modelo a uniones de más de una hilera donde sólo parte de la carga es transferida a un tornillo.

Los resultados obtenidos se comparan con evidencias experimentales obtenidas de la bibliografia mostrando una buena correlación. Algunos de los resultados presesntados son novedosos como los diagramas que muestran la apertura de la grieta (COD) en el momento de fallo. Estos gráficos son muy útiles para entender ciertas caracterísitcas de la ley cohesiva. Por ejemplo, mediante los diagramas del COD se demuestra que la primera parte de la ley cohesiva es la más importante para determinar la resistencia nominal de estructuras con agujeros. Finalmente, también se demuestra que si la ley cohesiva del material se puede determinar correctamente los

modelos presentados pueden substituir el uso de complejos modelos de daño continuo implementados en codigos de elementos finitos. Además, los resultados obtenidos permiten la definición de diagramas de diseño que permiten el estudio paramétrico de la resistencia de estructuras con agujeros bajo estados complejos de cargas.

Summary

Due to their superior specific properties many modern engineering structures such as aircraft, ships and bridges are made of quasi-brittle materials. These materials are characterized by formation of a relatively large fracture process zone before failure. The exitance of this region makes the strength of the structure depend on its size known by the *size effect*. Moreover, presence of holes in most of engineering structures is essential for different purposes. Open holes, for example, are required to act as windows, doors and access points in aeronautical structures. Furthermore, mechanically fastened joints, which require holes, are necessary for joining the different parts of these structures. As a result, studying of nominal strength and size effect of quasi-brittle structures that contain holes is a very important research topic.

One of the main purposes for an accurate strength prediction is to get a reliable design tool of a given structure. Since most of aircraft and aerospace structures contain many holes and are subject to multidirectional loading conditions, due to stress concentration, cracks will necessarily emanate from these holes before failure. Therefore, the nominal strength prediction of open hole specimens under biaxial loading conditions is very necessary for the safe design of these structures. Also, since bolted/pinned joints are common elements in many engineering structures and their failure can lead to catastrophic failure of these structures, their strength prediction is essential for an accurate design of the joints and, consequently, for the reliable design of the structure.

There are several models available in the literature that enable strength prediction of Open Hole (OH) and bolt-loaded quasi-brittle structures. However, it is well known that the analytical models have the privilege over the other models for their ability to predict the behavior of a structure in a few minutes. Consequently, they provide fast design tools for predicting nominal strength of a given structure.

Based on the above, the main contribution of this work is to introduce analytical models able to create simple design charts that would allow designers to quickly determine the strength of quasi-brittle structures containing circular holes. Cohesive Zone Models (CZM) are an excellent tool to model quasi-brittle structures with holes in which a large failure process zone is confined in a plane. Also, the CZM is able to predict the effect of the structure size on its strength. Moreover, it is one of the few models (or the only model) that takes into account the material cohesive law explicitly. Therefore, most of the presented models in this work are based on the CZM.

The global objective of this thesis is expected to be achieved through three partial objectives. The first objective is focused on development of an analytical model able to predict nominal strength and failure envelope of isotropic quasi-brittle OH specimens under biaxial loading conditions. In this model, the nominal strength is analyzed taking into account the hole radius and the biaxiality load ratio. The model is formulated based on the CZM considering various shapes of the cohesive law. Other approaches implementing the different methods of the critical distance theories are also presented and compared with the results of the cohesive crack model.

The second objective of this thesis is to introduce an analytical model to predict the net-tension strength of single-fastener double-lap joints in isotropic quasi-brittle structures. The model is formulated based on the CZM. The effect of the material cohesive law, the contact stress distribution due to presence of the bolt, the specimen size and the hole radius to joint width ratio on the strength of the joint are considered in this model. As the majority of bolted joints in engineering structures are multi-bolt joints, the last objective of this thesis is to extend the previous model to handle the multi-fastener double-lap joints.

The obtained results are compared with the available experimental data with good agreement. Some of these results are new such as plots of the Crack Opening Displacement (COD) at failure. These plots are very useful in understanding some characteristics of the cohesive law. For instance, the importance of the initial part of the cohesive law in computing the strength of isotropic quasi-brittle structures with holes is confirmed with the COD charts. Also, the slope of the first part of the cohesive law can be obtained with the presented results of the strength. Finally, if

the material cohesive law is completely determined by some experimental procedure, the introduced models can be considered as a reliable alternative to the use of complex continuum damage models implemented in finite element models. Further, the obtained results are suited for fast definition of simple design charts and for effective parametric studies of open hole specimens and mechanically fastened joints in isotropic quasi-brittle structures.

Chapter 1

Introduction

1.1 Overview

Quasi-brittle materials, such as laminated composites, possess superior specific properties with respect to traditional engineering materials. High specific stiffness, high specific strength and low weight as well as fatigue resistance are examples of the excellent properties offered by these materials compared with traditional ones. For this reason, modern engineering structures such as aircraft, ships, bridges and also medical structures like dental implants are often made of quasi-brittle materials.

Many of these structures requires open holes or cut-outs to act as windows, doors and as access points. Moreover, most of them are manufactured, initially, from several parts. These parts must be joined together to produce the whole structure. Welding, adhesion and mechanical fastening are the most common ways for this purpose. In many situations there is a need to disassemble and assemble some of these parts for shipping, inspection, repair and replacement if it is necessary. Bolted joints are the best option in this case. As as a result, the presence of open holes and loaded holes, for mechanically fastened joints, is essential for structures that are made of quasi-brittle materials.

Usually, loading conditions in the aforementioned structures are complex. For instance Open Hole (OH) specimens under biaxial loading conditions and bolted joints under combined bearing-bypass loading are a sample of problems to be studied in these structures. Presence of stress concentrators significantly reduce the load-carrying capacity of a structure due to associated high stresses. Therefore, accurate

and reliable models for analyzing failure behavior are very necessary for the safe design of these structures.

1.2 Motivation and Objectives

As shown in the previous section, there is insisting demands to reliable and fast design tools of quasi-brittle structures. An accurate strength prediction is one of the most important demands to get safe and reliable design tools of a given structure.

There are several models available in the literature that enable strength prediction of OH and bolt-loaded quasi-brittle structures. Finite element based models are accurate and can handel complex geometries. However, they are computationally expensive and very time consuming which makes them not suitable for the industry where the results must be obtained quickly. Experimental work is reliable but it is also very expensive and time consuming. On the other hand, it is well known that the analytical models have the privilege over the other models for their ability to predict the behavior of a structure in a few minutes. Consequently, they provide fast design tools for predicting nominal strength of a given structure.

Based on the above, the global objective of this thesis is to create simple design charts that would allow designers to quickly determine the strength of quasi-brittle structures containing circular OHs or loaded holes due to presence of mechanically fastened joints. These charts are obtained by means of analytical models. This global objective is expected to be achieved through three partial objectives.

The first objective is concerned with introducing analytical models for strength prediction of OH specimens under biaxial loading conditions. The main model is based on the Cohesive Zone Model (CZM). In this model the effect of the shape of the cohesive law on strength computation is studied. Other models based on different methods of the Critical Distance Theories (CDTs) are also introduced and compared with the first one. In all models, the effect of the hole size and the biaxiality load ratio on the nominal strength is investigated.

The second objective is to develop an analytical model able to predict the net-tension strength of single-fastener double-lap joints that are made of quasi-brittle materials. The developed model is based on the CZM. The effects of the material cohesive law, the contact stress distribution due to presence of the bolt, the joint size

and the hole radius to joint width ratio on the strength of the joint are considered in this model.

The majority of mechanically fastened joints in aerospace and many other engineering structures are multi-fastener joints. Therefore, the last objective of the present work is to extend the analytical CZM model to deal with this kind of joints. The effect of the bypass stresses on the joint net-tension strength is studied in this model. To calculate the bypass to the bearing load ratio in the joint, a simple analytical spring-based model is developed. The global model is able to predict the optimum geometry of the joints and, consequently, its maximum nominal strength.

1.3 Thesis Outline

According to the objectives of this thesis, its content is divided as follows:

Chapter 2 reviews the previous research relevant to this study. First, quasi-brittle materials and some of their applications are given. Next, the effect of the structure size on its strength is introduced. Then, different methods that are used in strength prediction of quasi-brittle structures containing holes are discussed.

Chapter 3 presents a general mathematical formulation for the problem of strength prediction and size effect of quasi-brittle structures with open or loaded holes. The formulation is based on the CZM. Thus, this chapter starts with an overview of the cohesive models and cohesive laws followed by the numerical formulation of the problem.

Chapter 4 is concerned with the nominal strength of quasi-brittle OH specimens under biaxial loading conditions. A brief introduction is first presented. Formulations based on the CZM and the different methods of the CDTs are presented in this chapter. Predictions obtained from all formulations are compared against each other and against the available experimental data. Also, the obtained results based on the size effect law are adjusted to match those obtained by the CZM formulation and the experimental data to estimate the parameters of the size effect law.

Net-tension strength of mechanically fastened joints made of quasi-brittle materials is presented in Chapter 5. To avoid the effect of secondary bending, only double-lap joints are considered in this work. Further, for simplicity, formulation of a single-fastener joints is presented in this chapter. The formulation is based on the

CZM taking into account the shape of the material cohesive law.

In Chapter 6, the model presented in Chapter 5 is extended to handle multi-fastener double-lap joints. A simple spring-based model is developed to analyze load distribution between the joint fasteners. The obtained plots provide a graphical optimization procedure for determining the optimum geometry of the joint and, as a consequence, its maximum net-tension strength.

Finally, conclusions and some related ideas for future work are presented in Chapter 7.

Chapter 2

Literature Review

2.1 Quasi-brittle Materials

When considering failure it is observed that many engineering materials are not perfectly brittle, but display some ductility and softening after reaching the strength limit. In these materials a nonlinear zone forms around the existing stress risers, such as cracks, inherent flaws, notches or holes, before collapse. This zone is known as Fracture Process Zone (FPZ). It includes two regions: The first one describes extrinsic dissipation mechanisms which are characterized by progressive softening or decrease of stress with increasing deformation, whereas the second region considers intrinsic dissipation mechanisms such as hardening plasticity or perfect plasticity.

In brittle materials, like glass, brittle ceramics and brittle metals, the size of the FPZ is negligible compared to the structure size and the entire fracture process takes place almost at one point ahead of the crack tip. In this case the whole body behaves elastically until rupture, and failure is abrupt. Linear Elastic Fracture Mechanics (LEFM) can be used to analyze the behavior of these materials. On the other hand, for ductile materials, such as ductile metals, the non-softening region forms most of the FPZ and the size of the FPZ is small but not negligible. The behavior of this kind of materials is treated by elasto-plastic fracture mechanics.

In between the two previous situations, there is a set of heterogeneous materials characterized by the presence of relatively large FPZ compared to the other structure dimensions before complete failure. These materials have negligible intrinsic dissipation mechanisms, while the major part of the FPZ undergoes progressive damage

with material softening due to microcracking, voids formation, interface breakage, and other similar phenomena. Moreover, failure of these materials is transitional from elastic to plastic failure according to the size of the FPZ (ℓ_{FPZ}) which, in turn, depends on the size of the structure. This phenomenon is known as the *size effect* on the strength and it will be discussed in the following section. These materials are called *quasi-brittle materials* and they are characterized by linear response up to failure. Fiber composites, nanocomposites, tough ceramics, concrete, modern tough alloys, dental cements, bones and rocks [1] are examples of quasi-brittle materials. Figure 2.1 shows the FPZ of laminated and particulate composites.

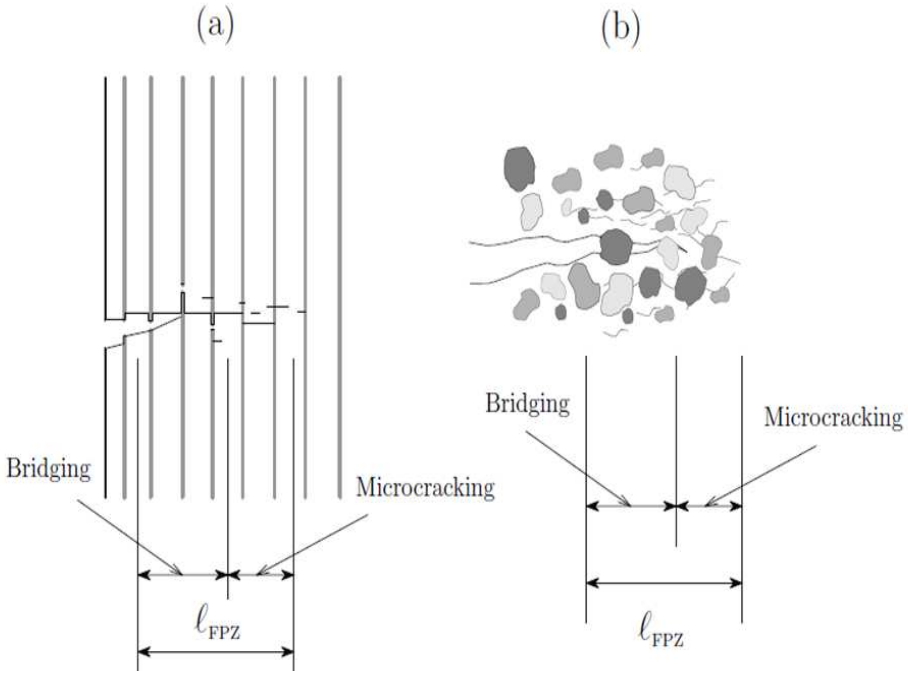

Figure 2.1: Fracture process zone in composite laminates (a) and in particulate composites (b).

2.2 Size Effect on the Strength

Stress analysis shows that failure of structures that are made of ideally brittle or perfectly plastic materials is material size independent [2]. In contrast, the formation of relatively large FPZ, which leads to a stable crack growth, prior to the attaintment

of the peak load in structures that are made of quasi-brittle materials is the reason for the size effect on their strength [1]. This can be explained by the existence of the FPZ which redistributes the stress concentration and thus delays the final failure. The dependency of strength on the size is known as the Size Effect Law (SEL). It states that, for geometrically similar structures, the nominal strength decreases with increasing the size of the specimen.

Due to the size effect it is expected that large structures can give much lower notched strengths than small test specimens. Therefore, a proper understanding of scaling effect -specimen size effect- is essential for safe and efficient use of these structures.

One of the most important parameters of scaling effects on the strength of structures with open holes is the hole size [3]. When dealing with failure prediction of OH specimens two extreme situations can be expected: brittle or ductile failure [1]. For specimens with small holes the FPZ almost occupy the whole size of the specimen and there is no stress concentration which means that the stress field throughout the specimen is almost constant. With increasing the external applied load this stress field approaches the material unnotched strength and the specimens fail according to the plastic limit. Therefore, specimens with small holes are notch insensitive and their failure is ductile. On the other extreme, in case of specimens with large holes, the relative size of the FPZ is negligible with respect to the specimen size and brittle failure is expected. For brittle failure the nominal strength depends on the elastic limit according to the stress concentration factor. As a result, brittle failure is notch sensitive. In between these extremes, quasi-brittle failure exists.

The nominal strength (σ_{Nf}) and expected failures of the OH specimens, under uniaxial tensile load, are described in Figure 2.2. In this figure $2W$ and R are respectively the specimen width and the hole radius, while $\bar{\sigma}_{Nf} = \sigma_{Nf}/\sigma_u$ is the normalized nominal strength with respect to the material ultimate tensile strength (σ_u).

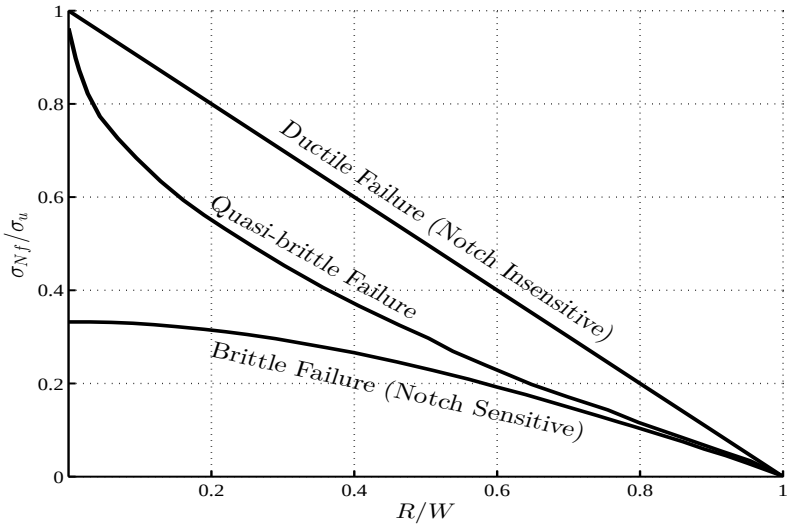

Figure 2.2: Notch sensitivity.

The SEL defines the transition from ductile to brittle failure with increasing the specimen size in quasi-brittle structures. It is defined by asymptotically matching the extreme responses of geometrically similar structures of different sizes [4–10]. It is initially developed for cracked structures and quickly expanded to specimens without stress singularities. Based on this law, the nominal strength is expressed as [11, 12]:

$$\sigma_{Nf} = f_t^{\infty} \left(1 + \frac{R_N}{R + \ell_{\text{SEL}}}\right)^{1/r} \tag{2.1}$$

where R is the characteristic size of the structure (hole radius in case of OH specimens), f_t^{∞} is the nominal strength for very large structure, R_N is a characteristic length related to the size of the FPZ, while ℓ_{SEL} and r are two adjusting parameters that bound the strength for very small specimens and control the slope of the transition from ductile to brittle response, respectively. If the nominal strength is defined as the mean stress at failure plane just before failure, the following relations are defined: $f_t^{\infty} = \sigma_u / K_t$ and $R_N = (K_t^r - 1)\ell_{\text{SEL}}$. Therefore, Equation (2.1) can be written in normalized form as [12]:

$$\bar{\sigma}_{Nf} = \left(\frac{K_t^{-r} + \bar{\ell}_{\text{SEL}}}{1 + \bar{\ell}_{\text{SEL}}}\right)^{1/r} \tag{2.2}$$

where $\bar{\ell}_{\text{SEL}} = \ell_{\text{SEL}}/R$ is related to the normalized length of the FPZ according to

the SEL. For cracked structures ($K_t \to \infty$) of large size, Equation (2.2) must agree with the LEFM law. Therefore, $r = 2$ and $\ell_{\text{SEL}} = \ell_M/(\pi F^2)$ when $R \to \infty$, where F is a geometrical parameter. It must be pointed out that ℓ_{SEL} depends on both of the specimen geometry through the parameter F and on the material through the material characteristic length (ℓ_M) which will be defined later. For OH specimens it is possible to fit the parameters of the SEL in Equation (2.2), ℓ_{SEL} and r, to the experimental results of geometrically similar specimens of different sizes. Figure 2.3 shows the predicted nominal strength using the SEL for OH specimens under uniaxial loading conditions, where $\bar{\ell}_M = \ell_M/R$. In this figure, $K_t = 3$ for a hole in an infinite isotropic plate and $\bar{\ell}_{\text{SEL}} = \bar{\ell}_M/\pi$ are used.

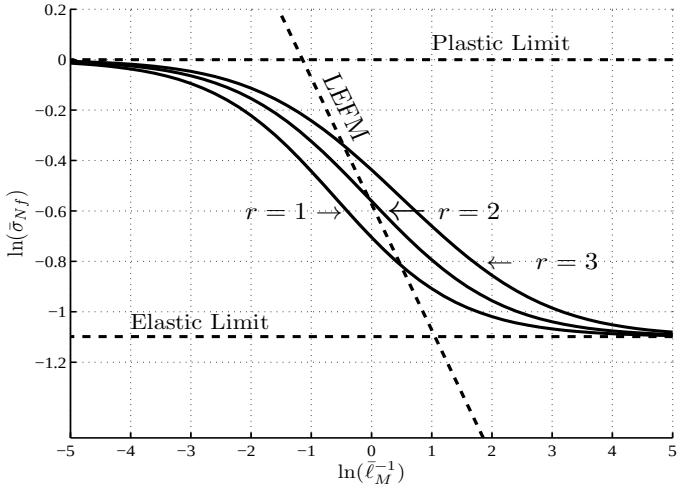

Figure 2.3: Nominal strength according to the SEL for OH specimens under uniaxial loading .

The effect of scaling on the OH tensile strength of quasi-isotropic composite laminates has been investigated by some researches [13–15]. In their study the ply and the laminate thicknesses as well as the hole diameter were investigated as the independent variables, whilst the ratios of hole diameter to the width and to the length were kept constant. They found that failure of specimens with single 0.125 mm thickness plies, no clustering, was brittle with the normal hole size effect. On contrary, specimens of the same overall thickness with four plies blocked together failed by delamination, with a trend of increasing strength with hole size (opposite to the usual hole size effect). This new finding was attributed to the formation

of delaminations at the edge of the hole. An intermediate response was found for specimens with 0.25 mm thick ply blocks where failure of small specimens was by delamination while large ones failed by fiber fracture. Finally, they concluded that the delamination plays an important role in the tensile strength and failure mechanisms of OH specimens. Also, the conventional hole size corrections may not always be applicable.

Other researchers [3, 16] studied the size effect on the OH compressive strength of quasi-isotropic laminates. They examined the effect of the hole size, stacking sequence and ply blocking on the compressive strength. Two generic quasi-isotropic stacking sequences were used in their investigations. The first one was fabricated with blocked plies $[45_n/90_n/-45_n/0_n]_s$ and the other with distributed layers $[45/90/-45/0]_{ns}$ with $n = 2$, 4 and 8 to control the total thickness of the laminate. Unlike the situation of the tensile strength, the hole size effect on the OH compressive strength has appeared in both of laminates with blocked and distributed plies. However, the laminate with blocked plies was less notch sensitive. Also, they concluded that the thickness effect on the compressive notched strength is negligible.

Camanho et al. [17] examined the size effect on the notched tensile strength of quasi-isotropic CFRP laminates with open holes experimentally as well as by means of a continuum damage model. The tested specimens were with stacking sequence of $[90/0/\pm 45]_{3s}$.

The size effect on the strength of composite laminates with central holes loaded in tension and compression has been investigated experimentally and analytically by Erçin et al. [18]. They compared the the size effect on the tensile and compressive strengths of these laminates. Two lay-ups were used in their experimental work namely $[90/0/\pm 45]_{3s}$ (laminate 1) and $[90_2/0_2/45_2/-45_2/90/0/45/-45]_s$ (laminate 2). All the tested specimens showed strength decreasing with respect to the hole size when the hole diameter to the specimen width ratio is kept constant for both tensile and compression loading.

2.3 Strength Prediction of Holed Structures

Behavior of quasi-brittle materials with stress concentrations due to presence of holes is of great importance in their design. This is because of the resulting strength reduction due to damage growth around these stress concentrators. It has been found that the crack initiation and propagation in OH and bolted joint problems are similar in tensile and net-tension failures, respectively [19]. This enables using the same approaches for strength determination in both of them.

Failure behaviour of quasi-brittle structures has been studied by several researches. Some of them investigated this behaviour experimentally. Others developed, numerical, semi-analytical and analytical models for predicting the notched strength of these structures. Most of the available semi-analytical models were based on the CDTs methods. These models and their drawbacks will be reviewed briefly in the next section. After that some experimental and numerical studies that have been conducted for strength prediction and notch sensitivity analysis of holed quasi-brittle structures are reviewed.

Models that are based on the CZM dealt with the drawbacks of the CDTs models. These models seem to be relevant for tensile and net-tension failure of OH and bolted joint problems especially in materials that satisfy the model hypothesis such as woven fabric and thin-ply laminates. Therefore, there is great attention to use the CZM approach in the present work, and hence the next chapter has been allocated to display these models.

2.3.1 Critical Distance Theories

It has been found that a parameter called characteristic length is a useful concept in failure analysis of quasi-brittle structures containing stress concentrations. This parameter, related to the size of the FPZ, controls the plastic to elastic transition of the structural strength and is determined experimentally [12]. Methods that assume that failure of quasi-brittle materials is affected by stress or energy flux acting on this characteristic length are called the Critical Distance Theories (CDTs) and they are widely used by the scientific community [20].

The CDTs have the common feature of combining a linear elastic analysis with a characteristic length. They are also called two-parameter models. This is because

of their ability to predict the notched strength by means of the material unnotched strength and the characteristic length. Due to the easiness of the elastic stress field computation by means of the finite element method and good agreement with the experimental data, these techniques are attractive for quick structural design. Recently, Taylor [21, 22] published a book and a review article dedicated to the CDTs to show their relevance and widespread usage. Lately, a comprehensive review to theses methods was presented in [12]. CDTs can generally be classified into three groups: (1) Stress based models, (2) fracture mechanics based models and (3) combined stress-fracture mechanics based models.

2.3.1.1 Stress Based Methods

Whitney and Nuismer [23] proposed two failure criteria to account for the hole size effect in strength prediction of composites under uniaxial loading. These models are based on the normal stress distribution (σ_y) adjacent to the edge of the notch and are called the Point Stress Method (PSM) and Average Stress Method (ASM). PSM postulates that the failure will occurs when the stress σ_y at some fixed distance $d_0 \equiv \ell_{\text{PSM}}$ from the hole boundary reaches the material unnotched strength σ_u. Similarly, ASM assumes that failure takes place when the average stress value of σ_y over a characteristic length $a_0 \equiv \ell_{\text{ASM}}$ ahead of the notch becomes equals σ_u. Both methods are explained graphically in Figure 2.4. Mathematically, the nominal strength based on the PSM and the ASM are expressed as:

$$\sigma_{Nf}^{\text{PSM}} = \sigma_y(x,0)|_{x=R+\ell_{\text{PSM}}} = \sigma_u \tag{2.3}$$

$$\sigma_{Nf}^{\text{ASM}} = \frac{1}{\ell_{\text{ASM}}} \int_0^{x=R+\ell_{\text{ASM}}} \sigma_y(x,0)\, dx = \sigma_u \tag{2.4}$$

where σ_{Nf}^{PSM}, σ_{Nf}^{ASM}, $d_0 \equiv \ell_{\text{PSM}}$ and $a_0 \equiv \ell_{\text{ASM}}$ are the nominal strengths and the characteristic lengths according to PSM and ASM, respectively.

PSM and ASM are applied by Tan [24, 25] for the strength prediction of fiber-reinforced composite laminates containing an elliptical opening. His results showed that theses methods have good correlation with the experimental data.

Camanho and Lambert [26] proposed a methodology based on the PSM and the ASM to predict the final failure and failure mode of OH composite laminates under

biaxial loading condition. Also, they applied their methodology to quasi-isotropic double-shear mechanically fastened joints. The stress distribution in this model was obtained numerically. The obtained results in their study were in good agreement with the experimental ones.

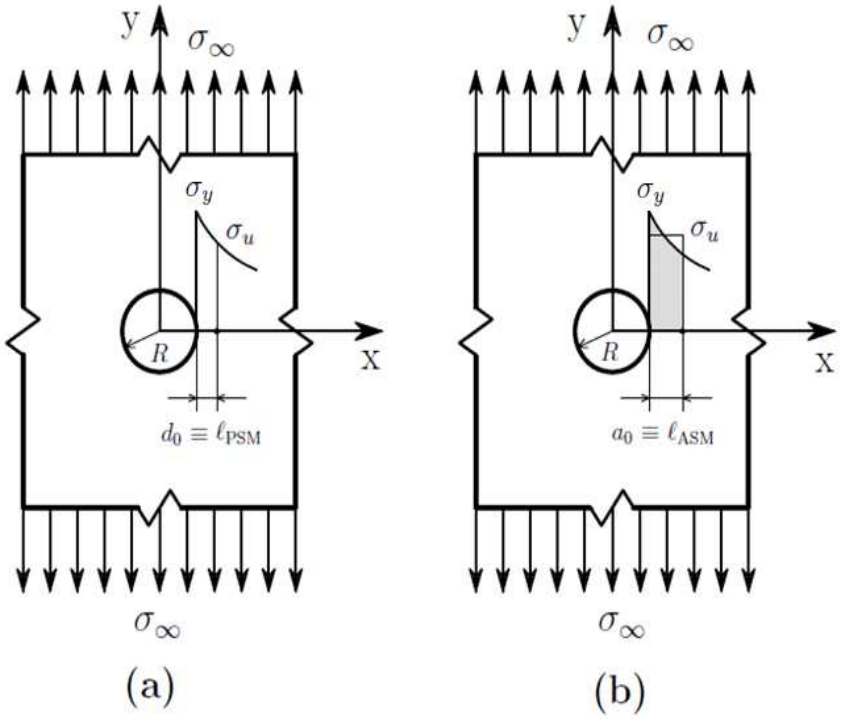

Figure 2.4: (a) Point stress method and (b) average stress method.

The damage growth and fracture at an open circular holes in quasi-isotropic woven glass fabric laminates, loaded in tension, has been studied by Belmonte et al. [27]. They concluded that the notched strength data can be adequately described by the PSM and ASM with the ASM being better than the PSM.

Some researchers [28–32] proposed a modification to the traditional PSM for predicting the notched strength of woven fabric composites. They introduced the characteristic length as a function of the specimen geometry. All of them concluded that the modified PSM predictions were better than those obtained by the traditional PSM and they are in good agreement with the experimental data.

Hwan et al. [33] proposed a similar modification to both of the PSM and ASM for strength prediction of braided composite plates with a central hole. They found

that both modified PSM and modified ASM gave better predictions of the nominal strength than traditional PSM and ASM for all kinds of braided composite plates.

The stress based models are also used for predicting the failure strength and the failure mode of mechanically fasted joints of quasi-brittle structures. Agarwal [34] used ASM to predict the failure strength and failure mode of double-shear single fastener composite joints. In his model the stress distribution around a fastener hole was calculated by means of a finite element analysis.

Whitworth et al. [35, 36] evaluated the bearing strength of pin-loaded composite joints by a model based on the PSM. In their study two-dimensional finite element analysis is used to calculate the stress profile around the fastener hole. They observed good agreement with experimental data of graphite/epoxy laminates when the bearing strength is computed as a function of edge distance to hole diameter. Whereas, when it is calculated as a function of plate width to hole diameter, conservative results were obtained.

2.3.1.2 Fracture Mechanics Based Methods

Fracture mechanics-based methods are based on linear elastic fracture mechanics. These methods assume the existence of a flaw of some characteristic length ahead of the notch and predict the nominal strength by the elastic solution. The Stress Intensity Factor (SIF) of a crack starting in a notch is expressed as:

$$K = \sigma_N \sqrt{\pi a}\, F(a) \tag{2.5}$$

where F is a shape factor that depends on the crack length (a), the material, the geometry and the loading conditions. F can be obtained from a finite element analysis. For OH specimens under uniaxial loading, the factor F is given as [37]:

$$F(a) = 1 + 0.358s + 1.425s^2 - 1.578s^3 + 2.156s^4 \quad \text{where} \quad s = \frac{R}{R+a} \tag{2.6}$$

An analytical solution obtained by Newman [37] can be used to derive the shape factor F for an isotropic plate with a cracked hole under biaxial loading and given as [38]:

$$\begin{aligned} F(a,\lambda) = (1-\lambda)(1 + 0.358s + 1.425s^2 - 1.578s^3 + 2.156s^4) \\ + \lambda(1 + 0.4577s + 0.7518s^2 - 0.8175s^3 + 0.8429s^4) \end{aligned} \tag{2.7}$$

where λ is the biaxiality load ratio.

The fracture mechanics-based methods include two models, namely the Inherent Flaw Model (IFM) and the Finite Fracture Mechanics (FFM). The IFM was developed initially by Waddoups et al. [39] for static failure of composite materials. This model predicts failure by assuming a flaw of size ℓ_{IFM} and applying linear elastic fracture mechanics. At failure the flaw size and the stress intensity factor reach their critical values, $a = \ell_{\text{IFM}}$ and $K = K_C$, and the nominal stress equals the notched strength, $\sigma_N = \sigma_{Nf}$. Accordingly, the σ_{Nf} can be given as:

$$K_C = \sqrt{EG_C} = \sigma_{Nf}\sqrt{\pi\ell_{\text{IFM}}}\, F(\ell_{\text{IFM}}) \;\text{ thus }\; \sigma_{Nf} = \sqrt{\frac{EG_C}{\pi\ell_{\text{IFM}}}}\, F^{-1}(\ell_{\text{IFM}}) \tag{2.8}$$

where K_C, E and G_C are critical stress intensity factor, the material Young's modulus and the critical fracture energy, respectively.

The FFM was proposed by Taylor et al. [40]. It considers the mean energy release rate of a crack growth with a characteristic length ℓ_{FFM} as the driving force. Based on the FFM the required energetic condition for failure onset can be stated as:

$$\frac{1}{\ell_{\text{FFM}}}\int_{a=0}^{\ell_{\text{FFM}}} G(a)\, da = G_C \tag{2.9}$$

Taking into account Irwin's relation $G = K^2/E$ and the form of the SIF in Equation (2.5), Equation (2.9) can be written as:

$$\frac{\pi\sigma_N^2}{E\ell_{\text{FFM}}}\int_{a=0}^{\ell_{\text{FFM}}} aF^2(a)\, da = G_C \tag{2.10}$$

At failure $\sigma_N = \sigma_{Nf}$ and therefore,

$$\sigma_{Nf} = \sqrt{\frac{EG_C\ell_{\text{FFM}}}{\pi\int_{a=0}^{\ell_{\text{FFM}}} aF^2(a)\, da}} \tag{2.11}$$

Both of IFM and FFM are explained graphically in Figure 2.5

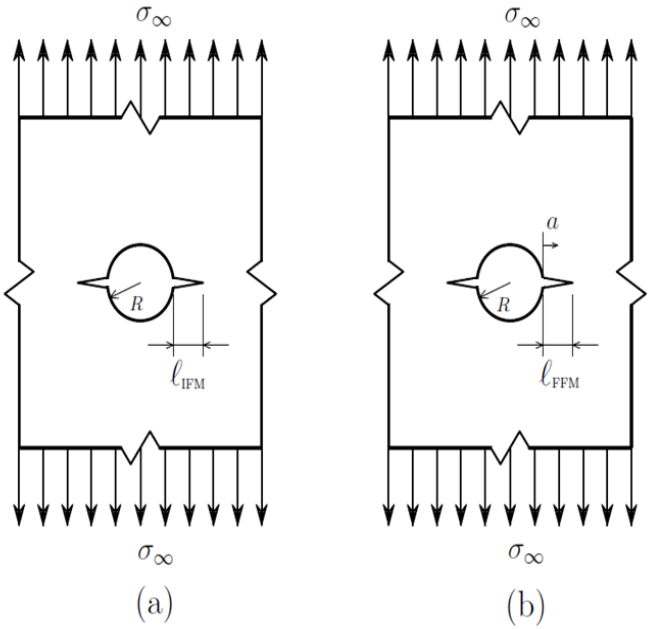

Figure 2.5: (a) Inherent flaw model and (b) Finite fracture mechanics.

Curtis and Grant [41] analyzed the failure of carbon fiber composite plates with unloaded and loaded holes by means of the ASM and the IFM. They found that the ASM gives better estimates of the failure strength for a wide range of loading conditions and failure modes. Schulz [42] predicted the net-tension strength of pin-loaded single-fastener laminated composite joints by using the IFM.

Irrespective of their advantages, the CDTs have some drawbacks. First, they assume that the characteristic length ideally depends on material parameters and not on the shape and size of the specimen despite it has been confirmed that it is a size and geometry dependent [12]. Second, they require experimentally determined parameters for each material, geometry and size which is an additional cost in time and money. Also, these approaches neglect the physical state of damage and the softening occurring, in most of quasi-brittle materials, prior to the ultimate failure.

2.3.1.3 Combined Methods

Almost all the previous methods rely on curve fitting of test data to determine the characteristic length and this is very expensive. Therefore, methods that are able to self-produce this parameter are promised. These methods are called combined

stress-fracture mechanics-based methods. The main assumption in these methods is that both of stress and energetic failure criteria are satisfied simultaneously just before failure. This can be achieved by considering the characteristic length as variable. Thus, equating the nominal strength defined by stress and fractures mechanics-based methods results in an equation in terms of this characteristic length. Solving it gives the characteristic length required for the same nominal strength based on both of the two criteria. One of great advantages of these methods is that the characteristic length as well as the nominal strength are defined solely by the material characteristic length $\ell_{\mathrm{M}} = EG_c/\sigma_u^2$.

Leguillon and Leguillon et al. [43, 44] coupled the PSM with the FFM for strength prediction of quasi-brittle materials. They compared their results with experiments in various domains: polymers, ceramics and rocks. Good agreement was found between their results and experimental data particularly in the case of holed specimens in tension and compression.

Belmonte et al.[27, 45] combined the ASM for damage growth with IFM for catastrophic failure at circular holes in quasi-isotropic GFRP and CFRP woven fabric laminates loaded in tension. Agreement between their theoretical results and experimental data has been demonstrated for three thicknesses of two woven types of quasi-isotropic CFRP based laminates. Also, their results showed that the proposed approach is applicable to a wide range of woven fabric CFRP laminates.

In Berbinau et al. [38], the failure of the repaired impact damaged laminate has been investigated. In their work the damaged area has been drilled and then the hole was plugged with a perfect-fit core made of a dissimilar material. They analyzed the laminate with the filled hole under biaxial tension-compression loading. They used the complex variable mapping method to determine the stress profile in the laminate. In this work the failure was predicted by coupling ASM with IFM.

Cornetti et al. [20] proposed a general model based on coupled ASM and FFM. The strength of three point bending tests of various relative crack depths and different sizes is predicted using the prosed model. Camanho et al. [46] used a coupled ASM-FFM model to predict the OH strength of composite laminates. Their results were compared with the experimental data obtained in quasi-isotropic carbon-epoxy laminates with good agreement.

Other combinations between the stress-based and the fracture mechanics-based

models -such as PSM-IFM, PSM-FFM, ASM-IFM and ASM-FFM- has been performed by Maimí et al. [12] for tensile strength prediction of cracked and OH specimens under uniaxial loading.

Catalanotti and Camanho [47] introduced a semi-analytical model for the prediction of the net-tension strength of mechanically fastened joints. Their model is based on the coupled ASM-FFM approaches. The stress distribution around the fastener hole and the stress intensity factor for the joint with two cracks emanating from the hole edge were calculated by means of the finite element method.

2.3.2 Experimental and Numerical Techniques

The previously discussed models for failure prediction of quasi-brittle structures can be classified as semi-analytical models. In addition to theses models, there are a lot of experimental and numerical studies which have been conducted for strength prediction and notch sensitivity analysis of holed quasi-brittle structures. In this section some of theses investigations are briefly reviewed.

O'Higgins et al. [48] compared between the tensile strength of high strength GFRP and CFRP OH specimens through an experimental study. They found that the OH CFRP specimens were stronger, while the OH GFRP specimens had greater ultimate strain. They found the higher levels of damage formation prior to failure that occurred in the OH CFRP specimens was the reason for their higher strength. Also, they found that the blocked-ply stacking sequences give higher damage levels and higher OH tensile strength than sub-laminate level stacking sequences.

Arteiro et al. [49] investigated the mechanical response of thin non-crimp fabric composites experimentally. They performed tensile and compressive tests in both notched and unnotched specimens. The notched tests included specimens with central cracks and with circular open holes loaded in tension and compression. They observed a size effect on the strength for both OH tension and compression tests. Also, they found an improved response to bolt-bearing loads for non-crimp fabrics over traditional composite materials.

The tension and compression strength of quasi-isotropic laminates with holes have been investigated by Wang et al. [50] by mean of experimental and numerical procedures. They conducted linear elastic and progressive damage approaches in their numerical analyses by using ABAQUS software package. They demonstrated

that the progressive damage approach was more accurate in un-notched and notched strength predictions.

O'Higgins et al. [51] performed an experimental and numerical study for tensile strength prediction of carbon/epoxy open-hole specimens. Their numerical model was based on a progressive damage analysis. The Hashin failure criteria have been chosen in their analysis. Also, the effects of shear nonlinearity have been taken into account in their model.

By using a mixed 2D/3D finite element model, Morais [52] predicted the open-hole tensile strength of quasi-isotropic $[0/\pm 45/90]_{ns}$ laminates under uniaxial loading.

The aforementioned references consider only OH specimens under uniaxial loading conditions, while most of aircraft and aerospace structures are exposed to multidirectional loading conditions. Therefore, there was a need for some studies considering specimens under biaxial loading. Unfortunately, multi-axial strength data is scarce because of the limited number of testing equipments and facilities available for these tests and the enormous cost involved [3, 16, 53]. Nevertheless, some experimental studies have considered laminated composite OH specimens under biaxial loading [53–55].

Huang et al. [53] studied the effect of the OH presence on the strength of $\pi/4$ quasi-isotropic carbon epoxy laminates under biaxial loading via an experimental work. They proposed an optimized design of a cruciform specimen for their biaxial test. The digital image correlation technique was used to measure the strain field in the hole neighborhood.

Khamseh and Waas [54] experimentally studied failure mechanisms of composite plates containing a circular hole under compressive biaxial loading. In their investigations the hole diameter to plate width ratio was kept in a range suitable for infinite plate assumption.

The effect of hole size on the failure of graphite/epoxy laminates under biaxial tension has been investigated experimentally by Daniel [55]. Four hole sizes were used in his investigation.

On the other hand, using numerical simulation, Shah et al. [56] predicted failure envelopes of OH specimens made of two different quasi-isotropic carbon fiber-epoxy composite laminates, namely, $[45/90/-45/0]_{4s}$ and $[0 \pm 60]_{5s}$.

As for mechanically fastened joints, experimental studies have been extensively used for investigation of failure mode and failure load of several types of joints [26, 47, 57–63].

Camanho and Lambert [26] studied the failure load and failure mode of double-lap pin and bolt-loaded composite joints. In this work the material of the tested joints was $[90/0/\pm 45]_{3s}$ Hexcel IM7-8552 carbon epoxy unidirectional laminate. Catalanotti and Camanho [47] investigated the net-tension failure of double-lap bolted joints that are made of the same material of the previous work. In these studies it is found that the net-tension strength of the joint has a value between the elastic and the plastic limits.

Failure strength and failure mode of composite laminates containing one or two pin-loaded holes have been studied by Chang et al. [57]. Different ply orientations were used in their investigations. Also, the two loaded holes were either in parallel or in series.

Bearing strength and failure mode of pinned joints of carbon-epoxy composite plates have been investigated by Aktaş et al. [58]. Effect of fiber orientations, end distance to hole diameter ratio (θ_e) and the hole diameter to the joint width ratio (θ_W) have been studied. They found that the full bearing strength was developed when θ_e and θ_W^{-1} ratios are equal to or greater than 4.

Yan et al.[59] assessed the clamping effects on the net-tension strength and failure response of composite laminates with bolt-filled holes. They concluded that in case of net-tension failure, clamping improves the strength of the joint regardless of the ply orientation.

Effect of the ratios θ_W and θ_e as well as the effect of woven fiber on the bearing strength of pin-loaded woven laminated composite have been examined by Okutan et al. [60]. Their results showed that the ultimate load capacity of woven-glass-fiber reinforced epoxy laminates with pin connections grew with both θ_W^{-1} and θ_e. However, for $\theta_W < 1/3$ and for $\theta_e > 2$ the effect of theses geometrical factors on the failure strength was insignificant.

A similar study has been performed by İçten and Karakuzu [61] to investigate the effect of θ_W and θ_e on the bearing strength and failure mode of pinned-joint carbon-epoxy woven composite plates. According to their results, the maximum bearing strength was reached when $\theta_W = 1/3$ and $\theta_e = 4$ and the bearing strengths

beyond theses values are very similar. When $\theta_e = 1$, the bearing strength is small and the failure mode is net-tension or shear-out. Net-tension failure occurred when $\theta_W = 0.5$ and the failure mode transformed to shear-out or bearing mode with decreasing θ_W. Also, bearing strength had the maximum value with fiber orientation $\theta = 0\,^\circ$ and decreased with increasing the fiber orientation to reach its minimum value at $\theta = 45\,^\circ$.

The influence of geometry and material characteristics on the tensile behaviour of single-lap composite joints has been investigated by Riccio and Marciano [62]. Different bolt diameters and different interfaces, composite-to-composite and composite-to-aluminum, were considered in this study. They found that the maximum sustainable load grew with bolt diameter. Also, the joints with composite-to-composite interface have been proven to be stronger that the composite-to-aluminum ones.

Jam and Ghaziani [63] explored the behaviour and the damage caused in bolted joints in sandwich structures with laminates mad of glass fiber and foam core.

Finally, numerical techniques are frequently used for strength prediction of the bolted joints [58, 61, 63]. Even though these techniques are accurate, they are complicated and very time consuming.

2.4 Concluding Remarks

A concise overview is given of various techniques concerned with the strength prediction of OH and bolt-loaded quasi-brittle structures. Many of the available models are semi-empirical approaches such as the CDTs methods. It is observed that almost all the reviewed methods were able to predict the size effect on the strength. Regarding CDTs, it seems that the ASM and the FFM model are the most accurate approaches for strength and size effect predictions of quasi-brittle structures containing central holes. However, the main drawback in theses semi-empirical models is the not understood physical meaning of the characteristic length used in theses approaches.

Numerical techniques can simulate complicated geometries with complex loading conditions and their predictions are accurate. However, these techniques require complex continuum damage models implemented in the finite element method and, therefore, they are still complicated and very time consuming.

Experimental observations showed that the tensile failure of OH specimens and net-tension failure of bolted joints are similar and that the local damage in these failure modes occurs in self-similar fashion. This is confirmed for specimens made of different quasi-brittle material such as woven GFRP and woven CFRP. As a result, the same numerical or analytical model can be used for strength prediction of both modes.

Experimental data of the bolted joints showed that the net-tension strength of the joint had a value between the elastic and the plastic limits. Also, it is found that quasi-isotropic laminates showed maximum bearing strength of the bolted joint problems. Since failure of this kind of laminates matches with the CZM hypothesis, as will be described in the next chapter, using the cohesive zone-based model in the present work is more motivated. Further, the strength of single-lap joints is lower than that of the double-lap ones. This is due to higher stress concentrations generated by the nonsymmetric geometry and loading.

The following part of this thesis considers a mathematical formulation of the nominal strength of OH specimens and net-tension strength of double-lap joints based on the cohesive zone model.

Chapter 3

Mathematical Formulations Based on the CZM

3.1 Overview of the Cohesive Models

Many design criteria are based on limits imposed by the ultimate strength of the materials. As long as these limits are not violated, the structure is safe and the collapse is unlikely to happen. However, many structures fail despite their ultimate strength is never exceeded. This may be due to the inherent defects of the material, or the structure, or because of the defects that grow to critical dimensions. As a result, the maximum load that can support a structure must be dependant not only on the strength of the material, but also on the size of the defects that may exist in the structural element.

Linear elastic fracture mechanics [64–66] has proven to be a useful tool for solving fracture problems provided a crack-like notch or flaw exists in the body and the size of the nonlinear zone ahead of the crack tip is negligible with respect to all other dimensions. Also, the linear elastic fracture mechanics assumes that the material behaves elastically until the complete failure. Unfortunately, this is not always the case. For instance, the size of plasticity in metals or the size of the FPZ in quasi-brittle materials are lager than to be neglected in studying of fracture of these materials. Therefore, more general fracture models capable of capturing larger energy dissipation mechanisms are needed.

The cohesive zone models, CZMs, have emerged as a powerful tool for simulation

of local non-linear fracture process. CZMs were proposed based on the assumption that the material non-linearities, plasticity in metals or FPZ in quasi-brittle materials, can be described by a cohesive zone around the crack tip [67–69]. The concept of the CZM was initially proposed by Dugdale [67] and Barenblatt [68], independently, as a possible alternative to the concept of fracture mechanics in perfectly brittle materials.

Dugdale [67] developed a microscopic plasticity model for ductile materials to represent the plastic deformation at the crack tip. Dugdale assumed that the stresses at the plastic zone, which exists near the crack tip, are constant and equal the material yield strength (σ_Y). Dugdale's model is known as strip-yield model. Later Barenblatt [68], independently, developed a similar model for brittle materials. Both of the Dugdale and Barenblatt models take into account the nonlinear behaviour at the crack tip by introducing cohesive forces at the crack surface. These cohesive forces represent the material resistance to fracture during the application of remote stress (σ_∞), thereby eliminating the stress singularity at the crack tip. The difference between the two cohesive zone models is that the cohesive stresses (σ_c) in the Barenblatt's model represent the forces of molecular cohesion of the material and they vary throughout the FPZ unlike their constant value as in Dugdale's model, as shown in Figure 3.1. These models are popularly known as Dugdale-Barenblatt model and their application has been extended to various fields of fracture mechanics.

Hillerborg et al. [69] extended the Dugdale-Barenblatt model to introduce a generalized cohesive zone model for non-linear fracture problems. In Hillerborg model it was assumed that the material is linear-elastic until damage initiation. In addition, the FPZ is considered as fictitious crack that is capable of transferring closure tension between its surfaces. This crack initiates, at damage onset, when the material tensile strength σ_u is reached. At this moment, the closure stress, or the cohesive stress, at the crack tip equals σ_u. As the crack propagates, the closure stress decreases with increasing the Crack Opening Displacement (COD) and vanishes when the COD reaches its critical value w_c. The energy dissipated in the damage zone, when the complete failure is reached, corresponds to the fracture energy which is a property of the material. The relation between the closure stress σ_c and the COD (w) is known as the tension-softening law or the Cohesive Law (CL) of the material,

see Figure 3.2. The CL is generally considered to be a material property [70]. In the following section, different shapes of the CL used in the analytical models and numerical implementations for failure prediction of the quasi-brittle materials will be illustrated.

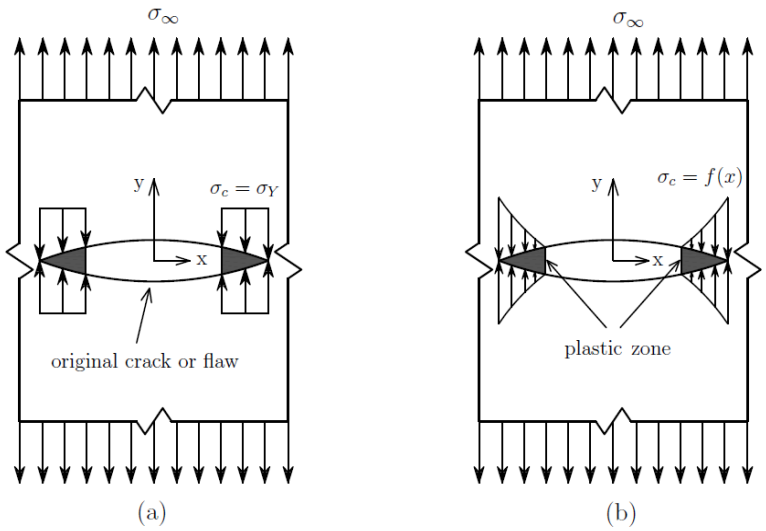

Figure 3.1: (a) Dugdale's and (b) Barenblatt's cohesive zone models.

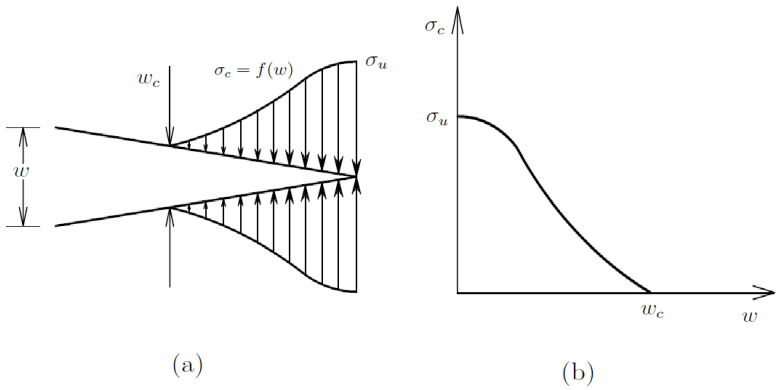

Figure 3.2: (a) Fictitious crack and (b) a general shape of the tension-softening law according to Hillerborg.

The CZMs are now widely used for studying different damage mechanisms of quasi-brittle materials. Plies delamination, friction between delaminated plies, plies

splitting, multiple matrix cracking within plies, fiber rupture or micro-buckling (kink band formation), process zones at crack tips representing crazing or other nonlinearity and large scale bridging by through-thickness reinforcement or by crack-bridging fibers are examples of these damage mechanisms [71].

Soutis et al. [72] studied the micro-buckling damage mechanism of carbon fiber-epoxy laminate containing a single hole using the CZM. In this work the damage around the open hole is represented by a cohesive crack.

Yang and Cox [71] used the CZM to represent delamination and splitting cracks in composite laminates. They presented a cohesive element for simulating three-dimensional mode-dependent process zones. In their formulation the delamination crack shape can follow its natural evolution, according to the evolving mode conditions calculated within the simulation. Fan et al. [73] developed an approach to implement the concept of the cohesive zone in FEM for simulation of delamination development in fibre composites and failure of adhesive joints. Ye and Chen [74] proposed a micro-mechanical model to simulate composites delamination via CZM-based FEM.

Maimí et al. [75] introduced an analytical model based on the CZM for nominal strength prediction of isotropic quasi-brittle structures. In their work the size of the specimen and the shape of the CL are taken into account. Also, a comparison between the obtained nominal strength of quasi-brittle structures based on the CZM and other CDTs was held by Maimí et al. [12].

On the other hand, for bolted joints, Ahmad et al. [76] developed a 3-D finite element model based on the CZM for modeling damage and fracture of double-lap bolted joints that fail by net-tension. In their work the joints were made of woven fabric composites. Hollmann [77] applied the CZM for simultaneous net-tension and shear-out failure analysis of composite laminates containing a bolt-loaded hole.

3.2 Cohesive Law

Most of quasi-brittle materials lose cohesion as the crack propagates. The material cohesive law defines the constitutive behaviour of the material at the FPZ. Results of strength predictions using cohesive models showed that the shape of the CL has a key role in crack propagation and in computing the nominal strength of the structures [12, 75, 78]. In spite of its importance there is still no fairly effective technique to determine its form. Moreover, its experimental determination is difficult. Therefore, in practice, it has been common to assume a parameterized shape for the CL to be used for the analytical models and numerical implementation.

If a meaningful modeling is desired, the choice of suitable CL for a given material is critical. Constant, linear, exponential and bilinear functions are the most common shapes of the CL, see Figure 3.3.

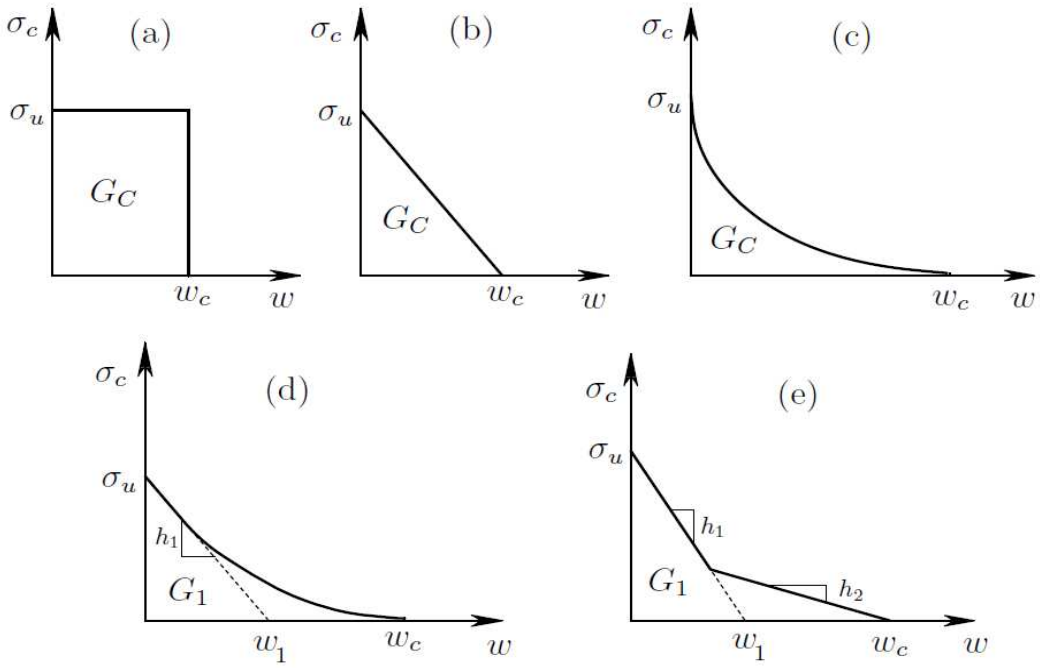

Figure 3.3: Constant (a), linear (b), exponential (c), curvilinear with initial linear part (d) and bilinear (e) shapes of the cohesive law

In Constant Cohesive Law (CCL) the cohesive stress σ_c is constant, and equals the material tensile strength σ_u, until some critical crack opening w_c. After that the

stresses drastically drop, as shown in Figure 3.3(a) where G_C is the critical fracture energy. CCL seems to be the best choice for typical yielding materials, like mild steel, [69]. It corresponds to the Dugdale model with $\sigma_u = \sigma_Y$ and the COD equals w_c at initiation of crack growth. Also, the CCL simulates the behaviour of some polymers. For the materials that exhibit some softening before failure such as some composites, the Linear Cohesive Law (LCL) shown in Figure 3.3(b) provides enough correct predictions of the structure behaviour and nominal strength. In case of CCL and LCL, only two parameters are necessary to fully define the material cohesive law. The first parameter is σ_u for the onset of softening and the second one is G_C, and theses parameters can be easily measured experimentally.

On the other hand, for materials like concrete, their softening law can be approximated by exponential function as shown Figure 3.3(c). The Exponential Cohesive Law (ECL) is defined by the same two parameters as in the CCL and LCL. However, it should be pointed out that the actual softening curve of concrete is rather curvilinear but has an initial linear part [70, 79], as shown in Figure 3.3(d). Despite this, the full curve can be approximated by a bilinear curve, as shown in Figure 3.3(e), and it has been proven that this approximation provides optimum solutions [80]. Also, the bilinear cohesive law is usually employed for composite laminates [12, 81], where the first part represents the brittle fiber failure while the second one corresponds to the fiber pull-out. The last two shapes of the CL need four parameters to be fully defined; σ_u and G_C are two of them. Other two additional parameters are needed to describe the shape (the slopes of the branches h_1 and h_2, the fracture energy G_1 which corresponds to crack opening w_1,...etc), but their measurement is not well established by the researchers.

In general, any proposed shape for the CL should have two features. The first one is that the material tensile strength is the cohesive stress at which the crack starts to open and it is given as:

$$\sigma_c(0) = \sigma_u \tag{3.1}$$

The second feature, or property, is that the area under the curve represents the total

fracture toughness G_C and it is given by:

$$G_C = \int_0^{w_c} \sigma_c(w)\, dw \tag{3.2}$$

For composite laminates there is no standard procedure to obtain G_C. However, adaptations of the compact tension test can define a value of G_C, which represents the bulk (global) laminate fracture toughness. Since this value dependent on the laminate stacking sequence, two laminates with different stacking sequence are considered two different materials with different cohesive laws.

Also, an important parameter for structural behavior is the so called material characteristic length ℓ_M. This length is considered as an inverse measure of the material embrittlement, the smaller ℓ_M the more brittleness of the material, and given by:

$$\ell_M = \frac{EG_C}{\sigma_u^2} \tag{3.3}$$

Finally, it has been widely recognized that the cohesive law is able to model the size effect on the structural strength [1, 6, 70, 79, 82]. The cohesive law can be implemented in finite element codes by means of cohesive elements [69, 83, 84] or by smearing the cohesive law in the solid element [85–88]. If the bulk response is assumed as linear and small displacements are considered, the equilibrium equations can be applied by imposing Dugdale's finite stress condition. This condition states that the stress intensity factor due to the remote stresses is in equilibrium with the stress intensity factor due to the cohesive stresses [12, 72, 75].

In the present work analytical models based on the Dugdale-Barenblatt CZM are developed to predict the nominal strength and size effect of quasi-brittle structures containing OH and pin-loaded holes. In these formulations the Dugdale's finite stress condition is imposed as will be described in the following sections.

3.3 Nominal Strength Based on the CZM

As shown in the previous chapter, many of the available models that enable strength prediction of OH and bolt-loaded holes quasi-brittle structures are semi-empirical approaches such as the CDT methods. In most of these models the material softening that occurs before fracture is neglected and this drawback can be

treated when using the CZM. Also, experimental observations showed that for tensile fracture of OH specimens and net-tension failure of bolted joints the local damage occurs in a self-similar fashion which is suitable for the the applicability of the CZM. This was confirmed for specimens that were made of different quasi-brittle material such as woven GFRP and woven CFRP [19] which are extensively used in the manufacturing of many engineering structures. This makes the adoption of the CZM throughout the present work very motivating.

3.3.1 Hypotheses

When modeling failure behaviour of quasi-brittle materials based on the CZM there are some hypotheses that should be imposed. These hypotheses can be described as follows:

1. The material is assumed to be linear elastic up to the point of cracking initiation, where softening begins and proceed continuously, and the initiation criteria is of Rankine type. This means the cracking initiates when the maximum principle stress at the critical point reaches the material tensile strength. The crack is assumed to grow normal to the principal stress direction.

2. The cohesive law is assumed to be a material property. As a consequence, the fracture energy is assumed to be constant.

3. Only extrinsic dissipation mechanisms due to damage are considered. This damage, or the FPZ, is assumed to be modeled with a localized plane where the dissipation mechanisms take place. Thus, in CZMs, the other sources of nonlinearity such as plasticity are not taken into account.

3.3.2 General Formulation for Holed Structures

As already alluded in the previous chapter, the existence of holes in most of engineering structures is very essential. These holes can be open holes and the structure is subjected to complex loading conditions such as biaxial loading. In other situations these holes are loaded holes as in the case of bolted joint connections. Therefore, in this section a general formulation based on the CZM for nominal strength prediction of isotropic quasi-brittle structures with holes is presented.

Since the linear elastic analysis is assumed to be valid, the principle of super-

position is applicable. For a specimen under generic loading condition as shown in Figure 3.4, the total solution can be obtained by the superposition of two solutions. The first one is the solution of an open hole specimen with open crack of length equal to the size of the FPZ and subjected to the total external applied loads. The second solution is the solution of the same specimen but only with cohesive stresses at the FPZ. This superposition is illustrated graphically in Figure 3.4. In this figure σ_1, σ_2 and σ_3 refer to the external loads applied outside the hole while L_b is the bearing load. Also, in the following chapters this superposition will be described in details according to the actual existing loading conditions.

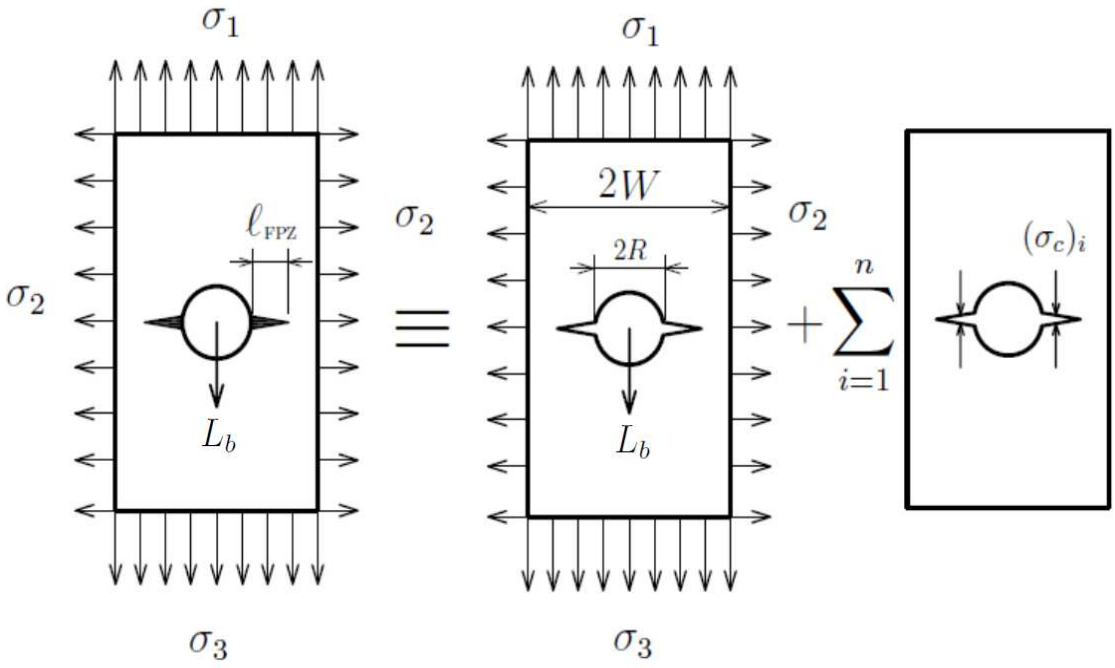

Figure 3.4: Generalized cohesive zone model.

For linear response and small displacements, the equilibrium equation can be obtained by imposing the Dugdale's finite stress condition. This condition states that since there is no singular stresses at the crack tip in the complete problem, the Stress Intensity Factor (SIF) due to the total external applied loads (K_E) must be in equilibrium with the SIF due to the cohesive stresses at the FPZ (K_{σ_c}), [67]:

$$K_E + K_{\sigma_c} = 0 \tag{3.4}$$

The cohesive stress profile at the FPZ can be approximated by the superposition of n problems with constant stress. Consequently, it is possible to define $K_{\sigma_c} = \sum_{i=1}^{n} \sigma_u(\bar{\sigma}_c)_i\sqrt{R}(\bar{K}_{\sigma_c})_i$, where $\bar{\sigma}_c = \sigma_c/\sigma_u$ is the normalized cohesive stress and $\bar{K}_{\sigma_c}(\bar{\ell}_{\mathrm{FPZ}}, \theta_W)$ is a normalized form of K_{σ_c}, while $\bar{\ell}_{\mathrm{FPZ}} = \ell_{\mathrm{FPZ}}/R$ is the normalized size of the FPZ and $\theta_W = R/W$ is a geometric parameter. Then, Equation(3.4) can be written in normalized form as [38, 75]:

$$\sigma_u\sqrt{R}\left(\bar{\sigma}_N\bar{K}_E + \sum_{i=1}^{n}(\bar{\sigma}_c)_i(\bar{K}_{\sigma_c})_i\right) = 0 \tag{3.5}$$

where $\bar{K}_E(\bar{\ell}_{\mathrm{FPZ}}, \theta_W, LP)$ is the normalized form of K_E and LP is a parameter that represents the loading condition, while $\bar{\sigma}_N = \sigma_N/\sigma_u$ is the normalized form of the nominal stress (σ_N). Therefore, the normalized nominal stress is defined by:

$$\bar{\sigma}_N = \beta_i(\bar{\sigma}_c)_i \tag{3.6}$$

where $\beta_i(\bar{\ell}_{\mathrm{FPZ}}, \theta_W, LP)$ is a vector that relates the normalized cohesive stress at position i to the normalized nominal stress.

The complete crack opening profile w can be computed by the superposition of the COD due to the total external applied loads (w_E) and the COD due to the cohesive stresses (w_{σ_c}). It can be written as:

$$w = w_E + w_{\sigma_c} = w_E + \sum_{i=1}^{n}(w_{\sigma_c})_i \tag{3.7}$$

Equation (3.7) can be written in a normalized form as [75, 89]:

$$w = \frac{R\sigma_u}{E}\left(\bar{\sigma}_N\bar{w}_E + \sum_{i=1}^{n}(\bar{\sigma}_c)_i(\bar{w}_{\sigma_c})_i\right) \tag{3.8}$$

where $\bar{w}_E(\bar{\ell}_{\mathrm{FPZ}}, \theta_W, LP)$ and $\bar{w}_{\sigma_c}(\bar{\ell}_{\mathrm{FPZ}}, \theta_W)$ are the normalized forms of the corresponding CODs, respectively. As the crack opening profile is discretized in n steps, the total crack opening at position i can be related to the cohesive stress at position j of the FPZ by means of Equations (3.8) and (3.6) as:

$$\bar{w}_i = f_{ij}(\bar{\sigma}_c)_j \tag{3.9}$$

where $\bar{w}_i = w_i E/(R\sigma_u)$ is the normalized total crack opening at position i and $f_{ij}(\bar{\ell}_{\text{FPZ}}, \theta_W, LP)$ is the profile that relates the crack opening at position i to the stress at position j.

For a given shape of the cohesive law $\bar{\sigma}_c(\bar{w})$ and parameters θ_W and LP, the nominal stress can be obtained for a certain size of the FPZ, $\bar{\ell}_{\text{FPZ}}$, using the system of equations in (3.6) and (3.9). Since the nominal strength is the maximum nominal stress before failure ($\bar{\sigma}_{Nf}$) and the critical $\bar{\ell}_{\text{FPZ}}$ that is required to produce this value of stress is unknown, the following condition must be imposed:

$$\frac{\partial \bar{\sigma}_N}{\partial \bar{\ell}_{\text{FPZ}}} = 0 \tag{3.10}$$

By solving the system of equations in (3.6) and (3.9) with the condition in Equation (3.10), it is possible to obtain an expression for $\bar{\sigma}_{Nf}(\theta_W, \bar{\ell}_M, LP)$, the critical size of the FPZ $\bar{\ell}_{\text{FPZ}}(\theta_W, \bar{\ell}_M, LP)$ and the maximum normalized crack opening at failure $\bar{w}_N(\theta_W, \bar{\ell}_M, LP)$.

3.3.3 The Validity of the Model

There are many materials that meet the model hypothesis such as ceramics, some polymers, metals under fatigue loads and some composites especially those with random or particulate reinforcement.

In composite laminates failure mechanisms can be, broadly, divided into in-plane and out-of-plane failure modes. Matrix tensile cracking at location of stress concentration, matrix shear cracking between fibers in off-axis plies, macroscopic splitting cracks (in splitting), fiber rupture (in tension), fiber micro-buckling (in compression) are in-plane failure mechanisms. This is because they, typically, occur in individual plies and are mostly related to in-plane stresses. Whereas delamination is an out-of-plane damage mode and its evaluation is dictated by the interlaminar stresses [71].

Interaction of the aforementioned damage mechanisms depends on the material properties of individual layer, geometry, stacking sequence and loading conditions. The resulting complex damage mode from this interaction governs the macroscopic mechanical response of the laminate. For instance, during the stable growth of the damage zones, preceding the final failure, the formation of new free surfaces

of subcritical cracks will alter the load paths and result in load redistribution and, consequently, increasing the strength of the structure. The combined effects of the competing damage processes generally lead to nonlinearity in macroscopic stress-strain curves. This non-linearity, as mentioned before, can be modeled using the CZMs.

The described analytical formulation based on the CZM is applicable for composite laminates under some assumptions. For OH specimens under biaxial loading the model is valid under two conditions. The first one is that the laminate should be delamination and ply-splitting resistant. This can be achieved by avoiding ply clustering, stitching the laminate, using thin plies or woven fabric plies [13, 90, 91]. Delamination resistant laminates are usually considered as a result of good design [92]. The second condition is that the laminates are isotropic from elastic, strength and toughness point of view. The elastic isotropy can be rigorously fulfilled if the laminate is composed by quasi-isotropic sublaminates, for example sublaminates with stacking sequence $[0/\pm 60]_s$, $[0/\pm 45/90]_s$ or $[0/\pm 36/\pm 72]_s$. On the other hand, the strength and toughness isotropy will never strictly be reached, but the anisotropy is reduced by reducing the mismatch angle between the plies that compose the laminate [90, 93]. In the case that the principal stress direction as well as the direction of the failure plane are kept constant, the model can be applicable only assuming elastic isotropy.

In addition of localized damage the net tension strength of bolted joints requires that the failure plane is normal to load direction. It happens in almost all isotropic and orthotropic laminates with principal directions aligned with the loads. The results presented in this thesis are only valid for isotropic materials but its generalization to anisotropic materials requires the redefinition of the functions β_i and f_{ij}. Since these are obtained from two dimensional elasticity solutions with stress boundary conditions, the differential equation that defines the stress state depends on the roots of a four order characteristic polynomial [94]. Therefore, for a general anisotropic material the solution depends on four nondimensional material parameters that defines its anisotropy. For orthotropic materials, with material directions aligned with the load, only two nondimensional parameters are required to characterize completely the functions β_i and f_{ij}. If further symmetries exist, as for example cross-ply laminates with the same Young modulus in the load direction and perpen-

dicularly, one material parameter is required. Finally, it must be noted that in the case of laminated composites the material properties that fed up the model are the homogenized properties of the laminate. Therefore, two laminates with different stacking sequences are considered two different materials.

Chapter 4

Open Hole Specimens under Biaxial Loading

4.1 Introduction

Most of aircraft and aerospace structures are made of quasi-brittle materials. These structures contain many holes and are subject to multidirectional loading conditions. Due to the industrial importance of these structures, the development of stress concentrations arising from the existing holes has been always of great concern. The prediction of the ultimate notched strength remains the main challenge in the simulation of their mechanical response [95].

Quasi-brittle materials develop a stable FPZ before failure, whose size ℓ_{FPZ} depends on the material characteristic length $\ell_M = EG_C/\sigma_u^2$. The reason of the influence of the size effect on the structure's strength (Figure 4.1b) is linked to the development of this FPZ. Due to the importance of this effect, it must be considered in the predictions of the nominal strength of quasi-brittle structures [13, 82, 96–99].

When dealing with failure prediction of open hole specimens two extreme situations can be expected: brittle or ductile failure. Specimens with small holes are notch insensitive: the perturbation of the stress field caused by the hole is enclosed in a region smaller than the length of the FPZ and the specimen fails according to the plastic limit (line P Figure 4.1a). On the other extreme, specimens with large holes are notch sensitive and the relative size of the FPZ is negligible with respect to the specimen size; herein brittle failure is expected (line E Figure 4.1a). The

nominal strength for brittle failure is predicted by the elastic limit depending on the value of the stress concentration factor (K_t). For a hole in an infinite plate it depends on the load biaxiality ratio (λ) so that $K_t = 3 - \lambda$. The transition from ductile to brittle failure occurs smoothly by increasing the hole radius.

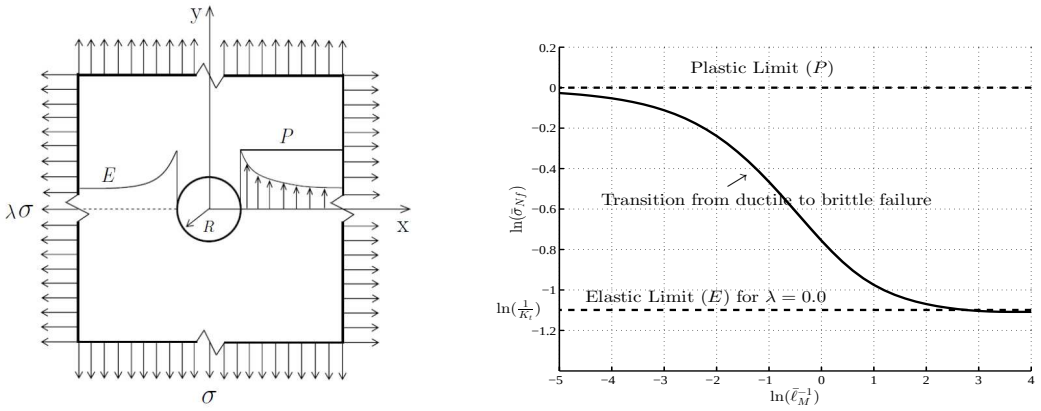

(a) Open hole specimen under biaxial loading (b) Size effect law on the structural strength

Figure 4.1: Loading condition and size effect law

As shown in Chapters 3 and 4, there is a shortage in analytical models and numerical simulations that investigate the nominal strength of quasi-brittle structures subjected to multidirectional loading conditions. So, the objective of this chapter is to introduce analytical models able to find the nominal strength of isotropic quasi-brittle OH specimens under biaxial loading conditions.

This chapter is organized as follows: in Sections 4.2 and 4.3 a formulation based on the CZM and its results are presented; in Section 4.4 the obtained results based on the SEL are presented and compared with those of the CZM and the available experimental data; formulations based on CDTs are introduced in Section 4.5; in Section 4.6 the obtained results of the CDT models are showed as well as a general discussion; and finally the conclusions of the presented work are listed at the end of the chapter.

4.2 Formulation Based on the Cohesive Zone Model (CZM)

In this section the nominal strength of infinite quasi-brittle open hole specimens under biaxial loading conditions, as shown in Figure 4.1 (a), is analyzed. The presented model is based on the Dugdale/Barenblatt CZM. The complete solution of this problem under the hypothesis of linear elastic analysis can be obtained by summation of two solutions as shown in Figure 4.2. The first one is the solution of an open hole with a crack of length ℓ_{FPZ} and an applied biaxial remote stress. The second is the solution of a specimen with cohesive stress at FPZ.

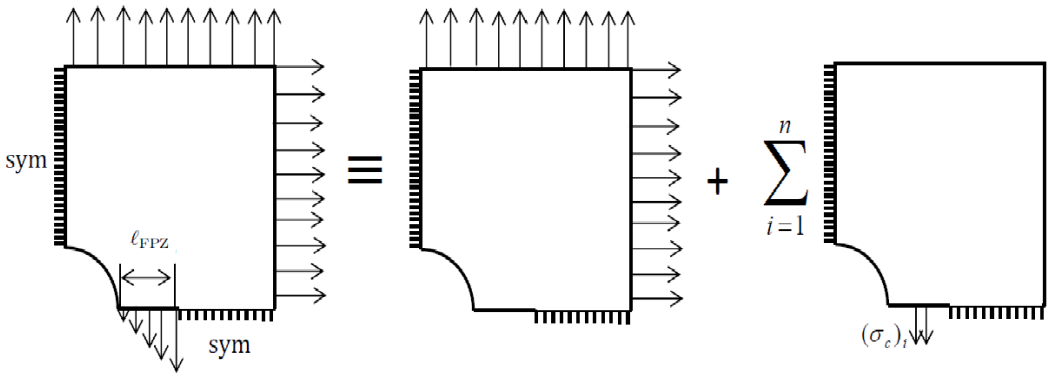

Figure 4.2: Open hole specimen with a failure process zone modeled as a superposition of two linear problems.

As no singular stresses are present in the complete problem, the total stress intensity factor K must be null [67]:

$$K = K_E + K_{\sigma_c} = 0 \tag{4.1}$$

where K_E and K_{σ_c} are the stress intensity factors due to the applied remote stresses (σ and $\lambda\sigma$) and the cohesive stress at the FPZ, respectively. Equation (4.1) can be written in normalized form as [38, 75]:

$$K = \sigma_u \sqrt{R} \left(\bar{\sigma}_N \, \bar{K}_E \left(\bar{\ell}_{\text{FPZ}}, \lambda \right) + \sum_{i=1}^{n} (\bar{\sigma}_c)_i \, \bar{K}(\bar{\ell}_{\text{FPZ}}, i/n) \right) = 0 \tag{4.2}$$

In Equation (4.2), the non-dimensional forms of the stress intensity factors, $\bar{K}_E$ and $\bar{K}$, can be obtained from the literature [38, 75]. Consequently, it is possible to define $\bar{\sigma}_N$ with respect to $(\bar{\sigma}_c)_i$ as:

$$\bar{\sigma}_N = (\bar{\sigma}_c)_i \; \beta_i(\bar{\ell}_{\mathrm{FPZ}}, \lambda) \tag{4.3}$$

where β_i is a vector relating the normalized stress at position i to the normalized remote stress.

As described in Chapter 3, the total crack opening profile w is obtained by the superposition of the displacement caused by the remote stress w_E and the displacement due to the cohesive stresses w_{σ_c}. In a normalized form, it can be written as [38, 75]:

$$w = R\frac{\sigma_u}{E}\left(\bar{\sigma}_N \; \bar{w}_E(\bar{\ell}_{\mathrm{FPZ}}, \lambda) + \sum_{i=1}^{n} (\bar{\sigma}_c)_i \; \bar{w}_c(\bar{\ell}_{\mathrm{FPZ}}, i/n)\right) \tag{4.4}$$

where $\bar{w}_E$ and $\bar{w}_c$ define the normalized crack opening profile under a remote stress and a cohesive stress at position i, respectively. If the crack opening profile is discretized in n steps, the crack opening at position i can be related to the stress at position j of the FPZ with the following expression:

$$\bar{w}_i = f_{ij}(\bar{\ell}_{\mathrm{FPZ}}, \lambda) \; (\bar{\sigma}_c)_j \tag{4.5}$$

where $\bar{w}_i = E/(R\sigma_u)w_i$ is the normalized crack opening at position i, f_{ij} is the profile that relates the crack opening at position i to the stress at position j and $(\bar{\sigma}_c)_j$ is the normalized cohesive law relating the normalized stress with respect to the normalized crack opening displacement. As ℓ_{FPZ} is unknown, it is necessary to look for the maximum of the remote stresses with respect to it. Accordingly, the following condition should be imposed:

$$\frac{\partial \bar{\sigma}_N}{\partial \bar{\ell}_{\mathrm{FPZ}}} = 0 \tag{4.6}$$

By solving the system of Equations in (4.5) and (4.3) with the condition in Equation (4.6) for a given cohesive law $\bar{\sigma}_c(\bar{w})$ it is possible to obtain expressions for the nominal strength $\bar{\sigma}_{Nf}(\lambda, \bar{\ell}_M)$, $\bar{\ell}_{\mathrm{FPZ}}(\lambda, \bar{\ell}_M)$ and the maximum crack opening $\bar{w}_N(\lambda, \bar{\ell}_M)$ at failure load. A more convenient way to normalize the crack opening displacement

is $\tilde{w}_N(\lambda, \bar{\ell}_M) = \bar{w}_N/(2\bar{\ell}_M)$.

4.3 Results of the Cohesive Zone Model

The cohesive law defines the constitutive behavior of the FPZ. This is defined by an onset criteria defined with the stresses and a critical fracture energy that corresponds to the complete area under the cohesive law. When computing the nominal strength of notched structures the shape of the cohesive law is also of importance [12, 75]. In Figure 4.3 different shapes of the cohesive laws those used in the present formulation are shown.

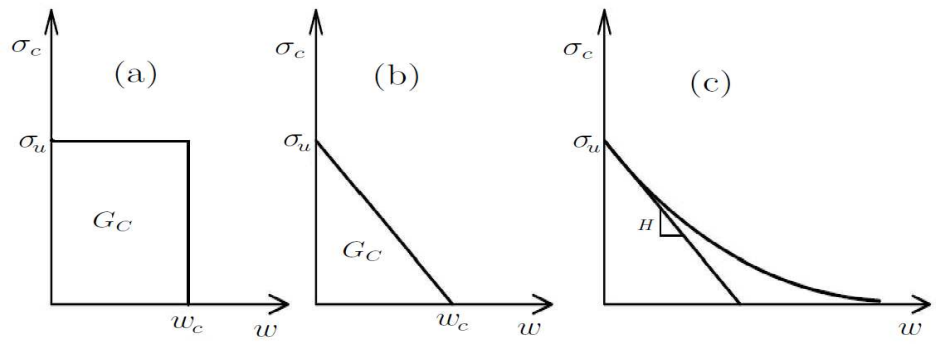

Figure 4.3: (a) Constant cohesive law, (b) linear cohesive law and (c) linear and exponential cohesive laws with the same initial slope

In the constant cohesive law the nominal strength is reached at a crack opening of $w_N = G_C/\sigma_u$, ($\tilde{w}_N = 1/2$), that corresponds to the moment when the FPZ is completely developed and a crack starts to grow in a self-similar way. The normalized nominal strength and corresponding failure envelopes for a constant cohesive law are shown in Figure 4.4.

In the case of small holes with large λ ratios, it is no longer acceptable to consider that the FPZ grows in only one plane. On the contrary, as the FPZ starts growing in one plane, say in the x direction, high stresses of similar magnitude appear in the perpendicular, say y, direction. This case corresponds to the area enclosed by the dotted line in Figure 4.4 (b). Experimental results actually show that in the specific case case of $\lambda = 1$ three equally spaced cracks emanate from the hole [55].

This is reasonable because this crack distribution pattern requires less energy than four equally spaced cracks.

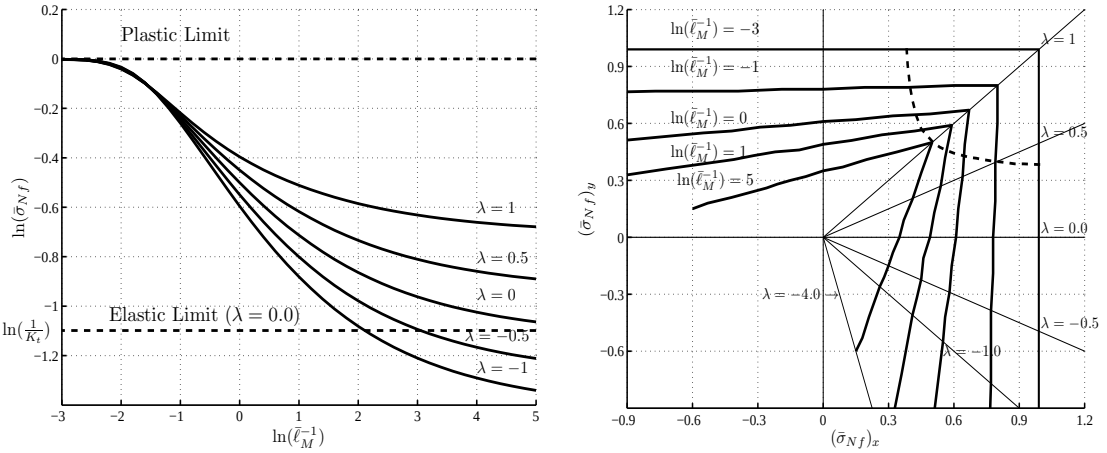

(a) Normalized nominal strength with respect to the nondimensional hole radius for different λ

(b) Predicted failure envelopes for different nondimensional hole radii

Figure 4.4: Normalized nominal strength and failure envelopes based on constant cohesive law

With the linear cohesive law the failure is reached before the FPZ is completely developed and the crack opening at failure is $w_N < 2G_C/\sigma_u$ [100]. The normalized crack opening displacement, the size of the FPZ at failure normalized with respect to ℓ_M ($\tilde{\ell}_{FPZ} = \ell_{\text{FPZ}}/\ell_M$), the nominal strength and the corresponding failure envelopes for the linear cohesive law are shown in Figure 4.5. For specimens with small and large holes the failure load is obtained at very small crack openings. Thus, it seems that the initial part of the cohesive law is an important parameter in the nominal strength prediction of the open hole specimens especially for small and large holes. Also, it is observed that as the stress concentration factor increases (while λ decreases) the crack opening displacement at failure becomes larger. Therefore, the initial part of the cohesive law will gain importance as λ tends to one.

An important conclusion from the crack opening displacement plot for the linear cohesive law is that after the critical crack opening ($\tilde{w}_N$) the shape of the cohesive law does not play any role in the determination of the nominal strength. In a linear cohesive law, for very small and very large hole radii, the nominal strength depends on the initial slope of the cohesive law and not on the total critical fracture energy. This means that a better way to normalize the material characteristic length is to

use the initial slope of the cohesive law (H), as shown in Figure 4.3 (c). If the material characteristic length is defined as:

$$\ell_M = \frac{E}{2H} \tag{4.7}$$

for a linear cohesive law it is equivalent to Equation (3.3), but it becomes equal to half this value in case of an exponential cohesive law. In Figure 4.6 the response of a linear and exponential cohesive law has been normalized with the expression (4.7) where LCL and ECL refers to linear and exponential cohesive law.

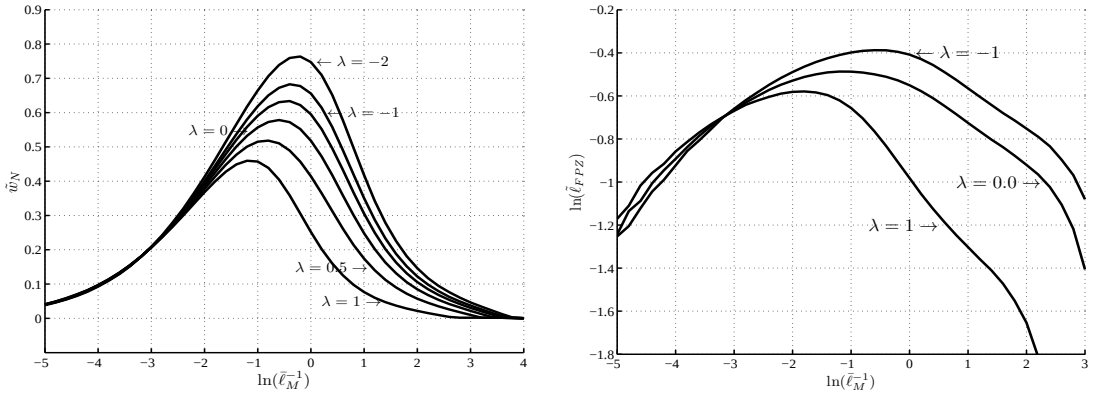

(a) Crack opening displacement at failure for different values of λ

(b) Fracture process zone at failure for different values of λ

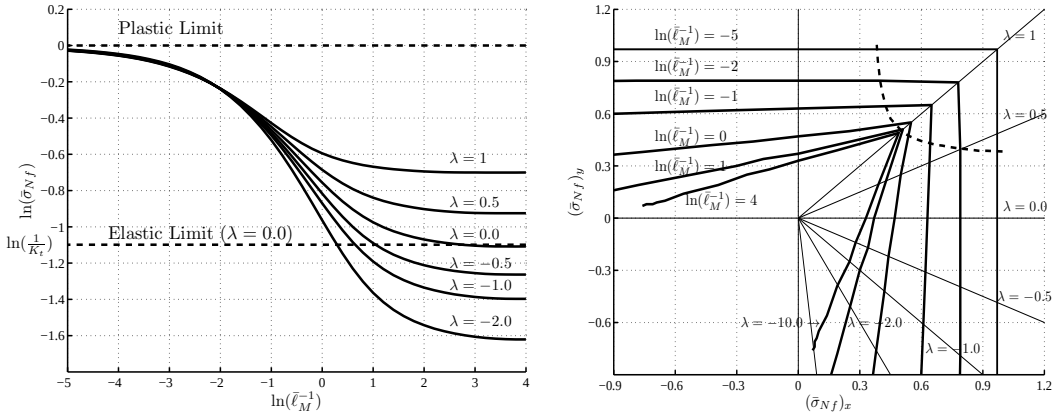

(c) Predicted nominal strength with respect to the nondimensional hole radius for different λ

(d) Predicted failure envelopes for different nondimensional hole radii

Figure 4.5: Crack opening displacement, fracture process zone, normalized nominal strength and failure envelopes based on linear cohesive law

Since the COD is related with the size of the FPZ, results of Figure 4.5 (b) can

explain the obtained shape in COD plots.

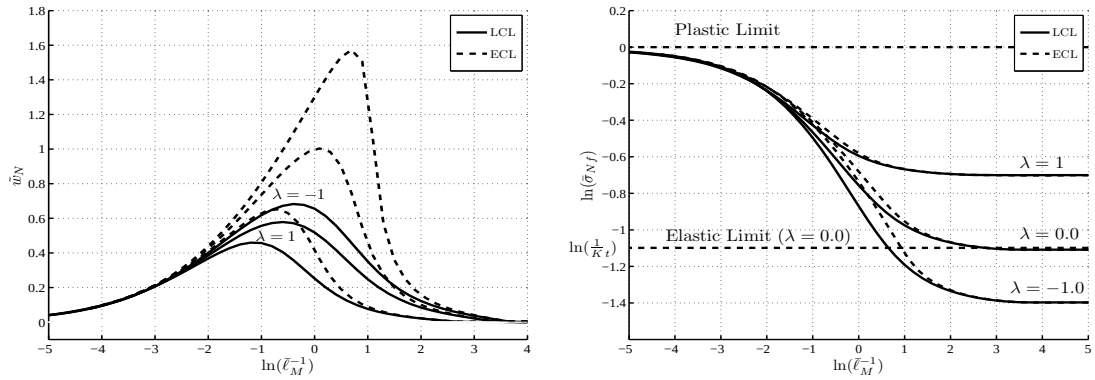

(a) Crack opening displacement at failure based on LCL and ECL for different values of λ

(b) Predicted nominal strength based on LCL and ECL for different values of λ

Figure 4.6: Importance of the initial slope of the cohesive law in failure analysis of the open hole specimens

The results in Figure 4.6 show that a material with a linear cohesive law of a given critical fracture energy will respond almost in the same way as a material with an exponential cohesive law with twice the fracture energy (but the same initial slope H). This is specially true when λ approaches one because of the small values of each stress concentration factor and the obtained $\tilde{w}_N$. This means that the results in Figure 4.5 can be used for any cohesive law if its initial part is specified in a proper way.

When the hole radius tends to zero, a material strength criterion is defined. As shown in Figures 4.4 (b) and 4.5 (d) the Rankine failure envelope is reached. This is due to the onset criterion defined in the cohesive law. To reach another failure surface it is required to take into account normal stresses parallel to the crack in the strength onset of the cohesive law. Presently, only some models consider these stresses [73, 101]. Most of the cohesive models implemented in finite elements codes as ABAQUS [102] do not take them into account.

4.4 Results Based on the Size Effect Law

For OH specimens under biaxial loading it is possible to fit the parameters of the SEL, described in Equation (2.2), to the linear and the constant cohesive laws. As

mentioned before, under biaxial loading conditions the stress concentration factor that defines the maximum normal stress at hole boundary with respect to the remote stress corresponds to $K_t = 3 - \lambda$. In Figure 4.7 the predictions of the SEL adjusted to the results obtained by the LCL and the CCL as well as to the experimental results of reference [55].

The best fitting to the experimental data is obtained with the parameters $r = 0.8$ and $\bar{\ell}_{\mathrm{SEL}} = \bar{\ell}_{\mathrm{M}}/\pi$, as shown in Figure 4.7 (a). With these values, for small holes and high values of λ there is an error between the SEL and the LCL with maximum value of 10.7 % for $\lambda = 1$. In case of CCL, the parameters $r = 2.7$ and $\bar{\ell}_{\mathrm{SEL}} = \bar{\ell}_{\mathrm{M}}/\pi$ results in a good agreement.

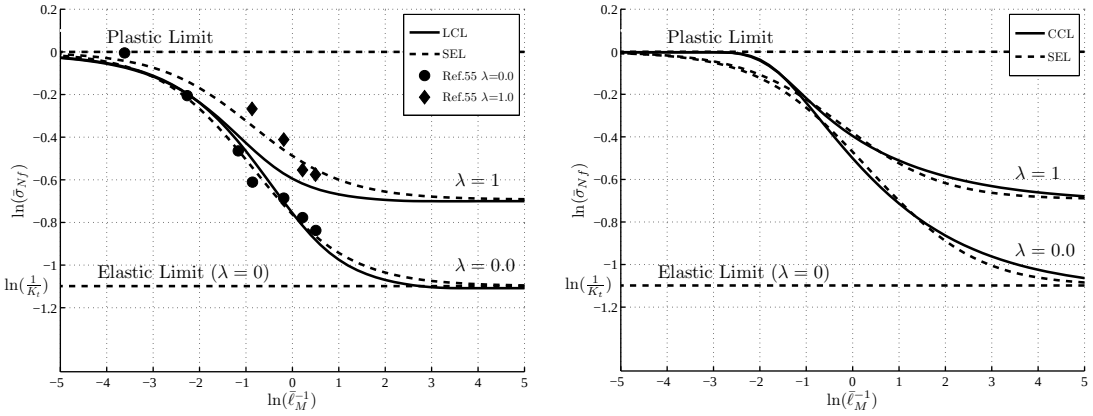

(a) The SEL adjusted to the LCL and the experimental data

(b) The SEL adjusted to the CCL

Figure 4.7: Predicted nominal strength based on the SEL

4.5 Formulations Based on Critical Distance Theories (CDTs)

Models based on CDTs have been used with remarkable success to adjust experimental results for various kinds of materials, especially for quasi-brittle materials. Its main advantage is that they are easy to implement. The stress based methods depend on the elastic stress field. The hoop and radial stress fields at the failure plane for a hole in an infinite plate under biaxial loading in the normalized form,

$\bar{\sigma}_{\theta\theta}$ and $\bar{\sigma}_{rr}$, can be expressed as [24]:

$$\bar{\sigma}_{\theta\theta}(\bar{x},0) = \frac{1}{2}\left\{(1+\lambda)\left[1+(1+\bar{x})^{-2}\right]+(1-\lambda)\left[1+3(1+\bar{x})^{-4}\right]\right\} \tag{4.8a}$$

$$\bar{\sigma}_{rr}(\bar{x},0) = \frac{-1}{2}\left\{\left[(1+\bar{x})^{-2}-1\right]\left[2\lambda-3\lambda(1+\bar{x})^{-2}+3(1+\bar{x})^{-2}\right]\right\} \tag{4.8b}$$

where $\bar{x} = x/R$ is the normalized distance to the intended point measured from the hole boundary.

The PSM considers failure when the strength criteria is satisfied at a characteristic distance ℓ_{PSM} of the hole boundary. In the ASM the stress is averaged over a line of some characteristic length ℓ_{ASM}. The normalized nominal strength can be defined by means of the linear elastic stresses defined in equation (4.8a) as [12, 23]:

$$\bar{\sigma}_{Nf}^{\mathrm{PSM}} = 2\left\{(1+\lambda)\left[1+(1+\bar{\ell}_{\mathrm{PSM}})^{-2}\right]+(1-\lambda)\left[1+3(1+\bar{\ell}_{\mathrm{PSM}})^{-4}\right]\right\}^{-1} \tag{4.9a}$$

$$\bar{\sigma}_{Nf}^{\mathrm{ASM}} = \frac{2(1+\bar{\ell}_{\mathrm{ASM}})^3}{(\bar{\ell}_{\mathrm{ASM}}+2)(2\bar{\ell}_{\mathrm{ASM}}^2+4\bar{\ell}_{\mathrm{ASM}}+3-\lambda)} \tag{4.9b}$$

where $\bar{\ell}_{\mathrm{PSM}}$ and $\bar{\ell}_{\mathrm{ASM}}$ are the normalized characteristic lengths in PSM and ASM, respectively. In the stress based methods the characteristic length is fitted by adjusting the response of large size fracture-mechanics specimens. The characteristic length must be fitted to asymptotically obtain the linear elastic fracture mechanics response [12, 23], resulting in:

$$\bar{\ell}_{\mathrm{PSM}} = \frac{\bar{\ell}_{\mathrm{M}}}{2\pi} \;\text{ and }\; \bar{\ell}_{\mathrm{ASM}} = \frac{2\bar{\ell}_{\mathrm{M}}}{\pi} \quad \text{where} \quad \bar{\ell}_{\mathrm{M}} = \frac{\ell_{\mathrm{M}}}{R} = \frac{E\,G_C}{R{\sigma_u}^2} \tag{4.10}$$

According to the IFM a crack emerges from the hole boundary and the strength is defined by linear elastic fracture mechanics. The FFM considers the mean energy release rate of a crack growth with a characteristic length as a driving force. The normalized nominal strength can be represented as [12, 40]:

$$\bar{\sigma}_{Nf}^{\mathrm{IFM}}(\bar{\ell}_{\mathrm{IFM}},\lambda) = \sqrt{\frac{\bar{\ell}_{\mathrm{M}}}{\pi\,\bar{\ell}_{\mathrm{IFM}}}}\;F^{-1}(\bar{\ell}_{\mathrm{IFM}},\lambda) \tag{4.11a}$$

$$\bar{\sigma}_{Nf}^{\mathrm{FFM}}(\bar{\ell}_{\mathrm{FFM}},\lambda) = \sqrt{\frac{\bar{\ell}_{\mathrm{FFM}}\,\bar{\ell}_{\mathrm{M}}}{\pi\int_{\bar{a}=0}^{\bar{\ell}_{\mathrm{FFM}}}\bar{a}\;F^2(\bar{a},\lambda)\;d\bar{a}}} \tag{4.11b}$$

where $\bar{a} = a/R$ is a normalized crack length and $F(\bar{a}, \lambda)$ is a shape factor that can be obtained from the bibliography as in Berbinau et al. [38], similar to Equation (2.7).

In IFM and FFM the characteristic length is fitted for a small crack in an infinite specimen to reach the material strength, or the plastic limit for very small specimens, [12, 39] resulting in:

$$\bar{\ell}_{\text{IFM}} = \frac{\bar{\ell}_{\text{M}}}{\pi} \text{ and } \bar{\ell}_{\text{FFM}} = \frac{2\bar{\ell}_{\text{M}}}{\pi} \tag{4.12}$$

It must be pointed out that in the present work the characteristic lengths of the cracked specimen, in Equations (4.10) and (4.12), are used for the open hole specimens.

Finally, a modification of the CDTs emerges when both a stress and fracture mechanics criteria are imposed to be simultaneously fulfilled. Choosing one of the criteria of Equation (4.9) and equating it to a fracture-mechanics criterion, Equation (4.11), we get a common length of FPZ for both criteria. For example when the ASM is coupled with the FFM the normalized length $\bar{\ell}_{\text{FPZ}}$ can obtained, for a given ℓ_{M} and λ, by solving the following equation:

$$\frac{4\pi\ \bar{\ell}_{\text{FPZ}}\ \bar{\ell}_{\text{M}}^{-1} \int_{\bar{\ell}=0}^{\bar{\ell}_{\text{FPZ}}} [(1+\bar{\ell})\ F^2(\bar{\ell}, \lambda)]\ d\bar{\ell}}{\left(\int_{\bar{\ell}=0}^{\bar{\ell}_{\text{FPZ}}} \left((1+\lambda)[1+(1+\bar{\ell})^{-2}] + (1-\lambda)[1+3(1+\bar{\ell})^{-4}] \right)\ d\bar{\ell} \right)^2} = 1 \tag{4.13}$$

Using the resulted value of $\bar{\ell}_{\text{FPZ}}$, the normalized nominal strength can be obtained as:

$$\bar{\sigma}_{Nf}^{\text{ASM-FFM}} = \frac{2(1+\bar{\ell}_{\text{FPZ}})^3}{(\bar{\ell}_{\text{FPZ}}+2)(2\bar{\ell}_{\text{FPZ}}^2 + 4\bar{\ell}_{\text{FPZ}} + 3 - \lambda)} \tag{4.14}$$

However, no physical meaning shall be attributed to the length ℓ_{FPZ}.

4.6 Results of CDTs and Discussion

The predicted nominal strength based on CDTs is shown in Figure 4.8. Taking into account the different combination of stress and energetic methods, the obtained nominal strength is illustrated in Figure 4.9. For very small hole specimens the nominal strength is correctly predicted and the plastic limit is reached for all of the applied methods. However, for specimens with very large holes the nominal strength

is incorrectly predicted: the reached elastic limit in the fracture mechanics based methods is 1.12 times smaller than the expected value, $1/K_t$, as shown in Figure 4.8 (b). This deviation from the usual elastic limit in IFM and FFM is due to the free edge effect. For other methods, the elastic limit is correctly reached.

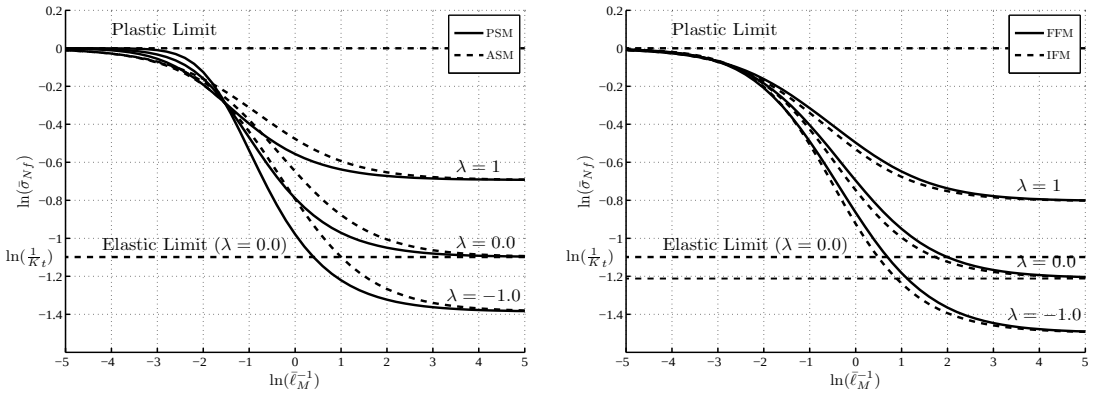

(a) Predicted nominal strength based on PSM and ASM for different values of λ

(b) Predicted nominal strength based on IFM and FFM for different values of λ

Figure 4.8: Nominal strength based on CTDs.

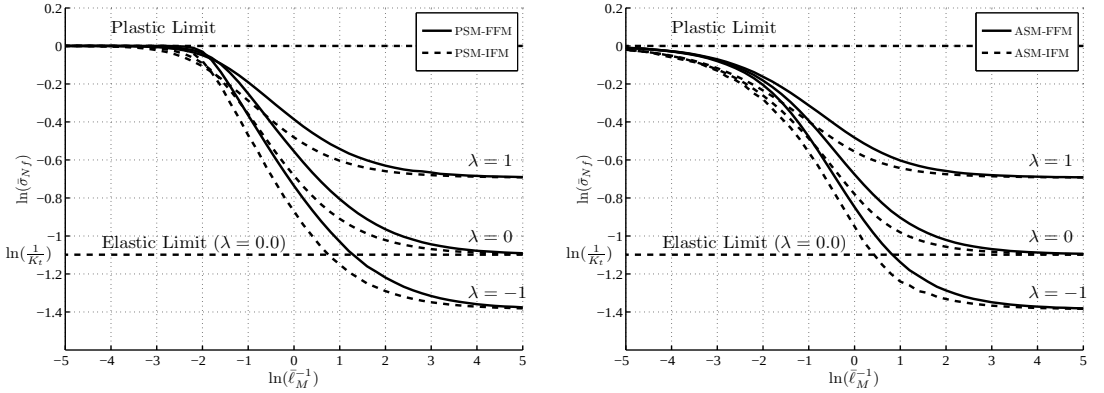

(a) Predicted nominal strength based on combined PSM-FFM and PSM-IFM methods for different values of λ

(b) Predicted nominal strength based on combined ASM-FFM and ASM-IFM methods for different values of λ

Figure 4.9: Nominal strength based on combined CTDs.

The predicted failure envelopes based on CDTs are shown in Figure 4.10. As in the CZM, the stress based methods and the fracture mechanics methods coincide with the Rankine theory for small hole radii.

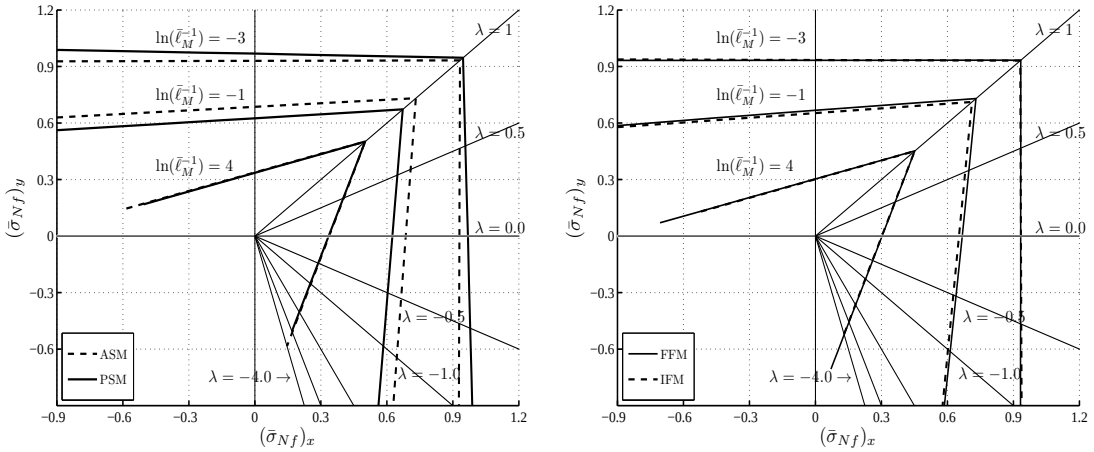

(a) Failure envelopes for different nondimensional hole radii based on PSM and ASM

(b) Failure envelopes for different nondimensional hole radii based on IFM and FFM

Figure 4.10: Predicted failure envelopes based on CTDs.

To obtain another failure criterion the stress based methods are easier than the other methods, CZM or fracture mechanics based methods. In this case, in order to take into account the effect of the radial stress in the failure process, the Von-Mises failure criterion can be imposed instead of the adopted Rankine type in the original PSM and ASM. Consequently, the normalized nominal strength based on a modified PSM (S_N^{MPSM}) and a modified ASM (S_N^{MASM}) can be defined by means of the linear elastic stresses from Equation(4.8) as:

$$\bar{\sigma}_{Nf}^{\text{MPSM}} = \left[\bar{\sigma}_{rr}^2(\bar{\ell}_{\text{PSM}}, 0) - \bar{\sigma}_{rr}(\bar{\ell}_{\text{PSM}}, 0)\bar{\sigma}_{\theta\theta}(\bar{\ell}_{\text{PSM}}, 0) + \bar{\sigma}_{\theta\theta}^2(\bar{\ell}_{\text{PSM}}, 0)\right]^{-1/2} \tag{4.15a}$$

$$\bar{\sigma}_{Nf}^{\text{MASM}} = \frac{\bar{\ell}_{\text{ASM}}}{\int_{\bar{x}=0}^{\bar{\ell}_{\text{ASM}}} \left[\bar{\sigma}_{rr}^2(\bar{x}, 0) - \bar{\sigma}_{rr}(\bar{x}, 0)\bar{\sigma}_{\theta\theta}(\bar{x}, 0) + \bar{\sigma}_{\theta\theta}^2(\bar{x}, 0)\right]^{1/2} d\bar{x}} \tag{4.15b}$$

Due to the complexity of the load in Equation (4.15b), it is solved numerically.

Figure 4.11 (a) shows the predicted failure envelopes based on the modified ASM. The obtained results show that an ellipsoidal failure type is reached as the hole radius tends to zero. Some quasi-brittle materials fit better to this type of failure, as in the case of $[0/\pm 45/90]_s$ graphite/epoxy laminate, according to [55]. For this reason, when the experimental results of [55] are fitted for $\lambda = 0$ it is found that the best fitting-minimum error-for biaxial loading is obtained from modified ASM due to its ellipsoidal failure type, as shown in Figure4.11 (b). In Figure 4.11 MASM refers to

the modified average stress method.

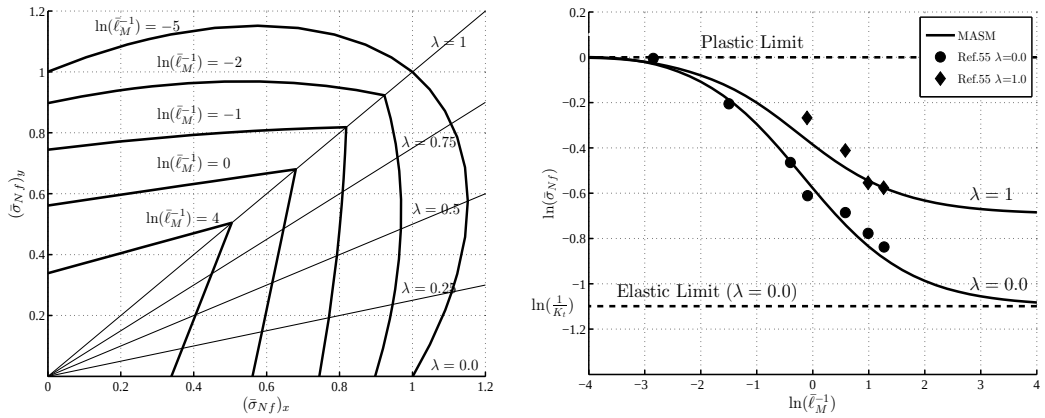

(a) Predicted failure envelopes for different nondimensional hole radii based on MASM

(b) Experimental results on graphite/epoxy laminate adjusted by MASM

Figure 4.11: Failure envelopes based on MASM and experimental results fitted to MASM

Another possibility to obtain a failure theory with fracture mechanics methods relies in considering that the fracture toughness depends on the biaxiality ratio. It is well known that the critical fracture energy depends on T-stress. Unfortunately, while the fracture toughness decreases in many material with respect to the triaxiality ratio, the strength usually increases until reaching a constant value [101]. On the other hand, the CZM, which represents the physical process of failure more precisely, shows that for small holed specimens the failure is reached at null crack opening. Therefore, the failure theory must be applied to the strength criterion, not on the fracture toughness.

Finally, the obtained results show that all of the presented models, namely CZM and CDTs models, are able to predict the decrease of the strength with respect to the hole radius. CZM have the advantage to link the material cohesive law with the nominal strength, the length of the FPZ and the critical crack opening. Again, an interesting conclusion with CZM is that the critical fracture energy is not an appropriate measure of the notch sensitivity. This is so because failure depends on the first part of the cohesive law, while its tail -that can dissipate an important amount of energy- is only important in cracked specimens of large size [12, 75].

On the other hand, CDTs models assume that the nominal strength can be

computed with the elastic stress field and a material characteristic length, which is a material property. Although the CDTs models offer an acceptable fitting to the experimental results in general, the characteristic length is usually fitted with the experimental results obtained for specimens with the same geometry. Furthermore, the best fitting to experimental results is obtained for variable characteristic length [29, 30]. As the CZM predicts that failure is reached at variable length of the FPZ, it comes out that both hypothesis can not be simultaneously fulfilled.

4.7 Conclusions

The nominal strength and the failure envelope of open hole isotropic quasi-brittle structures under multi-directional loading have been presented in this chapter. Different shapes of the cohesive law were used in the problem formulation. The effect of the hole radius and the load biaxiality ratio on the structures nominal strength have been studied.

It is observed that the first part of the cohesive law seems the most important parameter in the prediction of the nominal strength. Also, the linear cohesive law can represent any cohesive law when the slope of the initial part of the cohesive law is adjusted in a proper way. This is specially true when the biaxiality ratio tends to one.

The obtained results from the adopted CZM are similar to those obtained from the different methods of the CDTs and to the available experimental results. The modified ASM provides a more accurate strength prediction than those obtained with the other models in case of materials that exhibit an ellipsoidal failure surface. The obtained graphs can be readily used as design charts for quasi-brittle structures with open hole after rescaling their dimensions.

Chapter 5

Single-fastener Double-lap Joints

5.1 Introduction

Most of aircraft and aerospace structures contain many components joined together. These components should be occasionally disassembled for inspection and, eventually, replacement of the damaged parts. Bolted joints are a preferred option as mechanical fasteners for this purpose because they can be easily assembled and disassembled. Although riveted joints are more difficult to remove than bolted joints, they are widely used in these structures.

Since these joints act as load transfer elements in many engineering structures, the performance of these structures is greatly dependent on their behavior. Reliable design of the mechanically fastened joints requires an accurate prediction of its strength depending on the expected type of failure. Bearing, net-tension, shear-out and cleavage are the most frequent types of failure encountered in bolted joint connections. Net-tension and cleavage failures are abrupt, whereas bearing and shear-out are more ductile.

In bolted joints, there are more than one measure of the stresses applied to the joint. They are defined by the bearing load (L_b) divided by some characteristic length of the structure. At the same time they can be normalized with respect to the material strength σ_u. The remote stress (σ_∞) in its normalized form can be given by:

$$\bar{\sigma}_\infty = \frac{\sigma_\infty}{\sigma_u} = \frac{L_b}{2Wt\sigma_u} \tag{5.1}$$

where $\bar{\sigma}_\infty$ is the normalized remote stress, $2W$ is the joint width and t is the joint

thickness. This measure of the joint stress is the one used in the ASTM standards [103, 104].

Sometimes, it is more interesting to define the mean stress at failure plane σ_N by the bearing load divided by the net area, $\sigma_N = L_b/[2(W-R)t]$. This is the usual measure of stress in stress concentration handbooks as Peterson [105]. Another possibility is to use the hole radius as a measure of the applied stress [106], $\sigma_b = L_b/(2Rt)$, where σ_b is the bearing stress. These measures of stress, in normalized form, can be related by:

$$\bar{\sigma}_\infty = \bar{\sigma}_N(1-\theta_W) = \bar{\sigma}_b\theta_W \tag{5.2}$$

where $\bar{\sigma}_b = \sigma_b/\sigma_u$ is the normalized bearing stress and $\theta_W = R/W$ is the hole radius to the joint width ratio.

The net-tension strength of bolted joints in composites is neither defined by perfectly elastic nor perfectly plastic analysis [107, 108]. This intermediate response is attributable to the stable growth of the FPZ before failure in quasi-brittle materials. Under bearing load, the plastic and elastic limits are defined with respect to the normalized nominal stress as:

$$(\bar{\sigma}_N)_{\text{Plastic}} = 1 \qquad \text{and} \qquad (\bar{\sigma}_N)_{\text{Elastic}} = \frac{1}{K_t} \tag{5.3}$$

where K_t is the stress concentration factor due to the bearing stress. To define the corresponding normalized stresses with respect to the gross area or the hole radius, Equation 5.2 can be used.

The joint geometry, loading, strength limits and failure modes when the ratio of the end distance to the hole diameter ($\theta_e = e/(2R)$) is sufficiently large are shown in Figure 5.1. In this figure, e refers to the end distance and $(\bar{\sigma}_\infty)_f$ is the remote stress at failure$(\sigma_\infty)_f$ in its normalized form. The factor K_t depends on the contact stress profile due to the bolt and the geometric parameters θ_W and θ_e [105, 106]. Therefore, the elastic limit in Figure 5.1 is plotted according to Peterson's data [105]. Also, the bearing strength (S_b) depends mainly on the hole radius and the material compressive strength. The bearing limit in Figure 5.1 corresponds to a $[90/0/\pm45]_{3s}$ IM7-8552 CFRP laminate [17, 26], where $S_b = 737.8$ MPa and $\sigma_u = 845.1$ MPa. It must be noted that, at the bearing limit $\bar{\sigma}_{bf} \equiv \bar{S}_b$, where $\bar{S}_b = S_b/\sigma_u$ is the

normalized bearing strength and $\bar{\sigma}_{bf} = \sigma_{bf}/\sigma_u$ is the normalized form of the bearing stress at failure (σ_{bf}).

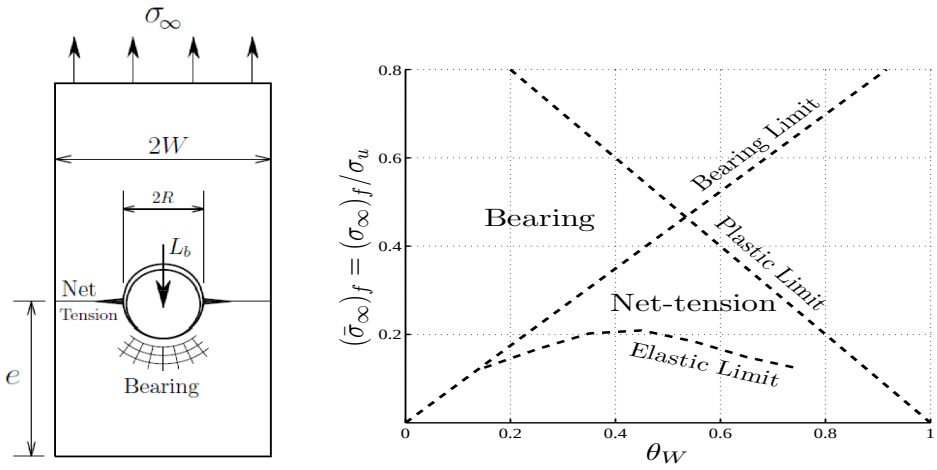

(a) Geometry and Loading (b) Strength limits and failure modes for large θ_e

Figure 5.1: Geometry, loading and failure modes of bolted joints when θ_e is large enough

Bearing failure is non-catastrophic and is characterized by damage accumulation and permanent deformation of the hole [26]. Typically, the bearing strength is defined when the permanent deformation is 4% of the hole diameter [104]. In composite materials this will happen before the other modes of failure when θ_W is less than 1/4 provided that θ_e is sufficiently large [109]. As θ_W increases, the failure mode shifts from bearing to net-tension failure. The maximum strength of the joint is expected around the transition from bearing to net-tension failure, within the range $1/4 \leqslant \theta_W < 2/3$ for many joints [110].

Literature of the previous chapters shows that there is a shortage in analytical models that predict the net-tension strength of the bolted joints. So, the objective of this chapter is to develop an analytical model capable of predicting the net-tension strength of single-fastener double-lap joints made of isotropic quasi-brittle material. This model is based on the CZM.

This chapter is organized as follows: In the next section a mathematical formulation of the problem based on the CZM is presented. The obtained results as well as a general discussion are presented in Section 5.3. Finally, conclusions are summarized at the end of the chapter.

5.2 Numerical model for net-tension failure

A numerical model for the net-tension failure of mechanically fastened joints of isotropic quasi-brittle structures is introduced in this section. The present formulation is based on the CZM. In this model the cohesive law defines the constitutive behavior at the FPZ. Therefore, it is expected that its shape will affect the computation of the net-tension strength of the joint as in the case of the nominal strength of notched structures [12, 75, 111]. To examine this influence, constant and linear shapes of the cohesive law are considered in the present model as shown in Figure 5.2.

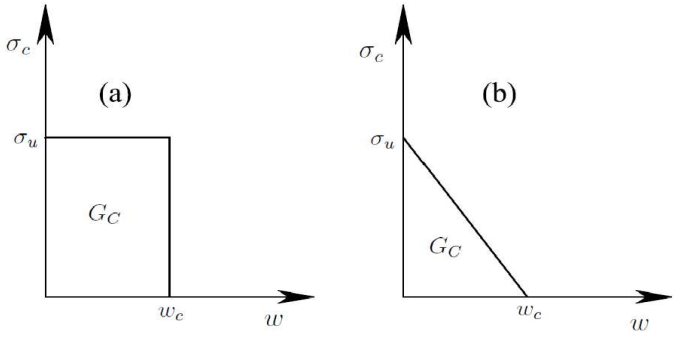

Figure 5.2: (a) Constant and (b) linear cohesive laws

Again, it must be pointed out that the applicability of the present model is limited to the joints of structures that are made of isotropic quasi-brittle materials. In these materials the damage, FPZ, can be modeled within a localized plane where the dissipation mechanisms take place. Also, it is assumed that the only source of nonlinearity is the localized FPZ.

Under these assumptions, the complete solution of the problem can be obtained by the superposition of the solution of two problems as shown in Figure 5.3. The first one is the solution of a loaded hole specimen with a critical crack length ℓ_{FPZ} and subjected to stresses due to the presence of the bolt. The second one is the solution of a specimen with cohesive stress σ_c at the FPZ.

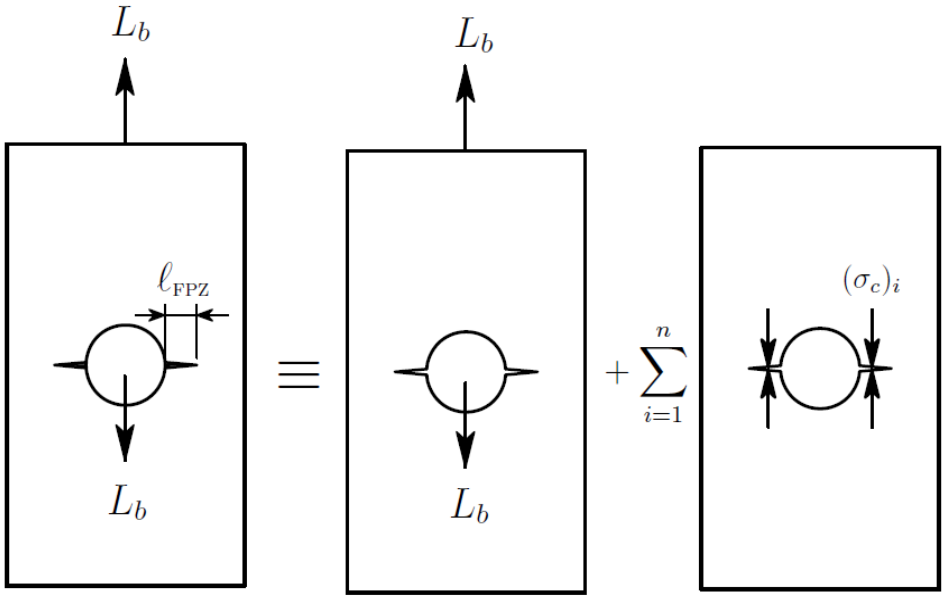

Figure 5.3: Bolted/pinned joint as a superposition of two problems

As stated in Chapter 3 the Dugdale's finite stress condition is given by:

$$K_E + K_{\sigma_c} = 0 \tag{5.4}$$

where $K_E = \bar{\sigma}_N \sigma_u \sqrt{R} \bar{K}_E \left(\bar{\ell}_{\text{FPZ}}, \theta_W\right)$ and $\bar{K}_E$ is its normalized form. Equation(5.4) can be written in normalized form as:

$$\sigma_u \sqrt{R} \left(\bar{\sigma}_N \bar{K}_E + \sum_{i=1}^{n} (\bar{\sigma}_c)_i (\bar{K}_{\sigma_c})_i \right) = 0 \tag{5.5}$$

The normalized SIF due to the cohesive stresses $\bar{K}_{\sigma_c}$ is given in Appendix A.1 [75, 89]. Using Equation (5.5), $\bar{\sigma}_N$ can be related to $(\bar{\sigma}_c)_i$ by:

$$\bar{\sigma}_N = (\bar{\sigma}_c)_i \; \beta_i(\bar{\ell}_{\text{FPZ}}, \theta_W) \tag{5.6}$$

The vector β_i which relates the normalized cohesive stress at position i to the normalized net-tension stress is given in Appendix A.1.

As before, the complete crack opening profile w is given by:

$$w = w_E + \sum_{i=1}^{n} (w_{\sigma_c})_i \tag{5.7}$$

Equation (5.7) can be written in a normalized form as:

$$\bar{w} = \bar{\sigma}_N \bar{w}_E + \sum_{i=1}^{n} (\bar{\sigma}_c)_i (\bar{w}_{\sigma_c})_i \tag{5.8}$$

The normalized forms of the CODs $\bar{w}_E$ and $\bar{w}_{\sigma_c}$ are given in Appendix A.1 [75, 89, 112]. As the crack opening profile is discretized in n steps, the relation between the crack opening at position i and the stress at position j of the FPZ is:

$$\bar{w}_i = f_{ij}(\bar{\ell}_{\mathrm{FPZ}}, \theta_W)(\bar{\sigma}_c)_j(\bar{w}_j) \tag{5.9}$$

The profile f_{ij} that relates the crack opening at position i to the stress at position j is described in Appendix A.1.

The condition of the maximum net-tension stress with respect to ℓ_{FPZ} is:

$$\frac{\partial \bar{\sigma}_N}{\partial \bar{\ell}_{\mathrm{FPZ}}} = 0 \tag{5.10}$$

For a given cohesive law $\bar{\sigma}_c(\bar{w})$, by the system of Equations in (5.9) and (5.6) it is possible to obtain the net-tension stress required for a given length of the FPZ. With the condition in Equation (5.10) the $\bar{\ell}_{\mathrm{FPZ}}(\theta_W, \bar{\ell}_M)$ that causes the net-tension failure is obtained. At this length the normalized nominal stress at failure, normalized net-tension strength, $\bar{\sigma}_{Nf}(\theta_W, \bar{\ell}_M)$ is determined. The normalized bearing stress at failure, $\bar{\sigma}_{bf}(\theta_W, \bar{\ell}_M)$, and the normalized remote stress at failure, $(\bar{\sigma}_\infty)_f(\theta_W, \bar{\ell}_M)$, can be obtained by means of Equation 5.2. Finally, the maximum normalized crack opening at failure, $\tilde{w}_N(\theta_W, \bar{\ell}_M)$, is also obtained.

It is important to point out that the SIFs of loaded holes have been studied by many authors [113–115]. Applying the principle of superposition to these factors and that of the open hole, it is possible to obtain an expression for the SIF of a bolted joint, Figure 5.4. Then, K_E can be expressed as:

$$K_E = \tfrac{1}{2}\left(K_{rb} + K_b\right) \tag{5.11}$$

where $K_{rb} = \bar{\sigma}_N \sigma_u \sqrt{R} \bar{K}_{rb}\left(\bar{\ell}_{\mathrm{FPZ}}, \theta_W\right)$ is the SIF due to the remote stress caused by the bearing load, $K_b = \bar{\sigma}_N \sigma_u \sqrt{R} \bar{K}_b\left(\bar{\ell}_{\mathrm{FPZ}}, \theta_W\right)$ is the SIF of the contact stress due to the bolt, and $\bar{K}_{rb}$ and $\bar{K}_b$ are their normalized forms, respectively. K_b depends on the assumed distribution of the contact stress due to the bolt. Expressions for $\bar{K}_b$ and $\bar{K}_{rb}$ are given in Appendix A.1 [75, 113, 114] based on the assumed contact stress profiles.

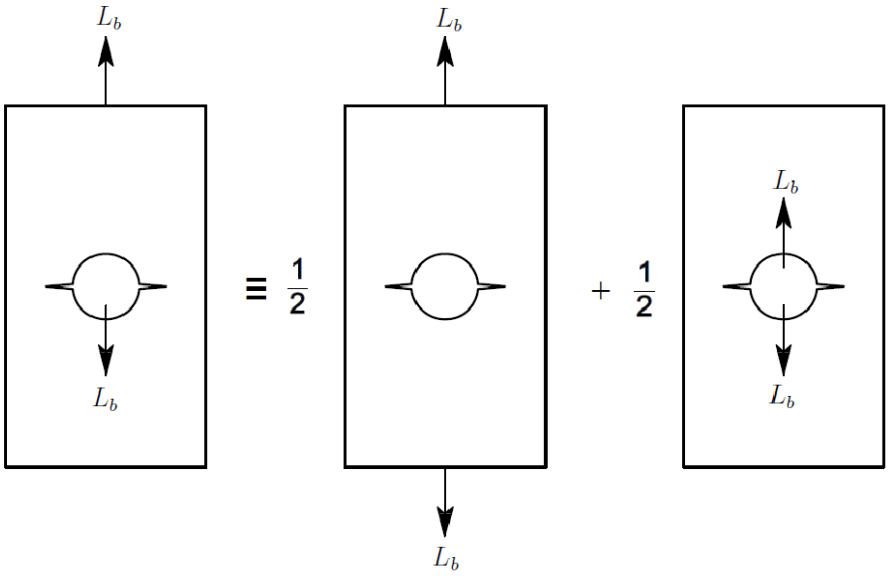

Figure 5.4: External loads as a superposition of two problems

Uniform and cosinusoidal stress distributions on the hole edge due to the presence of the bolt are introduced in the present model, Figure 5.5. In case of uniform stress distribution the contact stress due to the bolt (σ) can be expressed [113, 114] as $\sigma = \sigma_b$, while for the cosine distribution it is expressed [61, 106, 114, 116] as $\sigma = (4\sigma_b/\pi)\cos\theta$, where θ is the angle shown in Figure 5.5 (b).

Accordingly, the COD due to the external loads (w_E) can be given by:

$$w_E = \tfrac{1}{2}\left(w_{rb} + w_b\right) \tag{5.12}$$

where w_{rb} and w_b are the CODs due to the contact stress and the remote stress,

while $\bar{w}_{rb}$ and $\bar{w}_b$ are their normalized forms, respectively. Expressions for $\bar{w}_{rb}$ and $\bar{w}_b$ are introduced in Appendix A.1 [89, 112] depending on the functions of the corresponding SIFs.

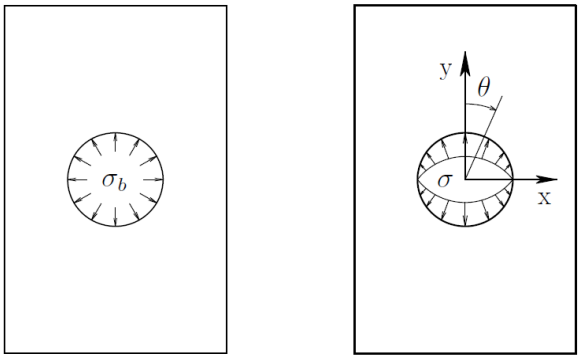

Figure 5.5: (a) Uniform and (b) cosinusoidal contact stress profiles due to bolt/pin

5.3 Results and discussions

5.3.1 Results for constant θ_W

In this section the ability of the cohesive law to predict the size effect on the joint net-tension strength has been examined. The size effect law defines the decrease of the structural strength by increasing the specimen size while keeping its geometry constant. This means that, for a constant θ_W, the source of embrittlement is the decrease of the relative size of FPZ with respect to the joint size.

The normalized nominal strength with respect to the nondimensional hole radius for different values of θ_W is presented in Figure 5.6. For all values of θ_W either with the linear or the constant cohesive laws, the net-tension strength increases when the hole radius decreases. This response is due to the larger relative size of the FPZ with respect to the joint size associated with small holes.

Also, for two materials with the same characteristic length, ℓ_M, it is observed that the predicted net-tension strength is higher with the constant cohesive law than with the linear one. It is known that for materials like concrete or composite, a bilinear softening function is appropriate. For other materials, such as some polymers, the

cohesive law is constant until some critical crack opening, after that the stresses drastically drop. As a result, for constant ℓ_M, a material with constant cohesive law must be less notch sensitive than a material with linear law. This implies that the shape of the material cohesive law affects the computation of the net-tension strength of the bolted joints.

Further, as shown in Figures 5.6 (a) and 5.6 (b) the predicted net-tension strength for the uniform stress distribution is higher than that obtained with the cosinusoidal one. This is reasonable because of the lower stress concentration factor associated with the uniform stress distribution due to the larger contact area between the bolt and the hole surface. However, the cosinusoidal stress distribution is more realistic when modeling mechanically fastened joints [61, 114, 116]. Therefore, the rest of this work is focused on this type of stress distribution.

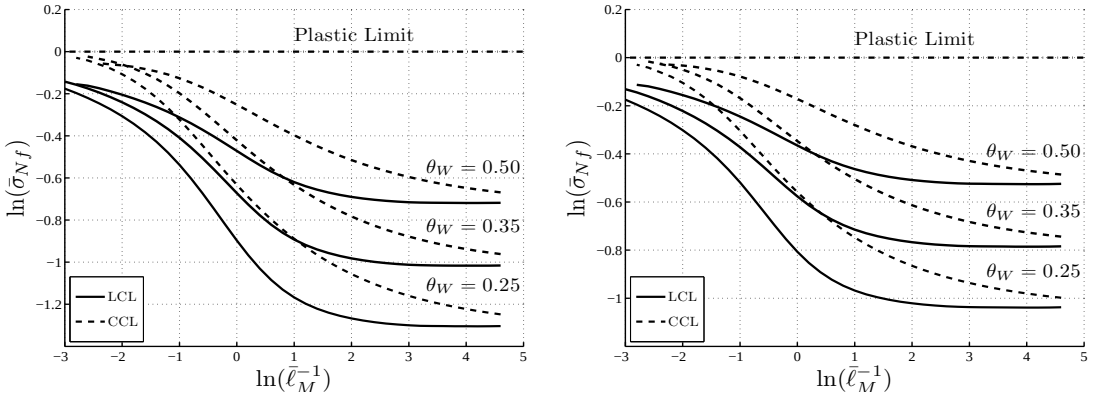

(a) Normalized nominal strength for cosinusoidal stress distribution

(b) Normalized nominal strength for uniform stress distribution

Figure 5.6: Normalized nominal strength with respect to nondimensional hole radius for different θ_W

The normalized CODs at failure due to cosinusoidal stress distribution for different values of θ_W and with the linear cohesive law is shown in Figure 5.7. It is observed that the COD grows with a decreasing θ_W due to the increment of the stress concentration factor. Also, for joints with small or large holes the joint net-tension strength is reached at small CODs for the different geometries. As a result, it can be concluded that the first part of the cohesive law is an important parameter in the determination of the net-tension strength of these joints.

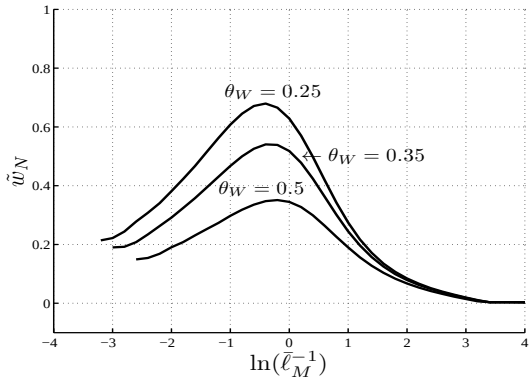

Figure 5.7: Normalized crack opening displacements at failure for cosinusoidal stress distribution and with LCL

5.3.2 Results for constant hole radius (R)

As mentioned before, for net-tension failure the nominal strength is defined between the elastic and the plastic limits. Figure 5.8 shows the bearing stress at net-tension failure with respect to θ_W for different values of $\bar{\ell}_M$ with both constant and linear cohesive laws. For each value of $\bar{\ell}_M$ the maximum load, with a minimum joint weight, is obtained at the limit between net-tension and bearing failure.

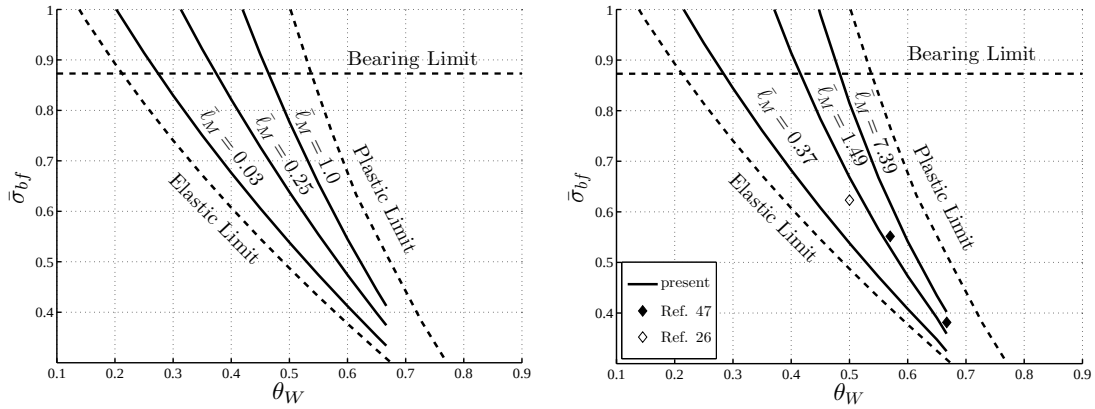

(a) Normalized bearing stress with CCL (b) Normalized bearing stress with LCL

Figure 5.8: Normalized bearing stress with respect to θ_W for CSD

For large W the bearing failure is reached and the failure is ductile. Again, the bearing limit in this figure and in the next one is for the $[90/0/\pm 45]_{3s}$ IM7-

8552 CFRP laminate presented in [17, 26] and assumed to be size and geometry independent.

The experimental results on quasi-isotropic $[90/0/\pm 45]_{3s}$ Hexcel IM7-8552 carbon epoxy laminate [26, 47] are adjusted with that of the linear cohesive laws as shown in Figure 5.8 (b). In those studies all specimens had the same hole radius $R = 3$ mm and all of them failed in net-tension mode. There is a reasonably good agreement between the present prediction and the experimental results.

5.3.3 Results for constant width (W)

The normalized remote stress at failure for different values of the normalized material characteristic length with respect to width ($\tilde{\ell}_M$) is shown in Figure 5.9, where $\tilde{\ell}_M = \ell_M/W$.

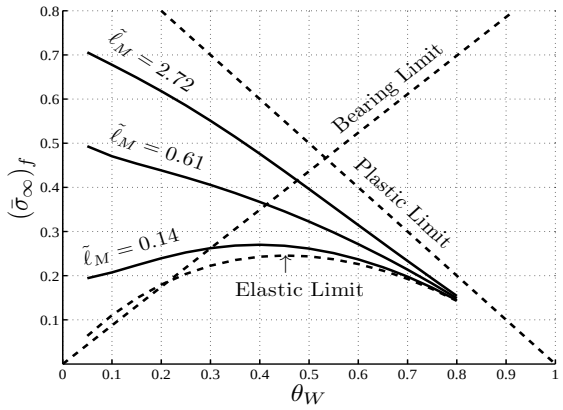

Figure 5.9: Normalized remote stress for CSD with LCL

For large joints (large W or small $\tilde{\ell}_M$) the optimum geometry of the joint corresponds to $\theta_W \approx 0.45$. Decreasing the hole radius results in lower net-tension strength even though the net section is larger. This is a consequence of the high stress concentration factor for a small values of θ_W. On the other hand, for small joints (large $\tilde{\ell}_M$) the maximum net-tension strength of the joint and its optimum geometry are defined when the net-tension strength equals the bearing strength.

5.4 Conclusions

The net-tension strength of single-fastener double-lap joints of isotropic quasi-brittle structures has been presented. The constant and the linear shapes of the material cohesive law were used in the problem formulation. The effects of the contact stress distributions in the hole boundary, the shape of the cohesive law, the joint size and the ratio between the hole radius and the joint width on the joint net-tension strength have been studied.

The contact stress distribution due to the presence of the bolt and the shape of the cohesive law affect the computation of the net-tension strength of the joint. Also, it is concluded that the first part of the cohesive law is an important parameter in the determination of the net-tension strength of these joints. The obtained predictions have been compared with the available experimental results with good agreement.

Finally, if the cohesive law of the material and its bearing strength are completely determined by some experimental procedure, the present model can be considered as a reliable alternative to the use of complex continuum damage models implemented in finite element models. Further, the obtained results are suited for fast definition of simple design charts and for effective parametric studies of mechanically fastened joints in isotropic quasi-brittle structures.

Chapter 6

Multi-fastener Double-lap Joints

6.1 Introduction

As mentioned in the previous chapter, mechanical fasteners are used extensively in aerospace and many other engineering structures as load transfer elements. However, the majority of mechanically fastened joints in these structures are multi-fastener joints. These joints act as weakness spots in the structure because of high stress concentrations due to the presence of holes and fasteners. Therefore, an accurate strength prediction of these joints is essential for a reliable design of the structure.

To determine a multi-fastener joint strength, first the load distribution between joint fasteners must be determined. Then, the critical bolt-hole is analyzed under its bearing and bypass stresses to obtain the joint strength according to the expected failure mode.

Load distribution in multi-bolt joints has been investigated by many authors using different methods. Some of them [117, 118] used experimental techniques in their investigations. Others used numerical methods such as the finite element method [119–121] and the boundary element method [122]. Analytical methods such as the complex variable approach [123, 124], the boundary collocation method [119, 125] and spring-based methods [126, 127] are also used to study the load distribution in these joints. Using these analyses it is possible to determine the critical fastener-hole. Accordingly, the ratio between the bearing and the bypass load of this hole can also be determined.

In multi-fastener joints, fasteners in the same row almost carry equal load portions [121–125] provided that all fasteners are symmetrically positioned in the joint and have the same clearance and friction conditions. In addition, the most loaded row in the joint is one of the most outer rows. Also, in single-column joints the critical fastener-hole is one of the most outer holes [117, 119, 120, 126, 127]. As a result, a multi-column joint can be approximated by a single-column joint. Figure 6.1 shows approximation of a multi-column double-lap joint as a single-column one, where L_{bi} is the bearing load of the corresponding fastener and i refers to the fastener number. Further, it is possible to approximate this single-column joint by a single-fastener joint as explained in the next section.

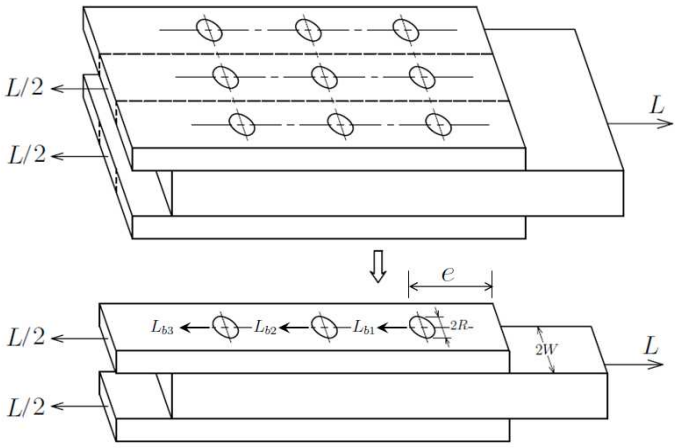

Figure 6.1: Approximation of a multi-column joint as a single column joint

As mentioned before, cleavage, shear-out, bearing and net-tension failures are the common failure modes encountered in mechanically fastened joints. Generally, the joints are designed to avoid shear-out and cleavage failures [121]. This can be achieved by using a sufficiently large edge distance and a sufficient number of off-axis plies in case of laminate joints that are made of unidirectional plies. Bearing failure is characterized by a permanent deformation of the hole. It is a gradual, progressive and in-plane failure mode. Being easy to detect and a non-catastrophic failure mode, it is desired in some practical applications [128]. Conversely, net-tension failure is an abrupt and catastrophic failure mode. In spite of its dangerousness, it is a primary failure mode in multi-bolt joints specially for large bypass loads [47, 49, 129]. Therefore, the net-tension strength prediction of these joints is of

great importance for a reliable design of many engineering structures.

In case of a single-fastener, the joint strength can be controlled with the joint geometry for a given material and applied load. A more complex load situation is encountered in multi-fastener joints. This is because of the interaction of the bearing-bypass stress concentrations. Therefore, the bypass stresses play an important role in controlling the failure of these joints [127]. A measure of the bypass ratio (ζ) can be defined as the ratio between bypass (L_B) and bearing load, L_b, as:

$$\zeta = \frac{L_B}{L_b} \tag{6.1}$$

The joint net-tension strength is the mean stress at failure plane ($\sigma_N = L/(2(W-R)t)$ just before failure. L is the sum of the bearing and the bypass load; in the most outer row it is the total load transferred by the joint. σ_N can be normalized with respect to the material strength σ_u as: $\bar{\sigma}_N = \sigma_N/\sigma_u$. Also, it is related to the normalized total remote stress ($\bar{\sigma}_\infty = \sigma_\infty/\sigma_u = L/(2Wt\sigma_u)$) and the normalized bearing stress ($\bar{\sigma}_b = \sigma_b/\sigma_u = L_b/(2Rt\sigma_u)$) by:

$$\bar{\sigma}_N = \frac{\bar{\sigma}_\infty}{1-\theta_W} = \frac{\bar{\sigma}_b \theta_W (1+\zeta)}{1-\theta_W} \tag{6.2}$$

For constant geometry -constant θ_W- the brittle failure is reached when the relative size of the FPZ with respect to the joint size, $\bar{\ell}_{\mathrm{FPZ}} = \ell_{\mathrm{FPZ}}/R$, is very small. This happens in very large joints. On the other extreme, when $\bar{\ell}_{\mathrm{FPZ}}$ is very large, the stress field in the whole joint approaches its material strength σ_u and the joint failure is ductile. This occurs in case of very small joints. The elastic and plastic limits are defined with respect to the normalized net-tension stress as:

$$(\bar{\sigma}_N)_{\mathrm{Elastic}} = \frac{1}{K_t} \qquad \text{and} \qquad (\bar{\sigma}_N)_{\mathrm{Plastic}} = 1 \tag{6.3}$$

where K_t is the stress concentration factor due to the combined bearing-bypass stresses, as shown in Figure 6.2 [105].

As the bypass load tends to zero, the joint response is the same as that of the single-fastener joint. Conversely, when it is close to the total applied load, the joint strength approaches that of the open hole specimen with the same material and geometry. For a material with a linear cohesive law, the expected net-tension

strength for these joints is shown in Figure 6.3. The predicted strengths in this figure correspond to $\theta_W = 0.128$ [75, 130].

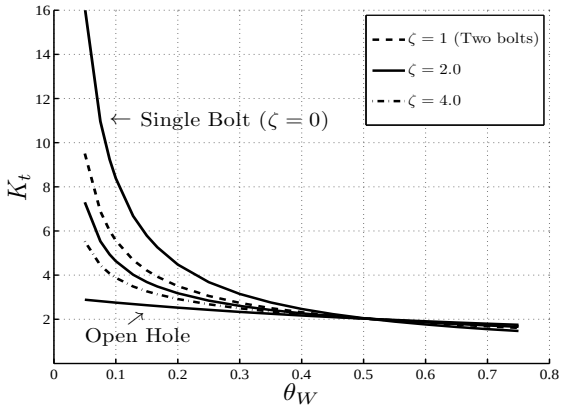

Figure 6.2: Stress concentration factors for multi-fastener joints

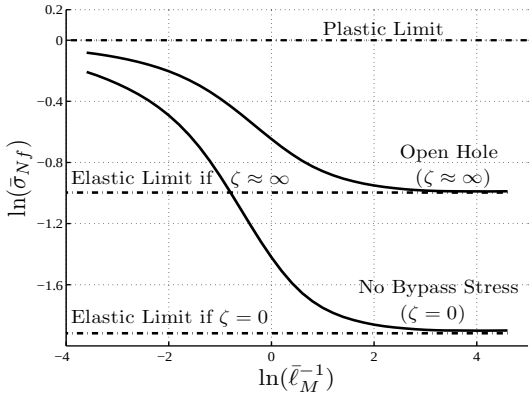

Figure 6.3: Expected net-tension strength

The literature shows that the problem of multi-fastener joints is very important in engineering structures. Also, it shows that the majority of the available models for predicting strength of multi-fastener joints are numerical models. It is well known that the analytical models have the advantage of its ability to predict the behavior of these joints in a few minutes. Thus, the main objective of this chapter is to develop an analytical model able to predict the net-tension strength of multi-fastener double-lap joints. The present model is based on the CZM which is able to predict the effect of the structure size on its strength. Moreover, it takes into account the material

softening that occurs before fracture which is neglected in most of the other models. The present model is restricted to the joints that are made of isotropic quasi-brittle materials.

This chapter is arranged as follows: In Section 6.2, a numerical model for net-tension failure of multi-fastener joints is presented. The obtained predictions are presented in Section 6.3. A general discussion is introduced in Section 6.4, where a simple analytical model for calculating the bypass to the bearing load ratio of the critical bolt in the joint is described. Moreover, it is explained how to find the optimum design of the joint. Finally, at the end of the chapter the conclusions are summarized.

6.2 Mathematical Formulation of the Problem

Multi-fastener joints can be modeled as a single-fastener joint under combined bearing-bypass loading conditions as shown in Figure 6.4 (a). As mentioned before, L_b represents the load supported by the critical fastener, whilst L_B represents the corresponding bypass load. The present formulation is based on the CZM. It is one of the few models (or the only model) that takes into account the cohesive law explicitly. In the previous chapter it is shown that the shape of the cohesive law affects the computation of net-tension strength of bolted joints [130]. Also, it has been confirmed that the linear cohesive law can represent any cohesive law when the slope of its initial part is adjusted in a proper way [75, 111]. Thus, only a triangular shape of the material cohesive law is considered in the present model, Figure 6.4 (b).

It is necessary to point out, again, that the following model is only applicable to the joints that are made of elastic isotropic quasi-brittle materials with localized (or extrinsic) dissipation mechanisms.

The actual stress profile due to the fastener presence is complex and dependent on several factors. Material properties of the fastener and connected parts as well as the fastener-hole friction and clearance are some of these factors. To develop a simple analytical model for the strength prediction of these joints it is not convenient to take all these factors into account. As a consequence, the following assumptions are imposed in the present formulation: (1) a cosine stress profile due to the presence

of the fastener is assumed and (2) the secondary bending and the fastener-hole clearance are neglected.

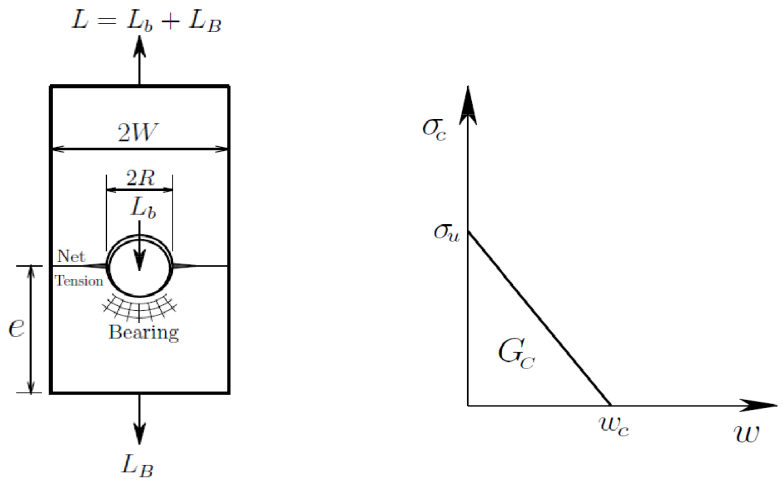

(a) Simplified multi-fastener joint (b) Linear cohesive law

Figure 6.4: Joint geometry, loading and its material cohesive law

A global solution of this problem can be obtained by applying the principle of superposition to three problems as shown in Figure 6.5. The first one is an open hole specimen with critical crack length ℓ_{FPZ} and subjected to a remote bypass load L_B. The second problem is a bolted-hole specimen with the same crack under bearing load L_b and a remote stress due to the bearing load $\sigma_{br} = L_b/(2Wt)$. Finally, the third one is a specimen with cohesive stress σ_c at the FPZ.

Provided that linear response and small displacements conditions are valid, Dugdale's finite stress condition can be imposed and given by [67, 72]:

$$K_E + K_{\sigma_c} = 0 \tag{6.4}$$

where $K_E = \bar{\sigma}_N \sigma_u \sqrt{R} \bar{K}_E \left(\bar{\ell}_{\text{FPZ}}, \theta_W, \zeta\right)$. K_E includes the SIF due to the bypass load (K_{rB}) and that of the fastener bearing load (K_f), as will be explained. Equation(6.4) can be written in normalized form as:

$$\sigma_u \sqrt{R} \left(\bar{\sigma}_N \bar{K}_E + \sum_{i=1}^{n} (\bar{\sigma}_c)_i (\bar{K}_{\sigma_c})_i \right) = 0 \tag{6.5}$$

The normalized SIF due to the cohesive stresses $\bar{K}_{\sigma_c}$ is given in Appendix A.2

[75, 89]. Using Equation (6.5), $\bar{\sigma}_N$ can be related to $(\bar{\sigma}_c)_i$ by:

$$\bar{\sigma}_N = (\bar{\sigma}_c)_i \; \beta_i(\bar{\ell}_{\mathrm{FPZ}}, \theta_W, \zeta) \tag{6.6}$$

The vector β_i which relates the normalized cohesive stress at position i to the normalized net-tension strength is given in Appendix A.2.

As before, the complete crack opening profile w is given by:

$$w = w_E + \sum_{i=1}^{n} (w_{\sigma_c})_i \tag{6.7}$$

where $w_E = (R\sigma_u \bar{\sigma}_N / E)\, \bar{w}_E \left(\bar{\ell}_{\mathrm{FPZ}}, \theta_W, \zeta\right)$. The normalized CODs $\bar{w}_E$ and $\bar{w}_{\sigma_c}$ are given in Appendix A.2 [75, 89, 112]. It is easy to write Equation (6.7) in a normalized form as:

$$\bar{w} = \bar{\sigma}_N \bar{w}_E + \sum_{i=1}^{n} (\bar{\sigma}_c)_i (\bar{w}_{\sigma_c})_i \tag{6.8}$$

where $\bar{w} = wE/(R\sigma_u)$ is the normalized total crack opening.The relation between the crack opening at position i and the stress at position j of the FPZ is:

$$\bar{w}_i = f_{ij}(\bar{\ell}_{\mathrm{FPZ}}, \theta_W, \zeta) \; (\bar{\sigma}_c)_j \tag{6.9}$$

The profile f_{ij} is described in Appendix A.2. To relate the obtained total COD to its critical value for a given cohesive law, it is more convenient to normalize it with respect to the material characteristic length as $\tilde{w}_N(\theta_W, \bar{\ell}_M, \zeta) = \bar{w}/(2\bar{\ell}_M)$.

For a given cohesive law $\bar{\sigma}_c(\bar{w})$, geometrical parameter θ_W and loading parameter ζ, the nominal stress can be obtained for a certain size of the FPZ using the system of equations in (6.6) and (6.9). The condition of the net-tension strength, the maximum nominal stress before failure, is:

$$\frac{\partial \bar{\sigma}_N}{\partial \bar{\ell}_{\mathrm{FPZ}}} = 0 \tag{6.10}$$

By solving the system of equations in (6.6) and (6.9) with the condition in Equation (6.10), it is possible to obtain an expression for $\bar{\sigma}_{Nf}(\theta_W, \bar{\ell}_M, \zeta)$, $\bar{\ell}_{\mathrm{FPZ}}(\theta_W, \bar{\ell}_M, \zeta)$ and the maximum normalized crack opening at failure $\tilde{w}_N(\theta_W, \bar{\ell}_M, \zeta)$. Also, the normalized bearing stress at net-tension failure $\bar{\sigma}_{bf}(\theta_W, \bar{\ell}_M, \zeta)$ and the normalized

remote stress at net-tension failure $(\bar{\sigma}_\infty)_f(\theta_W, \bar{\ell}_M, \zeta)$ can be obtained by means of equation 6.2.

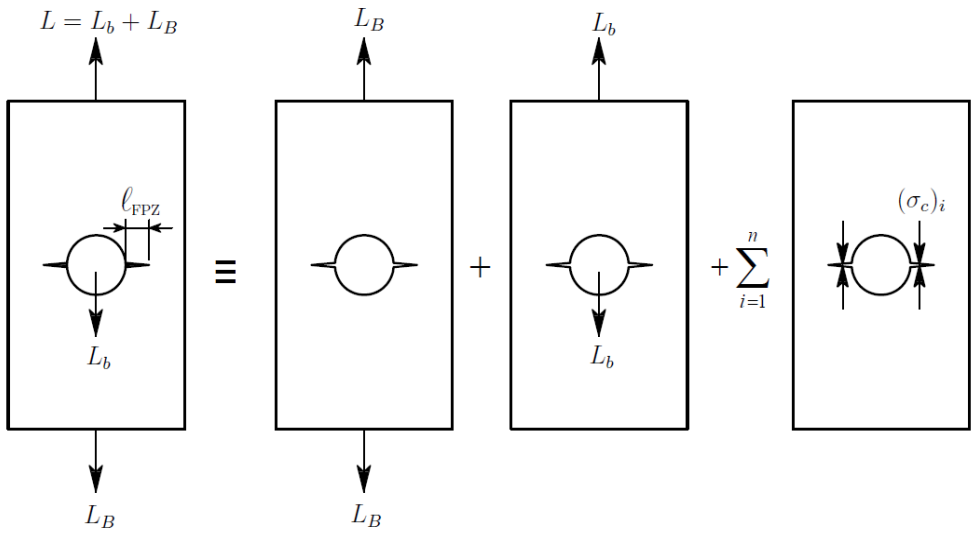

Figure 6.5: Bolted joint with bypass stresses as a superposition of three problems

K_E can be calculated as the superposition of the SIF due to the bypass load (K_{rB}) and the bearing load (K_f). It can be expressed as [113–115]:

$$K_E = K_{rB} + K_f = K_{rB} + \tfrac{1}{2}\left(K_{rb} + K_b\right) \tag{6.11}$$

To determine the SIF associated with the bearing load, we can consider the superposition of the problems shown in Figure 5.4. K_{rB}, K_{rb} and K_b can be written in a non-dimensional form in order to obtain K_E and its normalized form $\bar{K}_E$ as shown in Appendix A.2 [75, 113, 114].

Similarly, an expression for the COD due to the external loads (w_E) can be given by:

$$w_E = w_{rB} + \tfrac{1}{2}\left(w_{rb} + w_b\right) \tag{6.12}$$

where w_{rB}, w_{rb} and w_b are the CODs corresponding to the SIFs K_{rB}, K_{rb} and K_b respectively, while $\bar{w}_{rB}$, $\bar{w}_{rb}$ and $\bar{w}_b$ are their normalized forms, respectively. Expressions for these CODs are given in the Appendix [89, 112] according to the functions of the corresponding SIFs.

6.3 Results

The ability of the cohesive law to model the structure size effect on its strength has been confirmed [1, 12, 70, 75, 79, 82, 111, 130]. Again, the size effect law states that, for geometrically similar structures, the nominal strength decreases with increasing the size of the specimen. In this case, the relative size of the FPZ decreases and the specimen brittleness grows. Therefore, when θ_W is kept constant, the joint net-tension strength increases when decreasing the hole radius. The normalized net-tension strength with respect to the non-dimensional hole radius for different values of θ_W and ζ is presented in Figure 6.6.

The net-tension strength for small joints corresponds to the plastic limit and is independent of the bypass ratio. By increasing the joint size, the embrittlement on the structural strength results in a different nominal strength depending on the stress concentration factor. As can be seen in Figure 6.2 the stress concentration factor is larger for the bearing load than for the bypass load when $\theta_W < 0.5$. In these cases the remote load that causes the joint collapse grows with the bypass load. On the other hand, for $\theta_W > 0.5$ the net-tension strength is almost independent of the bypass ratio.

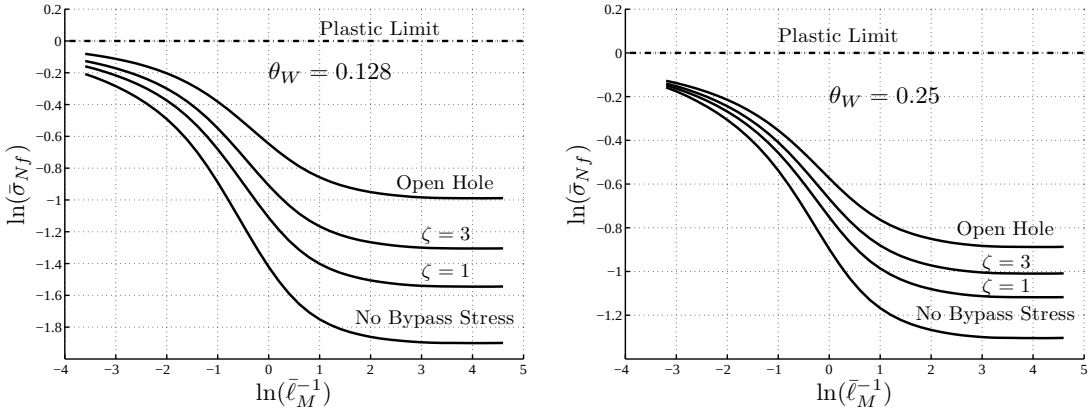

Figure 6.6: Normalized net-tension strength for different values of ζ and θ_W

The normalized CODs at failure for different values of θ_W and ζ are shown in Figure 6.7. Results predict larger crack openings in case of fastened joints with respect to open holed specimens. This is true for $\theta_W < 0.5$ and indeed reasonable because of the higher stress concentration associated with the fastener presence, as

shown in Figure 6.2. Also, the COD grows with lower bypass ratios due to higher stress concentrations. The important conclusion to be drawn from these plots is that, for small θ_W and large ζ the initial part of the cohesive law gains more importance in the net-tension strength computation of the joint.

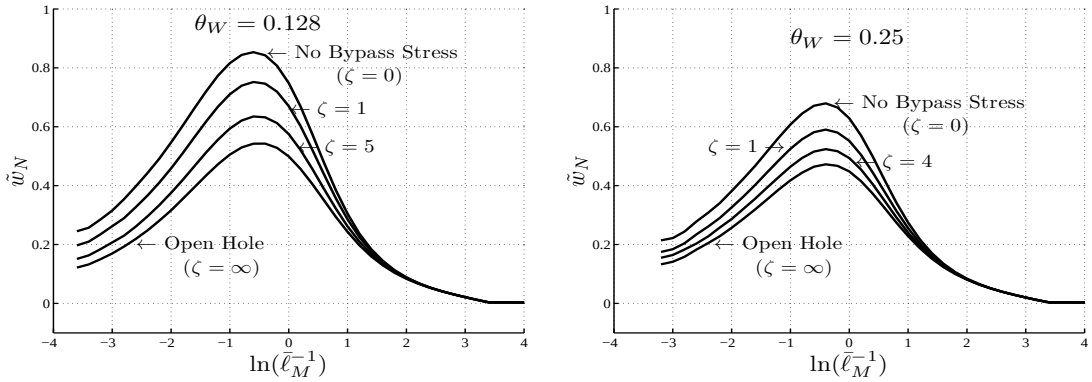

Figure 6.7: Normalized COD at failure for different values of ζ and θ_W

Figure 6.8 presents the normalized bearing-bypass stresses. In this figure $\bar{\sigma}_{nB}$ is the normalized bypass stress with respect to the net area and is given by:

$$\bar{\sigma}_{nB} = \frac{L_B}{2(W-R)t\sigma_u} = \frac{\zeta\bar{\sigma}_N}{1+\zeta} \tag{6.13}$$

while β is a measure of the bearing to bypass load ratio:

$$\beta = \frac{\bar{\sigma}_b}{\bar{\sigma}_{nB}} = \frac{1-\theta_W}{\zeta\theta_W} \tag{6.14}$$

The results of the model are consistent with the experimental results (⧫ and ◊) of Crews et al. [131] and Hart-Smith [107], as shown in Figures 6.8 (a) and 6.8 (b), respectively. In Crew's work all tested specimens had the same hole radius $R = 3.198$ mm and the same width $2W = 50$ mm. In his work, the net-tension failure is the dominant failure mode. Only one specimen (◊) failed in bearing mode and the others failed in net-tension. According to [132] the bearing strength S_b increases with respect to the bypass load. This can be explained by the compressive hoop stress caused by the bypass load under the bolt. This stress induces a confinement of fibers improving the compressive strength. This result is in accordance with the method presented in [26] for the determination of the elastic limit. On the other

hand, according to the point stress method applied in [26] the bearing strength decreases with the bypass load. However, in the present work S_b is assumed to be size, geometry and β independent as in Hart-Smith's and Crews's work [107, 131]. The bearing limit ($\bar{S}_b = S_b/\sigma_u$) shown in Figure 6.8 (a) is that of the $[0/45/90/-45]_{2s}$ graphite/epoxy laminate [131], where $S_b = 518$ MPa and $\sigma_u = 414$ MPa. In this figure the net-tension failure is defined below the bearing limit between the elastic and plastic limits. Results show that for small values of β the net-tension failure is the dominant failure mode.

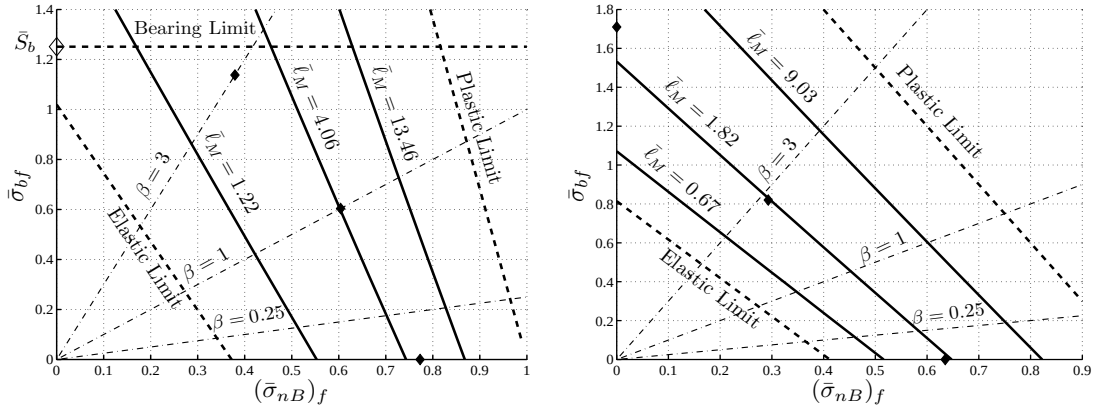

(a) Bearing-bypass stresses at failure, $\theta_W = 0.128$

(b) Bearing-bypass stresses at failure, $\theta_W = 0.25$

Figure 6.8: Normalized bearing-bypass stresses at net-tension failure

In Hart-Smith's work, the tested specimens are made of $[0/45/90/-45]_{2s}$ graphite/epoxy laminate with $\sigma_u = 468$ MPa. All specimens had a hole radius $R = 3.175$ mm and width $2W = 25$ mm. Also, all tested specimens failed in tension and therefore the bearing strength was not defined.

6.4 Discussion

6.4.1 Load distribution of single-column double-lap joints

For multi-bolt joints, determination of the load distribution between joint fasteners is of capital importance in their strength prediction. Fastener stiffness and stiffness of the connected parts as well as the bolt-hole clearance and the number

of bolts are the most important parameters on the load sharing between the joint fasteners.

Figure 6.9 (a) shows a single-column double-lap joint where t_I, t_O, E_I and E_O are the thicknesses of the inner and the outer plates and their corresponding Young's moduli respectively, while q and E_f are the fastener spacing and the fastener Young's modulus.

A simple spring model for load distribution analysis of these joints is shown in Figure 6.9 (b). In this model the non-linearity due to the bearing damage, the bolt-hole clearance and the secondary bending are neglected. k_I and k_O are the stiffnesses of the inner and the outer plates, respectively, while k_f and i are the fastener stiffness and the fastener number.

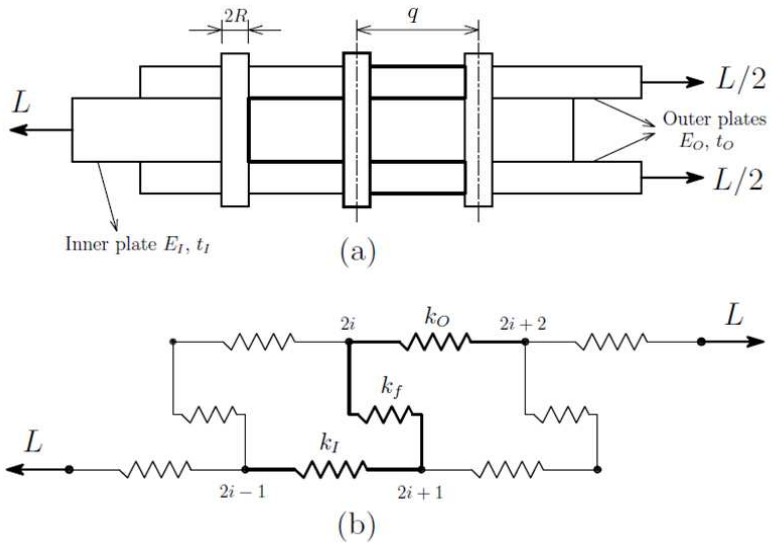

Figure 6.9: A double lap joint and a spring model for calculating its fasteners load sharing

The equilibrium equation, in matrix form, of an arbitrary bolt i is given by:

$$\begin{bmatrix} k_I & 0 & -k_I & 0 \\ 0 & k_O + k_f & -k_f & -k_O \\ -k_I & -k_f & k_I + k_f & 0 \\ 0 & -k_O & 0 & k_O \end{bmatrix} \begin{bmatrix} u_{2i-1} \\ u_{2i} \\ u_{2i+1} \\ u_{2i+2} \end{bmatrix} = \begin{bmatrix} L_{2i-1} \\ L_{2i} \\ L_{2i+1} \\ L_{2i+2} \end{bmatrix} \tag{6.15}$$

The global equilibrium equation is obtained by assembling the individual bolt equi-

librium equations relating the loads $\{L\}$ and the nodal displacements $\{u\}$. Since the global stiffness matrix and the global load vector are known, the global equilibrium equation can be solved for the displacement vector. Finally, the normalized load carried by any bolt i ($\bar{L}_{bi}$) can be easily determined as: $\bar{L}_{bi} = L_{bi}/L = k_f(u_{2i+1} - u_{2i})/L$ and the normalized bypass load ($\bar{L}_{Bi}$) as: $\bar{L}_{Bi} = (k_I(u_{2i-1} - u_{2i+1}) - k_f(u_{2i+1} - u_{2i}))/L$.

Practically, there are several empirical formulas used for the fastener stiffness calculation in lap-joints. Among these equations, Huth's [133] formula has the advantage of its applicability to double lap joints and is given by:

$$\frac{1}{k_f} = \left(\frac{t_I + t_O}{4R}\right)^m \frac{b}{N}\left(\frac{1}{t_I E_I} + \frac{1}{N t_O E_O} + \frac{1}{2 t_I E_f} + \frac{1}{2N t_O E_f}\right) \tag{6.16}$$

where m and b are two empirical parameters that are depend on the type and the material of the joint, while N equals 1 for single-lap and equals 2 for double-lap joints. It must be pointed out that in Huth's equation the fastener tightening and the fastener-hole clearance are not taken into account. The stiffness k_f combines the fastener stiffness and the local deformations of the plates. Therefore, the different terms in the parenthesis of Equation (6.16) represent the compliance of the inner and outer plates and that of the fastener.

Neglecting the hole effect, the connected parts between the fasteners can be approximated as bar elements and, therefore, their stiffnesses are given by:

$$k_I = \frac{2W t_I E_I}{q} \quad \text{and} \quad k_O = \frac{4W t_O E_O}{q} \tag{6.17}$$

Figure 6.10 shows the load distribution in three- and four-fastener double-lap joints based on the described model. The joint plates are of the same material, namely quasi-isotropic multi-layer symmetrical glass fiber laminates (GFRP), as described in [121]. The Young's moduli of the connected plates are $E_x = E_y = E_I = E_O = 25$ GPa, while the joint dimensions are $t_I = 2t_O = 30$ mm, $R = 7$ mm, $W = 30$ mm and $q = 60$ mm. The bolts are made of stainless steel with $E_f = 200$ GPa. The parameters that define the joint type in Equation (6.16) are taken as reported in reference [133]: $N = 2$, $m = 2/3$ and $b = 4.2$.

For symmetric double-lap joints with constant thickness and material properties

(Figure 6.9), the bypass to the bearing load ratio of the first, critical, row (ζ) depends on the two relative stiffnesses ($\bar{k}_O$ and $\bar{k}_I$) and the number of bolts (n): $\zeta(\bar{k}_O, \bar{k}_I, n)$, where $\bar{k}_O = k_O/k_f$ and $\bar{k}_I = k_I/k_f$. In the typical case in which $\bar{k}_O = \bar{k}_I = \bar{k}$, the load distribution between bolts depends on the relative stiffness $\bar{k}$. Using the empirical parameters, m and b, as described in [133] for bolted graphite/epoxy joints, the empirical Equation (6.16) results in $\bar{k} = 5.56$.

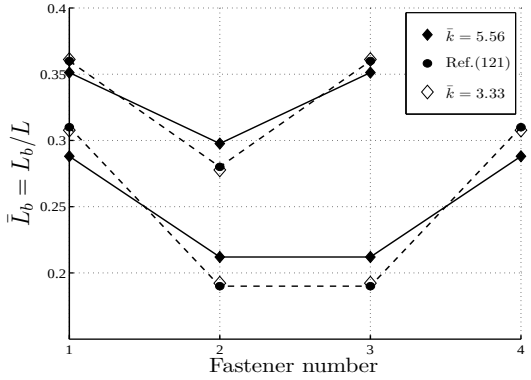

Figure 6.10: Load distribution in three- and four-fastener double lap joints

Since the current joint is made of GFRP, a better fitting to the results obtained by the finite element analysis [121] is found with $\bar{k} = 3.33$. Therefore, the discrepancy observed in Figure 6.10 can be assigned to the stiffness approximation.

The variation of ζ with respect to the number of bolts in the joint for different $\bar{k}$ is shown in Figure 6.11. For very stiff fasteners or very compliant arms, $\bar{k}$ tends to zero and ζ tends to one for any number of bolts. This means that only the bolts in both extremes of the column would be working. Conversely, for very compliant fasteners with stiff arms the bypass loading is equally distributed between the joint bolts and the parameter $\zeta = n - 1$.

On top of that, joints that are made of ductile materials are able to redistribute the bypass load among the bolts by means of plasticity at the hole boundary. This plastic flow contributes more to the reduction of fastener stiffness than to the reduction of the plate stiffness. As a result, the load is uniformly distributed between the bolts. This means that the number of bolts is of great importance on the load sharing between joint fasteners in that case. This is not the case for joints that are made of quasi-brittle materials -such as laminated composites- due to its brittle

nature. These materials are not able to relief the stress concentration. As a consequence, increasing the number of bolts -over a certain number- has a slight effect on the load distribution between the bolts.

Quasi-brittle materials have little or null ability to redistribute the load between the bolts by plastic flow in the net-tension area. But the fastener yielding and the stable bearing failure acts by reducing the fastener stiffness, thus helping to redistribute the load. Therefore, in joints with small θ_W ratios the onset of bearing damage produces a load redistribution that reduces the fastener load.

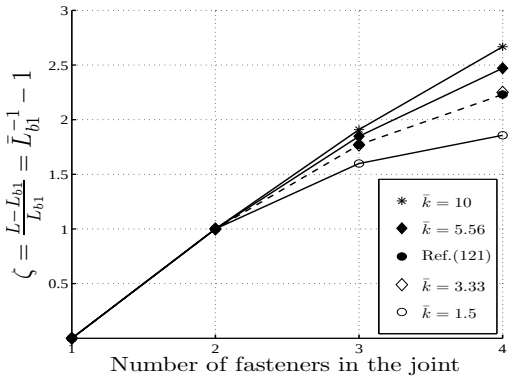

Figure 6.11: Variation of ζ with the number of fasteners in the joint

6.4.2 Optimal joint

When considering the optimal design of a mechanically fastened joint, the maximum joint strength is the objective. This goal can be obtained by changing some design variables under given constraints. Fastener-hole radius, joint width and hole-diameter-to-width ratio are among the geometrical design variables. If there are limitations to the joint dimensions, its maximum strength is attained at the optimum value of the parameter ζ.

Normally, the maximum joint strength is expected around the transition between the bearing and the net-tension failures. Bearing stress at failure against θ_W for different values of $\bar{\ell}_M$ and ζ is shown in Figure 6.12. In this figure and the next one the elastic and plastic limits are defined by means of Equations (6.2) and (6.3), whereas the bearing limit is for the $[0/45/90/-45]_{2s}$ graphite/epoxy laminate [131].

In addition, the net-tension failure is defined below the bearing limit and between the elastic and plastic limits.

For a joint with specified material and number of bolts, the optimum geometric parameter θ_W for a constant radius (constant $\bar{\ell}_M$) is obtained at the limit between the bearing and the net-tension failures. This is specially true for small joints (large $\bar{\ell}_M$) and small values of ζ. This optimum geometry produces a joint with maximum net-tension strength and minimum joint weight. Also, it is observed that for the same joint, as ζ increases, the failure mode turns from bearing to net-tension failure.

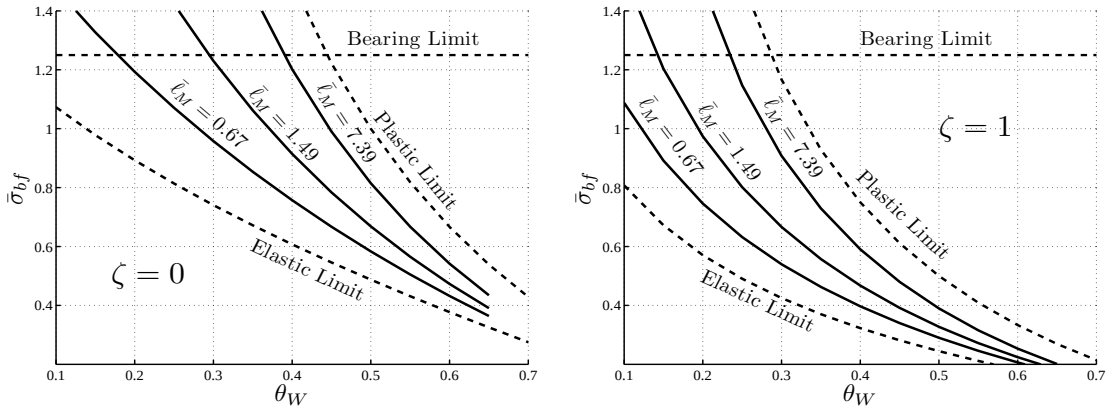

(a) Normalized bearing stress for single-bolt joint

(b) Normalized bearing stress for two-bolt joint

Figure 6.12: Normalized bearing stress at failure with respect to θ_W for different hole radiuses

Sometimes the design constraints are on the joint width, its own material and number of fasteners. In this situation the maximum strength of the joint is attained by changing the fastener-hole radius until the optimum joint geometry is obtained. Figure 6.13 shows the normalized total remote stress at failure against θ_W for different values of the normalized joint width, where $\tilde{\ell}_M = \ell_M/W$ is the inverse normalized width with respect to the material characteristic length of the joint.

For large joints (small $\tilde{\ell}_M$) the optimum geometry corresponds to $\theta_W \approx 0.45$ in case of single-fastener joints while it corresponds to $\theta_W \approx 0.3$ for two-fastener joints. In both cases the net-tension strength decreases if the hole radius decreases, in spite of the net area being larger. This is because of the high stress concentrations

associated with small θ_W as shown in Figure 6.2. Otherwise, for small joints (large $\tilde{\ell}_M$) the optimum joint geometry and its maximum strength are obtained when the net-tension strength and the bearing strength are equal.

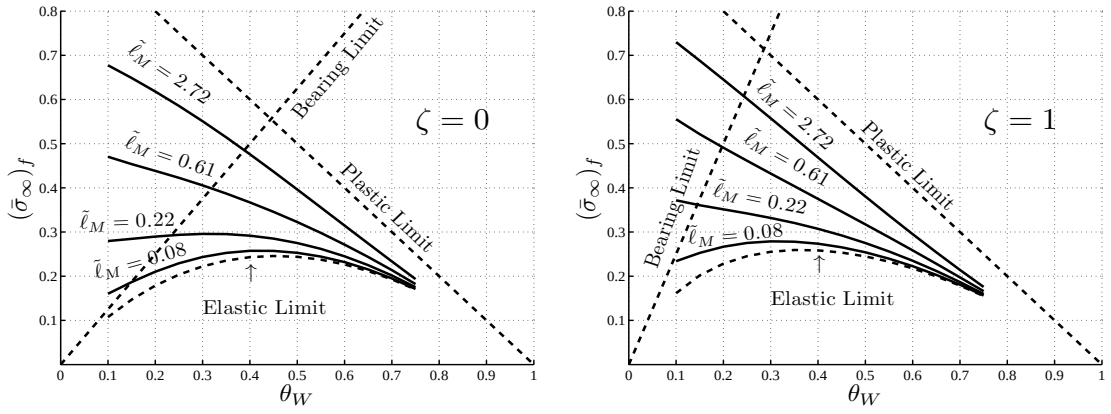

(a) Normalized remote stress for single-bolt joint (b) Normalized remote stress for two-bolt joint

Figure 6.13: Normalized remote stress at failure with respect to θ_W for different joint widths

An important conclusion from Figure 6.13 is that, when a single-fastener joint is designed for its optimum geometry, increasing the number of bolts has a very slight effect on its strength. However, increasing the number of bolts has a significant effect on the joint strength when the joint is designed for its new optimum geometry. That is, when we have more than one bolt the optimal geometry moves to smaller values of θ_W. For example, the optimum geometry of the joint of $\tilde{\ell}_M = 0.61$ with a single-fastener is $\theta_W \approx 0.33$ and its maximum strength is $(\bar{\sigma}_\infty)_f \approx 0.4$. Adding another bolt to this joint with the current geometry almost does not affect its strength. Whereas, when the two-bolt joint of $\tilde{\ell}_M = 0.61$ is used with its optimum geometry ($\theta_W \approx 0.2$), the maximum strength grows from $(\bar{\sigma}_\infty)_f \approx 0.4$ to $(\bar{\sigma}_\infty)_f \approx 0.5$.

When the joint geometry is mandatory, its maximum strength is reached by defining the optimum ζ to be used. For a given θ_W the optimum ζ is defined at the bearing limit in Figure 6.8 for each value of the hole radius by means of Equation (6.14). The optimum number of bolts to be used in the joint can be determined using this optimum ζ and a plot similar to Figure 6.11.

6.5 Conclusions

An analytical model able to predict the net-tension strength of multi-fastener double-lap joints is presented. The model is based on the cohesive zone model and is restricted to joints that are made of isotropic quasi-brittle materials. The effect of the bypass loads on the optimum geometry of the joint and, consequently, on its maximum strength has been studied. Also, a simple analytical spring-based model has been used for calculating the bypass to the bearing load ratio of the critical fastener in the joint.

The cohesive zone model is able to predict the joint size effect on its strength. The initial part of the cohesive law is an important parameter in joint strength computation. For small ratios of hole radius to joint width, as the bypass load increases, this initial part gains more importance in the computation of the joint net-tension strength.

An important conclusion is that, when a single-fastener joint is designed with its optimum geometry, increasing the number of bolts has a slight effect on its strength. But, if more than one bolt is used, the bypass load increases and a new geometric optimum can be found. This optimum design corresponds again to the condition of simultaneous bearing and net-tension failure. Furthermore, it is advisable for designers to even reduce a little bit the hole radius so that failure happens in the bearings. This brings two advantages together, namely, that it is possible to detect damage of the structure thus precluding catastrophic failure nd that, when three or more bolts are used, the non-linearity of the bearing bearing deformation helps in redistributing the load from the bolts of the outer rows to the central bolts.

Finally, the obtained results can be considered as valuable design charts for the double lap joints that are made of isotropic quasi-brittle materials. An important requirement for that is that the material cohesive law and the bearing strength of the joint be thoroughly defined by means of some experimental procedure.

Chapter 7

Conclusions and Future Work

7.1 Conclusions

Simple analytical models based on the physically-based CZM are introduced for the strength and the size effect predictions of quasi-brittle structures with holes. Various loading conditions are considered in this work. First, a model for structures with OHs and subjected to a biaxial loading condition is developed. Also, models for net-tension strength of double-lap joints under bearing and under coupled bearing-bypass loading conditions are introduced.

In light of the results and the discussions introduced in the previous chapters, the following conclusions can be drawn.

The CZM is able to predict the size effect on the strength of the structure. The shape of the material cohesive law affects the computation of the nominal strength of OH structures as well as the net-tension strength of the mechanically fastened joints. Materials with constant cohesive law resulted in higher nominal strength than materials with other shapes of the traction law. This is because the former materials are less notch sensitive than the latter ones. The initial part of the cohesive law and its slope are the most important parameters in strength predictions. For small ratios of hole radius to specimen width, or to joint width, these parameters gain more importance in the strength computation. Also, the linear cohesive law can represent any other cohesive law when the slope of its initial part is adjusted in a proper way. This is especially true when the biaxiality load ratio, λ, approaches one in case of OH specimens and for high values of the bypass load in case of multi-faster

joints.

For OH specimens under biaxial loading conditions, the nominal strength and the failure envelope have been obtained for different sizes of specimens. As the hole radius tends to zero, the Rankine failure envelope is reached. This is due to the onset criterion defined in the cohesive law. To reach another failure surface, the adopted CZM must be modified to take into account the stresses parallel to the crack in the strength onset criterion of the cohesive law. As for CDTs, a modification to the ASM has been introduced by imposing the Von-Mises failure criterion instead of the adopted Rankine type; and the ellipsoidal failure type is reached as the hole radius tends to zero. It is found that the modified ASM provides a more accurate strength prediction than that obtained with the other models in case of materials that exhibit an ellipsoidal failure surface.

For double-lab joints, analytical models capable of predicting the net-tension strength of single- and multi-fastener joints are presented. All models are based on the CZM and are restricted to joints that are made of isotropic quasi-brittle materials.

In case of single-fastener joints, the constant and the linear shapes of the material cohesive law were used in the problem formulation. In addition, uniform and cosinusoidal stress distributions on the hole edge due to the presence of the bolt are considered. The effects of the contact stress distributions, the shape of the cohesive law, the specimen size and the ratio between hole radius and the joint width on the joint strength have been studied. Results showed that the predicted net-tension strength for the uniform stress distribution is higher than that obtained with the cosinusoidal one. This is because of the lower stress concentration factor associated with the uniform stress distribution due to the larger contact area between the bolt and the hole surface. However, the cosinusoidal stress distribution is more realistic when modeling mechanically-fastened joints.

For multi-fastener joints, only the linear cohesive law and the cosinusoidal stress distribution are used in the mathematical formulation of the problem. The effect of the bypass loads on the optimum geometry of the joint and, consequently, on its maximum strength has been studied. For this purpose, a simple analytical spring-based model has been developed for calculating the load sharing between the joint fasteners and, thus, the bypass to the bearing load ratio of the critical fastener in

the joint. An important conclusion is that, when a single-fastener joint is designed with its optimum geometry, increasing the number of bolts has a slight effect on its strength. But if more than one bolt is used, the bypass load increases and a new optimum geometry can be found. This optimum design corresponds to the condition of simultaneous bearing and net-tension failure. Furthermore, it is advisable for designers to even reduce a little bit the hole radius so that failure happens in the bearings. This brings two advantages together, namely, that it is possible to detect damage of the structure thus precluding catastrophic failure, and that when three or more bolts are used, the non-linearity of the bearing deformation helps in redistributing the load from the bolts of the outer rows (the critical bolts) to the central bolts.

Generally, one of the most important conclusions in this work is that the initial part of the CL and its slope are the most important parameters in strength predictions. This mean that the fracture toughness is not an appropriate parameter to adjust the characteristic lengths used in the CDTs because only the first part of the CL is important in strength computing. Also, as shown in the presented results, failure is reached before the FPZ is completely developed and the crack opening at failure is less than its critical value. Hence, failure is reached before the regime of self-similar crack growth. Therefore, self-similar crack growth is not necessary condition in the presented models.

The main conclusion of the present work is that the introduced models are able to create simple design charts that would help designers to quickly determine the strength of structures with open holes and for double-lap joints made of isotropic quasi-brittle materials. An important requirement is that the material cohesive law and the bearing strength, in case of double-lap joints, be thoroughly defined by means of some experimental procedure. The introduced models are applicable to many materials that are of interest in industry. Ceramics, some polymers, metals under fatigue loads and delamination and ply-splitting resistant laminates are examples of these materials.

Finally, it must be emphasized that in case of laminated composites the material properties that fed up the introduced CZM models are the homogenized properties of the laminate. Since stacking sequence of a laminate is expected to affect its cohesive stresses and its bulk properties, two laminates with different stacking sequences are

considered two different materials with different cohesive laws. For anisotropic or orthotropic layered plates that are not fulfill the hypotheses of the presented models all expressions of the SIF and COD must be corrected.

7.2 Future Works

Probably the most interesting areas of work related to that presented in this thesis include:

(1) Determination of the cohesive law for the most applicable quasi-brittle materials such as the thin-ply laminates with different stack sequences. This could be done experimentally or by micromechanical models to, at least, obtain the general shape of the cohesive law.

(2) Determination of the bearing strength of the joint material to enable optimization of its geometry using the present model.

(3) The application of the open hole model to strength prediction of other shapes of cut-outs. Elliptical shape is an important example to be studied.

Bibliography

[1] Z. P. Bažant and J. Planas. *Fracture and size effect in concrete and other quasi-brittle materials*. CRC Press, Boca Raton, Florida, first edition, 1998.

[2] J. F. Labuz and L. Biolzi. Characteristic strength of quasi-brittle materials. *International Journal of Solids and Structures*, 35:4191–4203, 1998.

[3] J. Lee and C. Soutis. Measuring the notched compressive strength of composite laminates: specimen size effects. *Composites Science and Technology*, 68:2359–2366, 2008.

[4] Z. P. Bažant. Scaling theory for quasibrittle structural failure. *Proceeding of National Academic Sciences USA*, 101(37):13400–13407, 2004.

[5] Z. P. Bažant. Size effect in blunt fracture: Concrete, rock, metal. *Journal of Engineering Mechanics*, 110(4):518–535, 1984.

[6] Z. P. Bažant. Concrete fracture models: testing and practice. *Engineering Fracture Mechanics*, 69:165–205, 2002.

[7] Z. P. Bažant. Scaling of quasi-brittle fracture: Asymptotic analysis. *International Journal of Fracture*, 83:19–40, 1997.

[8] Z. P. Bažant. Size effect. *International Journal of Solids and Structures*, 37: 69–80, 2000.

[9] Z. P. Bažant and L. Cedolin. *Stability of Structures: Elastic, Inelastic, Fracture and Damage Theories*. Oxford University Press, New York, USA, 1991.

[10] Z. P. Bažant. Scaling of quasibrittle fracture: Hypotheses of invasive and lacunar fractality, their critique and weibull connection. *International Journal of Fracture*, 83:41–65, 1997.

[11] Z. P. Bažant and Q. Yu. Universal size effect law and effect of crack depth on quasi-brittle structure strength. *Journal of Engineering Mechanics*, 135(2): 78–84, 2009.

[12] P. Maimí, E. V. González, N. Gascons, and L. Ripoll. Size effect law and critical distance theories to predict the nominal strength of quasibrittle structures. *Applied Mechanics Reviews*, 65(2); doi: 10.1115/1.4024163, 2013.

[13] B. G. Green, M. R. Wisnom, and S. R. Hallet. An experimental investigation into the tensile strength scaling of notched composites. *Composites: Part A*, 38:867–878, 2007.

[14] M. R. Wisnom and S. R. Hallet. The role of delamination in strength, failure mechanisms and hole size effect in open hole tesile tests on quasi-isotropic laminates. *Composites: Part A*, 40:335–342, 2009.

[15] S. R. Hallet, B. G. Green, Jiang W.G., and M. R. Wisnom. An experimental and numerical invistigation into the damage mechanisms in notched composites. *Composites: Part A*, 40:613–624, 2009.

[16] C. Soutis and J. Lee. Scaling effects in notched carbon fibre/epoxy composites loaded in compression. *Journal of Materials Science*, 43:6593–6598, 2008.

[17] P. P. Camanho, P. Maimí, and C. G. Dávila. Prediction of size effects in notched laminates using continuum damage mechanics. *Composites Science and Technology*, 67:2715–2727, 2007.

[18] G. H. Erçin, P. P. Camanho, J. Xavier, G. Catalanotti, S. Mahdi, and P. Linde. Size effects on the tensile and compressive failure of notched composite laminates. *Composite Structures*, 96:736–744, 2013.

[19] H. Ahmad. Finit element-based stength prediction for notched and mechanically fastened woven fabriccomposites. PhD Thesis, Divison of Medical

and Aerospace Engineering, Faculty of Engineering and Physical Science, University of Surry, Guildford, United Kingdom., 2012.

[20] P. Cornetti, N. Pugno, A. Carpinteri, and D. Taylor. Finite fracture mechanics: A coupled stress and energy failure criterion. *Engineering Fracture Mechanics*, 73:2021–2033, 2006.

[21] D. Taylor. *The theory of critical distances. A new perspective in fracture mechanics*. Elsevier, first edition, 2007.

[22] D. Taylor. The theory of critical distances. *Engineering Fracture Mechanics*, 75:1696–1705, 2008.

[23] J. M. Whitney and R. J. Nuismer. Stress fracture criteria for laminated composites containing stress concentrations. *Journal of Composite Materials*, 8: 253–265, 1974.

[24] S. C. Tan. Laminated composites containing an elliptical opening.I. approximate stress analyses and fracture models. *Journal of Composite Materials*, 21:925–948, 1987.

[25] S. C. Tan. Effective stress fracture modes for unnotched and notched multidirectional laminates. *Journal of Composite Materials*, 22:322–340, 1988.

[26] P. P. Camanho and M. Lambert. A design methodology for mechanically fastened joints in laminated composite materials. *Composites Science and Technology*, 66:3006–3020, 2006.

[27] H. M. S. Belmonte, D. I. C. Manger, S. L. Ogin, P. A. Smith, and R. Lewin. Characterisation and modelling of the notched tensile fracture of woven quasi-isotropic GFRP laminates. *Composites Science and Technology*, 61:585–597, 2001.

[28] J. K. Kim, D. S. Kim, and N. Takeda. Notched strength and fracture criterion in fabric composite plates containing a circular hole. *Journal of Composite Materials*, 29:982–998, 1995.

[29] V. K. Srivastava. Notched strength prediction of laminated composite under tensile loading. *Materials Science and Engineering A*, 328:302–309, 2002.

[30] A. S. Rao, Y. Krishna, and B. N. Rao. Comparison of fracture models to assess the notched strength of composite/solid propellant tensile specimens. *Materials Science and Engineering A*, 385:429–439, 2004.

[31] B. S. Rao, R. Rudramoorthy, S. Srinivas, and B. N. Rao. Effect of drilling induced damage on notched tensile and pin bearing strengths of woven GFR-epoxy composites. *Materials Science and Engineering A*, 472:347–352, 2008.

[32] K. S. Ahmed, S. Vijayarangan, and A. C. B. Naidu. Elastic properties, notched strength and fracture criterion in untreated woven jute-glass fabric reinforced polyester hybrid composites. *Materials and Design*, 28:2287–2294, 2007.

[33] C. L. Hwan, K. H. Tsai, W. L. Chen, C. H. Chiu, and C. M. Wu. Strength prediction of braided composite plates with a center hole. *Journal of Composite Materials*, 0:1–12, 2011.

[34] B. L. Agarwal. Static strength prediction of bolted joint in composite material. *AIAA Journal*, 18(11):1371–1375, 1980.

[35] H. A. Whitworth, M. Othieno, and O. Barton. Failure analysis of composite pin loaded joints. *Composite Structures*, 59:261–266, 2003.

[36] H. A. Whitworth, O. Aluko, and N. A. Tomlinson. Application of the point stress criterion to the failure of the composite pinned joints. *Engineering Fracture Mechanics*, 75:1829–1839, 2008.

[37] J. C. Newman, Jr. A nonlinear fracture mechanics approach to the growth of small cracks. Technical Report 328, AGARD, 1983.

[38] P. Berbinau, C. Filiou, and C. Soutis. Stress and failure analysis of composite laminates with an inclusion under multiaxial compression tension loading. *Applied Composite Materials*, 8:307–326, 2001.

[39] M. E. Waddoups, J. R. Eisenmann, and B. E. Kaminski. Macroscopic fracture mechanics of advanced composite materials. *Journal of Composite Materials*, 5:446–454, 1971.

[40] D. Taylor, P. Cornetti, and N. Pugno. The fracture mechanics of finite crack extension. *Engineering Fracture Mechanics*, 72(7):1021–1038, 2005.

[41] A. R. Curtis and P. Grant. The strength of carbon fiber composite plates with loaded and unloaded holes. *Composite Structures*, 2(3):201–221, 1984.

[42] K. C. Schulz, P. Packman, and J. R. Eisenmann. A tension-mode fracture model for bolted joints in laminated composites. *Journal of Composite Materials*, 29:37–58, 1995.

[43] D. Leguillon. Strength or toughness? A criterion for crack onset at a notch. *European Journal of Mechanics A/Solids*, 21:61–72, 2002.

[44] D. Leguillon, D. Quesada, C. Putot, and E. Martin. Prediction of crack initiation at blunt notches and cavities - size effects. *Engineering Fracture Mechanics*, 74:2420–2436, 2007.

[45] H. M. S. Belmonte, S. L. Ogin, P. A. Smith, and R. Lewin. A physically-based model for the notched strength of woven quasi-isotropic CFRP laminates. *Composites, Part A*, 35:763–668, 2004.

[46] P. P. Camanho, G. H. Erçin, G. Catalanotti, S. Mahdi, and P. Linde. A finite fracture mechanics model for the prediction of the open-hole strength of composite laminates. *Composites: Part A*, 43:1219–1225, 2012.

[47] G. Catalanotti and P. P. Camanho. A semi-analytical method to predict net-tension failure of mechanically fastened joints in composite laminates. *Composite Science and Technology*, 76:69–76, 2013.

[48] R. M. O'Higgins, M. A. McCarthy, and C. T. McCarthy. Comparison of open hole tension characteristics of high strength glass and carbon fiber-reinforced composite materials. *Composites Science and Technology*, 68:2770–2778, 2008.

[49] A. Arteiro, G. Catalanotti, J. Xavier, and P. P. Camanho. Notched response of non-crimp fabric thin-ply laminates. *Composite Science and Technology*, 79:97–114, 2013.

[50] J. Wang, P. J. Callus, and M. K. Bannister. Experimental and numerical invistigation of the tension and compression strength of un-notched and notched quasi-isotropic laminates. *Composite Structures*, 64:297–306, 2004.

[51] G. S. O'Higgins, R. M. Padhi, M. A. McCarthy, and C. T. McCarthy. Experimental and numerical study of the open-hole tensile strength of carbon/epoxy composites. *Mechanics of Composite Materials*, 40(4):427–440, 2004.

[52] A. B. Morais. Open-hole tensile strength of quasi-isotropic laminates. *Composites Science and Technology*, 60:1997–2004, 2000.

[53] Y. Huang, S. H. Ha, J. Koyanagi, J. D. Melo, H. Kumazawa, and I. Susuki. Effects of an open hole on the biaxial strengths of composite laminates. *Journal of Composite Materials*, 44(20):2429–2445, 2010.

[54] A. R. Khamseh and A. M. Waas. Failure mechanisms of composite plates with a circular hole under remote static biaxial planar compressive loading. *Key Engineering Materials*, 120-121:463–488, 1996.

[55] I. M. Daniel. Behavior of graphite/epoxy plates with holes under biaxial loading. *Experimental Mechanics*, 20(1):1–8, 1980.

[56] P. D. Shah, J. D. Melo, C. A. Cimini, Jr, and M. Ridha. Evaluation of notched strength of composite laminates for structural design. *Journal of Composite Materials*, 44(2):2381–2392, 2010.

[57] F. Chang, R. A. Scott, and G. S. Springer. Failure of composite laminates containing pin loaded holes- Method of solution. *Journal of Composite Materials*, 18:225–278, 1984.

[58] A. Aktaş, R. Karakuzu, and B. Türkiye. Failure analysis of two-dimensional carbon-epoxy composite plate pinned joint. *Mechanics of Composite Materials and structures*, 6:347–361, 1999.

[59] Y. Yan, W. Wen, F. Chang, and P. Shyprykevich. Experimental study on clamping effects on the tensile strength of composite plates with a bolt-filled hole. *Composites: Part A*, 30:1215–1229, 1999.

[60] B. Okutan, Z. Aslan, and R. Karakuzu. A study of the effect of various geometric parameters on the failure strength of pin-loaded woven-glass-fiber reinforced epoxy laminate. *Composite Science and Technology*, 61:1491–1497, 2001.

[61] B. İçten and R. Karakuzu. Progressive failure analysis of pin-loaded carbon-epoxy woven composite plates. *Composite Science and Technology*, 62:1259–1271, 2002.

[62] A. Riccio and L. Marciano. Effects of geometrical and material features on damage onset and propagation in single-lap bolted composite joints under tensile load: Part I - experimental studies. *Journal of Composite Materials*, 39(23):2071–2090, 2005.

[63] J. E. Jam and N. O. Ghaziani. Numerical and experimental investigation of bolted joints. *International Journal of Engineering, Science and Technology*, 3(8):285–296, 2011.

[64] A. A. Griffith. The phenomena of rupture and flow in solids. *Philosophical Transactions of the Royal Society of London. Series A, Containing Papers of a Mathematical or Physical Character,*, 221:163–198, 1921.

[65] C. E. Inglis. Stress in a plate due to the presence of cracks and sharp corners. *Institution of Naval Architects*, 55:219–241, 1913.

[66] G. Irwin. Analysis of stresses and strains near to the end of crack traversing a plate. *Trans, ASME Journal of Applied Mechanics*, 24:361–364, 1957.

[67] D. S. Dugdale. Yielding of steel sheets containing slits. *Journal of the Mechanics and Physics of Solids*, 8(2):100–104, 1960.

[68] G. I. Barenblatt. The mathematical theory of equilibrium cracks in brittle fracture. *Advances in Applied Mechanics*, 7(C):55–129, 1962.

[69] A. Hillerborg, M. Modéer, and P. E Petersson. Analysis of crack formation and crack growth in concrete by means of fracture mechanics and finite elements. *Cement and Concrete Research,*, 6(6):773–781, 11 1976.

[70] M. Elices, G. V. Guinea, J. Gómez, and J. Planas. The cohesive zone model: advantages, limitations and chalenges. *Engineering Fracture Mechanics*, 69: 137–163, 2002.

[71] Q. Yang and B. Cox. Cohesive models for damage evaluation in laminated composites. *International Journal of Fracture*, 133:107–137, 2005.

[72] C. Soutis, N. A. Fleck, and P. A. Smith. Failure prediction technique for compression loaded carbon fibre-epoxy laminate with open holes. *Journal of Composite Materials*, 25:1476–1498, 1991.

[73] C. Fan, P. Y. Ben Jar, and J. J. Roger Cheng. Cohesive zone with continuum damage properties for simulation of delamination developement in fiber composites and failure of adhesive joints. *Engineering Fracture Mechanics*, 75: 3866–3880, 2008.

[74] Q. Ye and P. Chen. Prediction of the cohesive strength for numerically simulating composite delamination via CZM-based FEM. *Composites: Part B*, 42: 1076–1083, 2011.

[75] P. Maimí, D. Trias, E. V. González, and J. Renart. Nominal strength of quasi-brittle open hole specimens. *Composites Science and Technology*, 72 (10):1203–1208, 2012.

[76] H. Ahmad, A.D. Crocombe, and P.A. Smith. Strength prediction in CFRP woven laminate bolted double-lab joints under quasi-static loading using XFEM . *Composites: Part A*, 56:192–202, 2014.

[77] K. Hollmann. Failure analysis of bolted composite joints exhibiting in-plane failure modes. *Journal of Composite Materials*, 30:358–383, 1996.

[78] G. Alfano. On the influence of the shape of the interface law on the application of cohesive-zone models. *Composites Science and Technology*, 66(6):723–730, 2006.

[79] J. Planas, M. Elices, G. V. Guinea, F. J. Gómez, D. A. Cendón, and I. Arbilla. Generalizations and specializations of cohesive crack models. *Engineering Fracture Mechanics*, 70:1759–1776, 2003.

[80] M. Elices, C. Rocco, and C. Roselló. Cohesive crack modelling of a simple concrete: Experimental and numerical results. *Engineering Fracture Mechanics*, 76:1398–1410, 2009.

[81] C. G. Dávila, C. A. Rose, and P. P. Camanho. A procedure for superposing linear cohesive laws to represent multiple damage mechanisms in the fracture of compoites. *International Journal of Fracture*, 158(2):211–223, 2009.

[82] S. Morel and N. Dourado. Size effect in quasibrittle failure: Analytical model and numerical simulations using cohesive zone model. *International Journal of Solids and Structures*, 48:1403–1412, 2011.

[83] P. P. Camanho and C. G. Dávila. *Mixed-Mode Decohesion Finite Element for the simulation of Delamination in Composite Materials*. TM-2002-211737. NASA, 2002.

[84] A. Turon, P. P. Camanho, J. Costa, and C. G.Dávila. A damage model for the simulation of delamination in advanced composites under variable-mode loading. *Mechanics of Materials*, 38(11):1072–1089, 11 2006.

[85] Z. P. Bažant and B. H. Oh. Crack band theory for fracture of concrete. *Materials and Structures*, 16(93):155–177, 1983.

[86] G. Markeset and A. Hillerborg. Softening of concrete in compression localization and size effects. *Cement and Concrete Research*, 25(4):702–708, 5 1995.

[87] E. V. González, P. Maimí, A. Turon, P. P. Camanho, and J. Renart. Simulation of delamination by means of cohesive elements using an explicit finite element code. *Computers, Materials and Continua*, 9(1):51–92, 2009.

[88] P. Maimí, P. P. Camanho, J. A. Mayugo, and C. G. Dávila. A continuum damage model for composite laminates: Part II - computational implementation and validation. *Mechanics of Materials*, 39:909–919, 2007.

[89] T. N. Williams, J. C. Newman, Jr, and P. M. Gullett. Crack-surface displacements for cracks emanating from a circular hole under various loading conditions. *Fatigue Fract Engng Mater Struct*, 34(4):250–259, 2010.

[90] S. Shin, R. Y. Kim, K. Kawabe, and S. W. Tasi. Experimental studies of thinply laminated composites. *Composites Science and Technology*, 67:996–1008, 2007.

[91] T. Yokozeki, Y. Aoki, and T. Ogasawara. Experimental characterization of strength and damage resistance properties of thin-ply carbon fiber/toughned epoxy laminates. *Composite Structures*, 82:382–389, 2008.

[92] Handbook. *MIL-HDBK-17-3F: Composite Materials Handbook, Polymer matrix composites: materials usage, design, and analysis*, volume 17, v. 3. U.S. Department of Defense, 2002. ISBN 0803133529.

[93] T. A. Sebaey, E. V. González, N. B. Lopes, P. Maimí, and J. Costa. Damage resistance and damage tolerance of dispersed CFRP laminates: Effect of the mismatch angle between plies. *Composite Structures*, 101:255–264, 2013.

[94] S. G. Lekhnitskii. *Theory of elasticity of an anisotropic body*. Holdenday, 1963.

[95] M. J. Hinton and P. D. Soden. Predicting failure in composite laminates: the background to the exercise. *Composites Science and Technology*, 58:1001–1010, 1998.

[96] Z. P. Bažant and E. P. Chen. Scaling of structural failure. *Applied Mechanics Reviews*, 50(10):593–627, 1997.

[97] M. R. Wisnom. Size effects in the testing of fibre-reinforced composites. *Composites Science and Technology*, 59:1937–1957, 1999.

[98] G. J. Dvorak and A. P. Suvorov. Size effect in fracture of unidirectional composite plates. *International Journal of Fracture*, 95:89–101, 1999.

[99] Z. P. Bažant, Y. Zhou, D. Novák, and I. M. Daniel. Size effect on flexural strength of fiber-composite laminates. *Journal of Engineering Materials and Technology*, 126:29–37, 2004.

[100] G. Bao and Z. Suo. Remarks on crack-bridging concepts. *Applied Mechanics Reviews*, 45(8):355–366, August 1992.

[101] M. Anvari, I. Scheider, and C. Thaulow. Simulation of dynamic ductile crack growth using strain-rate and triaxiality-dependent cohesive elements. *Engineering Fracture Mechanics*, 73(15):2210–2228, 10 2006.

[102] ABAQUS inc. Abaqus 6.12 user's manual, 2012.

[103] D 953-02. *Standard test method for bearing strength of plastics*, volume 08.01.Plastics. ASTM International. West Conshohochen, PA: 2002.

[104] D5961/D5961M-05e1. *Standard Test Method for Bearing Response of Polymer-Matrix Composite Laminates*, volume 15.03. Composite Materials. ASTM International. West Conshohochen, PA: 2005.

[105] W. D. Pilkey and D. F. Pilkey. *Peterson's Stress Concentration Factors*. John Wiley & Sons, Inc., New York, third edition, 2011.

[106] H. John, Jr. Crews, and G. S. Hong. Stress-concentration factors for finite orthotropic laminates with a pin-loaded hole. Technical Paper 1862, NASA, 1981.

[107] L. J. Hart-Smith. Bolted joints in graphite-epoxy composites. Technical Report NASA CR-144899, National Aeronautics and Space Administration, USA, 1977.

[108] S. D. Thoppul, J. Finegan, and R. F. Gibson. Mechanics of mechanically fastened joints in polymer-matrix composite structures - A review. *Composites Science and Technology*, 69:301–329, 2009.

[109] R. Ujjin. Prediction of bearing failure in pin-loaded laminates. PhD Thesis, School of Mechanical and Manufacturing Engineering, University of New South Wales, Sydney, Australia., 2007.

[110] J. Ekh and J. Schön. Effect of secondary bending on strength prediction of composite, single shear lapjoints. *Composite Science and Technology*, 65: 953–965, 2005.

[111] A. M. Kabeel, P. Maimí, N. Gascons, and E. V. González. Nominal strength of quasi-brittle open hole specimens under biaxial loading conditions. *Composites Science and Technology*, 87:42–49, 2013.

[112] H. Tada, P. C. Paris, and G. R. Irwin. *The Stress Analysis of Cracks Handbook*. American Society of Mechanical Engineers, New York, third edition, 2000.

[113] J. C. Newman, Jr. An improved method of collocation for the stress analysis of cracked plates with various shaped boundaries. Technical Report D-6376, NASA TN, 1971.

[114] D. J. Cartwright and A. P. Parker. Opening mode stress intensity factors for cracks in pin-loads joints. *International Journal of Fracture*, 18(1):65–78, 1982.

[115] S. H. Ju. Stress intensity factors for cracks in bolted joints. *International Journal of Fracture*, 84:129–141, 1997.

[116] C. Echavarría, P. Haller, and A. Salenikovich. Analytical study of a pin-loaded hole in elastic orthotropic plates. *Composite Structures*, 79:107–112, 2007.

[117] V. P. Lawlor, M. A. McCarthy, and W.F. Stanley. An experimental study of bolt-hole clearance effects in double-lap, multi-bolt composite joints. *Composite Structures*, 71:176–190, 2005.

[118] P. J. Gray, R. M. O'Higgins, and C. T. McCarthy. Effects of laminate thickness, tapering and missing fasteners on the mechanical behaviour of single-lap, multi-bolt, countersunk composite joints. *Composite Structures*, 107:219–230, 2014.

[119] E. Madenci, S. Shkarayev, and B Sergeev. Analysis of composite laminates with multiple fasterners. *International Journal of Solids and Structures*, 35 (15):1793–1811, 1998.

[120] C. T. McCarthy, M. A. McCarthy, and V. P. Lawlor. Progressive damage analysis of multi-bolt composite joints with variable bolt-hole clearances. *Composites: Part B*, 36:290–305, 2005.

[121] L. Feo, G. Marra, and A. S. Mosallam. Stress analysis of multi-bolted joints for FRP pultruded composite structures. *Composite Structures*, 94:3769–3780, 2012.

[122] J. M. Zhang. Design and analysis of mechanically fastened composite joints and repairs. *Engineering Analysis with Boundary Elements*, 25:431–441, 2001.

[123] Y. Xiong. An analytical method for failure prediction of multi-fastener composite joints. *International Journal of Solids and Structures*, 29:4395–4409, 1996.

[124] V. Kradinov, A. Barut, E. Madenci, and D. R. Ambur. Bolted double-lap composite joints under mechanical and thermal loading. *International Journal of Solids and Structures*, 38:7801–7837, 2001.

[125] B. Sergeev, E. Madenci, and D. R. Ambur. Influence of bolt spacing and degree of anisotropy in single-lap joints. *Computers and Structures*, 76:89–103, 2000.

[126] M. A. McCarthy, C. T. McCarthy, and G. S. Padhi. A simple method for determining the effects of bolt-hole clearance on load distribution in single-column multi-bolt composite joints. *Composite Structures*, 73:78–87, 2006.

[127] C. T. McCarthy and P. J. Gray. An analytical model for the prediction of load distribution in highly torqued multi-bolt composite joints. *Composite Structures*, 93:287–298, 2011.

[128] H. S. Li, S. Xia, and D. M. Luo. A probabilistic analysis for pin joint bearing strength in composite laminates using subset simulation. *Composites: Part B*, 56:780–789, 2014.

[129] J. Zhang, F. Liu, L. Zhao, and B. Fei. A novel characteristic curve for failure prediction of multi-bolt composite joints. *Composite Structures*, 108:129–136, 2014.

[130] A. M. Kabeel, P. Maimí, N. Gascons, and E. V. González. Net-tension strength of double lap joints taking into account the material cohesive law. *Composite Structures*, 112:207–213, 2014.

[131] J. H. Crews, Jr, and R. A. Naik. Combined bearing and bypass loading on a graphit/epoxy laminate. *Composite Structures*, 6:21–40, 1986.

[132] F. Liu, L. Zhao, S. Mehmood, J. Zhang, and B. Fei. A modified failure envelope method for failure prediction of multi-bolt composite joints. *Composite Science and Technology*, 83:54–63, 2013.

[133] H. Huth. Influence of fastener flexibility on the prediction of load transfer and fatigue life for multiple-row joints. *Fatigue in Mechanically Fastened Composite and Metallic Joints, ASTM STP927*, pages 221–250, 1986.

Appendices

A.1 Normalized SIFs and CODs for Single-fastener Joints

$$\bar{K}_b\left(\bar{\ell}_{\mathrm{FPZ}},\theta_W\right)=\begin{cases}(\theta_W^{-1}-1)\sqrt{\pi\left(1+\bar{\ell}_{\mathrm{FPZ}}\right)}f_{1\mathrm{U}}F_2 & \text{for Uniform Stress Distribution (USD)}\\ (\theta_W^{-1}-1)\sqrt{\pi\left(1+\bar{\ell}_{\mathrm{FPZ}}\right)}f_{1\mathrm{C}}F_2 & \text{for Cosinusoidal Stress Distribution (CSD)}\end{cases}$$

$$\bar{K}_{rb}\left(\bar{\ell}_{\mathrm{FPZ}},\theta_W\right)=(1-\theta_W)\sqrt{\pi\left(1+\bar{\ell}_{\mathrm{FPZ}}\right)}f_2F_2$$

$$\bar{K}_{\sigma_c}\left(\bar{\ell}_{\mathrm{FPZ}},\theta_W,i/n\right)=2\sqrt{\left(1+\bar{\ell}_{\mathrm{FPZ}}\right)/\pi}\;F_3F_4$$

$$\beta_i=-\frac{4(F_3)_i(F_4)_i}{\pi(1-\theta_W)F_1F_2}$$

where

$$f_{1\mathrm{U}}=\tfrac{2}{\pi}\sqrt{1-s}\,(s+0.519s^2-0.073s^3+0.092s^4+0.211s^5)\,[s+\tfrac{\pi}{2}(1-s)]$$

$$f_{1\mathrm{C}}=\tfrac{2}{\pi}\sqrt{1-s}\,(s+0.555s^2-0.75s^3+2.19s^4-0.31s^5)\,[s+\tfrac{\pi}{2}(1-s)]$$

$$f_2=\sqrt{1-s}\,(1+0.358s+1.425s^2-1.578s^3+2.156s^4)$$

$$F_1=\begin{cases}\theta_W^{-1}f_{1\mathrm{U}}+f_2 & \text{for USD}\\ \theta_W^{-1}f_{1\mathrm{C}}+f_2 & \text{for CSD}\end{cases}$$

$$F_2=\sqrt{\sec\left(\frac{\pi\theta_W}{2}\right)\sec\left(\frac{\pi\theta_W}{2s}\right)}$$

$$F_3\left(\bar{\ell}_{\mathrm{FPZ}},i/n\right)=\left[\left(1+\frac{A_1}{1-s}+\frac{3A_2}{2(1-s)^2}\right)\arcsin\left(\gamma\right)+\left(\frac{A_1}{1-s}+\frac{(4-\gamma)A_2}{2(1-s)^2}\right)\sqrt{1-s^2}\right]_{\gamma=\bar{b}_i}^{\gamma=\bar{c}_i}$$

$$F_4\left(\bar{\ell}_{\mathrm{FPZ}},\theta_W,i/n\right)=A_0^{-1}\left[\arcsin\left(\frac{\sin\left(\frac{\pi\theta_W}{2s}\bar{c}_i\right)}{\sin\left(\frac{\pi\theta_W}{2s}\right)}\right)-\arcsin\left(\frac{\sin\left(\frac{\pi\theta_W}{2s}\bar{b}_i\right)}{\sin\left(\frac{\pi\theta_W}{2s}\right)}\right)\right]\sqrt{\sec\left(\frac{\pi\theta_W}{2s}\right)}$$

$$s=\left(1+\bar{\ell}_{\mathrm{FPZ}}\right)^{-1},\;A_0=\arcsin\left(\bar{c}_i\right)-\arcsin\left(\bar{b}_i\right),\;A_1=-0.02s^2+0.558s^4,$$

$$A_2=0.221s^2+0.046s^4,\;\bar{c}_i=1-\left[(i-1)/n\right]\left(s\;\bar{\ell}_{\mathrm{FPZ}}\right)\;\text{and}\;\bar{b}_i=1-(i/n)\left(s\;\bar{\ell}_{\mathrm{FPZ}}\right)$$

(A-1)

$$\bar{w}_b\left(\bar{x},\bar{\ell}_{\mathrm{FPZ}},\theta_W\right)=\begin{cases}4(\theta_W^{-1}-1)\left(1+\bar{\ell}_{\mathrm{FPZ}}\right)\left(1-\bar{x}^2\right)^{0.5}f_{1\mathrm{U}}F_2H & \text{for USD}\\ 4(\theta_W^{-1}-1)\left(1+\bar{\ell}_{\mathrm{FPZ}}\right)\left(1-\bar{x}^2\right)^{0.5}f_{1\mathrm{C}}F_2H & \text{for CSD}\end{cases}$$

$$\bar{w}_{rb}\left(\bar{x},\bar{\ell}_{\mathrm{FPZ}},\theta_W\right)=4(1-\theta_W)\left(1+\bar{\ell}_{\mathrm{FPZ}}\right)\left(1-\bar{x}^2\right)^{0.5}f_2F_2H$$

$$\bar{w}_{\sigma_c}\left(\bar{x},\bar{\ell}_{\mathrm{FPZ}},\theta_W,i/n\right)=\frac{8}{s\pi}\int_{\bar{x}}^{1}\frac{\bar{a}F_3F_4F_B}{\sqrt{\bar{a}^2-\bar{x}^2}}d\bar{a}$$

$$f_{ij}=(\bar{w}_E)_i\beta_j+(\bar{w}_{\sigma_c})_{ij}$$

where

$$H=1+A\left(\frac{1-\bar{x}}{1-s}\right)+B\left(\frac{1-\bar{x}}{1-s}\right)^m,\ m=8-5(1+\bar{\ell}_{\mathrm{FPZ}})^{-20}$$

$$A=-0.14(1+\bar{\ell}_{\mathrm{FPZ}})^{-4}+0.46\bar{\ell}_{\mathrm{FPZ}}(1+\bar{\ell}_{\mathrm{FPZ}})^{-2.7}$$

$$B=0.37(1+\bar{\ell}_{\mathrm{FPZ}})^{-0.85}-0.36(0.5+\bar{\ell}_{\mathrm{FPZ}})^{-1.5}+0.168(0.6+\bar{\ell}_{\mathrm{FPZ}})^{-2.8}$$

$$F_B=1+A_1\left(\frac{1-\gamma}{1-s}\right)+A_2\left(\frac{1-\gamma}{1-s}\right)^2,\ \gamma=\frac{\bar{x}}{\bar{a}},\ \bar{x}=\frac{1}{2}\left(\bar{b}+\bar{c}\right)$$

$$\bar{w}_E=0.5(\bar{w}_b+\bar{w}_{rb})=2(1-\theta_W)\left(1+\bar{\ell}_{\mathrm{FPZ}}\right)\left(1-\bar{x}^2\right)^{0.5}F_1F_2H$$

$$(\bar{w}_{\sigma_c})_{ij}=\frac{8}{s\pi}\int_{\bar{x}_i}^{1}\frac{\bar{a}(F_3)_j(F_4)_j(F_B)_i}{\sqrt{\bar{a}^2-\bar{x}_i^2}}d\bar{a}$$

(A-2)

A.2 Normalized SIFs and CODs for Multi-fastener Joints

$$\bar{K}_b\left(\bar{\ell}_{\mathrm{FPZ}},\theta_W,\zeta\right)=\tfrac{1-\theta_W}{\theta_W(1+\zeta)}\sqrt{\pi\left(1+\bar{\ell}_{\mathrm{FPZ}}\right)}f_{1\mathrm{C}}F_2$$

$$\bar{K}_{rb}\left(\bar{\ell}_{\mathrm{FPZ}},\theta_W,\zeta\right)=\tfrac{1-\theta_W}{1+\zeta}\sqrt{\pi\left(1+\bar{\ell}_{\mathrm{FPZ}}\right)}f_2F_2$$

$$\bar{K}_{rB}\left(\bar{\ell}_{\mathrm{FPZ}},\theta_W,\zeta\right)=\tfrac{\zeta(1-\theta_W)}{1+\zeta}\sqrt{\pi\left(1+\bar{\ell}_{\mathrm{FPZ}}\right)}f_2F_2$$

$$\bar{K}_E\left(\bar{\ell}_{\mathrm{FPZ}},\theta_W,\zeta\right)=\bar{K}_{rB}+\tfrac{1}{2}\left(\bar{K}_{rb}+\bar{K}_b\right)$$

$$\bar{K}_{\sigma_c}\left(\bar{\ell}_{\mathrm{FPZ}},\theta_W,i/n\right)=2\sqrt{\left(1+\bar{\ell}_{\mathrm{FPZ}}\right)/\pi}\;F_3F_4$$

$$\beta_i=-\frac{4(F_3)_i(F_4)_i}{\pi(1-\theta_W)F_1F_2}$$

where

$$f_{1\mathrm{C}}=\tfrac{2}{\pi}\sqrt{1-s}\left(s+0.555s^2-0.75s^3+2.19s^4-0.31s^5\right)\left[s+\tfrac{\pi}{2}(1-s)\right]$$

$$f_2=\sqrt{1-s}\left(1+0.358s+1.425s^2-1.578s^3+2.156s^4\right)$$

$$F_1=\frac{1}{1+\zeta}\left(\theta_W^{-1}f_{1\mathrm{C}}+(2\zeta+1)f_2\right)$$

$$F_2=\sqrt{\sec\left(\frac{\pi\theta_W}{2}\right)\sec\left(\frac{\pi\theta_W}{2s}\right)}$$

$$F_3\left(\bar{\ell}_{\mathrm{FPZ}},i/n\right)=\left[\left(1+\frac{A_1}{1-s}+\frac{3A_2}{2(1-s)^2}\right)\arcsin\left(\gamma\right)+\left(\tfrac{A_1}{1-s}+\tfrac{(4-\gamma)A_2}{2(1-s)^2}\right)\sqrt{1-s^2}\right]_{\gamma=\bar{b}_i}^{\gamma=\bar{c}_i}$$

$$F_4\left(\bar{\ell}_{\mathrm{FPZ}},\theta_W,i/n\right)=A_0^{-1}\left[\arcsin\left(\frac{\sin\left(\frac{\pi\theta_W}{2s}\bar{c}_i\right)}{\sin\left(\frac{\pi\theta_W}{2s}\right)}\right)-\arcsin\left(\frac{\sin\left(\frac{\pi\theta_W}{2s}\bar{b}_i\right)}{\sin\left(\frac{\pi\theta_W}{2s}\right)}\right)\right]\sqrt{\sec\left(\frac{\pi\theta_W}{2s}\right)}$$

$$s=\left(1+\bar{\ell}_{\mathrm{FPZ}}\right)^{-1},\;A_0=\arcsin\left(\bar{c}_i\right)-\arcsin\left(\bar{b}_i\right),\;A_1=-0.02s^2+0.558s^4,$$

$$A_2=0.221s^2+0.046s^4,\;\bar{c}_i=1-\left[(i-1)/n\right]\left(s\;\bar{\ell}_{\mathrm{FPZ}}\right)\;\text{and}\;\bar{b}_i=1-(i/n)\left(s\;\bar{\ell}_{\mathrm{FPZ}}\right)$$

(A-3)

$$\bar{w}_b\left(\bar{x},\bar{\ell}_{\mathrm{FPZ}},\theta_W,\zeta\right)=\frac{4(1-\theta_W)}{\theta_W(1+\zeta)}\left(1+\bar{\ell}_{\mathrm{FPZ}}\right)\left(1-\bar{x}^2\right)^{0.5}f_{1\mathrm{C}}F_2H$$

$$\bar{w}_{rb}\left(\bar{x},\bar{\ell}_{\mathrm{FPZ}},\theta_W,\zeta\right)=\frac{4(1-\theta_W)}{1+\zeta}\left(1+\bar{\ell}_{\mathrm{FPZ}}\right)\left(1-\bar{x}^2\right)^{0.5}f_2F_2H$$

$$\bar{w}_{rB}\left(\bar{x},\bar{\ell}_{\mathrm{FPZ}},\theta_W,\zeta\right)=\frac{4\zeta(1-\theta_W)}{1+\zeta}\left(1+\bar{\ell}_{\mathrm{FPZ}}\right)\left(1-\bar{x}^2\right)^{0.5}f_2F_2H$$

$$\bar{w}_E\left(\bar{x},\bar{\ell}_{\mathrm{FPZ}},\theta_W,\zeta\right)=\bar{w}_{rB}+\tfrac{1}{2}\left(\bar{w}_{rb}+\bar{w}_b\right)=2\left(1-\theta_W\right)\left(1+\bar{\ell}_{\mathrm{FPZ}}\right)\left(1-\bar{x}^2\right)^{0.5}F_1F_2H$$

$$\bar{w}_{\sigma_c}\left(\bar{x},\bar{\ell}_{\mathrm{FPZ}},\theta_W,i/n\right)=\frac{8}{s\pi}\int_{\bar{x}}^{1}\frac{\bar{a}F_3F_4F_B}{\sqrt{\bar{a}^2-\bar{x}^2}}d\bar{a}$$

$$f_{ij}\left(\bar{x},\bar{\ell}_{\mathrm{FPZ}},\theta_W,\zeta\right)=(\bar{w}_E)_i\beta_j+(\bar{w}_{\sigma_c})_{ij}$$

where

$$H=1+A\left(\frac{1-\bar{x}}{1-s}\right)+B\left(\frac{1-\bar{x}}{1-s}\right)^m,\ m=8-5(1+\bar{\ell}_{\mathrm{FPZ}})^{-20}$$

$$A=-0.14(1+\bar{\ell}_{\mathrm{FPZ}})^{-4}+0.46\bar{\ell}_{\mathrm{FPZ}}(1+\bar{\ell}_{\mathrm{FPZ}})^{-2.7}$$

$$B=0.37(1+\bar{\ell}_{\mathrm{FPZ}})^{-0.85}-0.36(0.5+\bar{\ell}_{\mathrm{FPZ}})^{-1.5}+0.168(0.6+\bar{\ell}_{\mathrm{FPZ}})^{-2.8}$$

$$F_B=1+A_1\left(\frac{1-\gamma}{1-s}\right)+A_2\left(\frac{1-\gamma}{1-s}\right)^2,\ \gamma=\tfrac{\bar{x}}{\bar{a}},\ \bar{x}=\tfrac{1}{2}\left(\bar{b}+\bar{c}\right)$$

$$(\bar{w}_{\sigma_c})_{ij}=\frac{8}{s\pi}\int_{\bar{x}_i}^{1}\frac{\bar{a}(F_3)_j(F_4)_j(F_B)_i}{\sqrt{\bar{a}^2-\bar{x}_i^2}}d\bar{a}$$

(A-4)